Quantitative Texture analysis in MR Imaging in the assessment of Alzheimer's disease

Stephanos Leandrou

Supervisor: Prof. Panicos Kyriacou

School of Mathematics, Computer Science and Engineering
Research Centre for Biomedical Engineering

This dissertation is submitted for the degree of

Doctor of Philosophy

City, University of London

February 2021

"Σε κάθε όνειρο παλιό, καινούργιο πάνω χτίζω
έμαθα φως μου στη ζωή, απλά να συνεχίζω"

-Mantinada: is the most common form of folk song and is widespread across Crete.

Abstract

Alzheimer's disease (AD) is a progressive neurodegenerative disease which is clinically characterized by cognitive impairment and memory loss. Anatomically, AD initially affects specific structures within the Medial Temporal Lobe (MTL), which are essential for declarative memory. A definitive diagnosis of AD relies on post-mortem biopsy therefore, clinical assessment and cognitive tests are currently used. However, these tests are not sensitive to detect AD in an early stage.

The aim of this research was to investigate the usefulness of quantitative Magnetic Resonance Imaging (MRI) and specifically of texture features in the assessment of Mild Cognitive Impairment (MCI) which is the pre-dementia stage and AD. Firstly, two types of magnetic fields where investigated in order to examine whether, a stronger MR magnetic field would benefit quantitative imaging analysis derived from texture features. Secondly, texture features were extracted from the entorhinal cortex and evaluated in the diagnosis and prediction of MCI and AD. To the best of our knowledge this is the first research that investigated how the MR field strength affects texture features and used entorhinal cortex texture features on the assessment of AD.

The main results of this PhD showed that (1) texture features could provide more sensitive measures when they are extracted from stronger MRI magnetic field, such as 3T, compared to 1.5T. From a disease classification and prediction perspective, (2) entorhinal cortex texture features provide better classification between Normal Controls (NC), MCI and AD subjects, and (3) better prediction of the conversion from MCI to AD. In conclusion, this research has shown for the first time in the literature that entorhinal cortex texture features from MRI could contribute towards the early classification of AD.

Table of contents

Contents

List of Abbreviations

AD	Alzheimer's disease
ADBD	Alzheimer's disease Bid Data
ADI	Alzheimer's disease International
ADNI	Alzheimer Disease Neuroimaging Initiative
ANN	Artificial Neural Network
Aβ	Amyloid β
APP	Amyloid Precursor Protein
ApoE4	Apolipoprotein e4
ASM	Angular Second Moment
AUC	Area Under Curve
CAD	Computer-Aided Diagnosis
CDR	Clinical Dementia Rate
CFL	Classifier Fusion and Labelling
CLEAR	Constant Level Appearance
CSF	Cerebrospinal Fluid
CMRgI	Cerebral Metabolic Rate for Glucose
DA	Discriminant Analysis
DTI	Diffusion Tensor Imaging
GLCM	Gray Lever Co-occurrence Matrix
GM	Gray Matter
GMRF	Gaussian-Markov Random Fields
GWAS	Genome Wide Association Studies
ELISA	Enzyme-Linked Immunosorbent Assays
EMS	Expectation-Maximization Segmentation
ENIGMA	Enhancing Neuro Imaging Genetics through Meta-Analysis
EOAD	Early-onset AD
FDA	Food and Drug Administration
FDG	Fluorodeoxyglucose
FLAIR	Fluid Attenuation Inversion Recovery
FTLD	Frontotemporal Dementia
LOAD	Late-onset AD
MCI	Mild Cognitive Impairment
NFTs	Neurofibrillary Tangles
MMSE	Mini Mental State Examination
MRI	Magnetic Resonance Imaging
MPRAGE	Magnetization Prepared - RApid Gradient Echo
MTL	Medial Temporal Lobe

NINCDS/ADRDA	National Institute of Neurological and Communicative Disorders and Stroke and the Alzheimer's disease and Related Disorders Association
NC	Normal Controls
NIA	National Institute on Aging
NIBIB	National Institute of Biomedical Imaging and Bioengineering
NODDI	Neurite Orientation Dispersion and Density Imaging
OASIS	Open Access Series of Imaging Studies
PET	Positron Emission Tomography
PiB	Pittsburgh compound B
PURE	Phased-Array Uniformity Enhancement
P-tau	Phosphorylated Tau
ROI	Region Of Interest
ROC	Receiver Operating Characteristic (curve)
RLM	Run Length Matrix
SNR	Signal to Noise Ratio
SVM	Support Vector Machine
T	Tesla
T-Tau	Total Tau
VBM	Voxel Based Morphometry
WM	White Matter

List of Tables

List of Figures

Declaration

I hereby declare that the work presented within this thesis has been conducted by myself, unless otherwise cited or acknowledged. The work is entirely of my own composition and has not been submitted, in whole or in part, for any other degree at the City University, London or any other institution.
Prior to commencing my PhD, Cy-Tera supercomputer of the Cyprus Institute was used to run the software needed to prepare my data downloaded from the Alzheimer's Disease Neuroimaging Initiative (ADNI) database.

Stephanos Leandrou

March 2021

List of Publications

Journal Papers

1. **Leandrou Stephanos**, Styliani Petroudi, Constantino Carlos Reyes-Aldasoro, Panayiotis A Kyriacou, Constantinos S Pattichis. Quantitative MRI Brain Studies in Mild Cognitive Impairment and Alzheimer's disease: A Methodological Review. IEEE Reviews in Biomedical Engineering, volume 11, pp. 97-111, January 2018. DOI: 10.1109/RBME.2018.2796598

2. A. S. Panayides, M. Pattichis, **S. Leandrou**, C. Pitris, A. Constantinidou, and C. S. Pattichis, "Radiogenomics for Precision Medicine With A Big Data Analytics Perspective," IEEE J Biomed Health Informatics, volume 23, Issue 5, pp. 2063-2079, December 2018. DOI: 10.1109/JBHI.2018.2879381

3. **Leandrou S.,** D. Lamnisos, G. Mamais, Panicos A. Kyriacou, Constantinos S. Pattichi. Assessment of Alzheimer's Disease Based on Texture Analysis of the Entorhinal Cortex. Original Research Article, Frontiers Aging Neuroscience, volume 12:176, July 2020. DOI: 10.3389/fnagi.2020.00176

4. **Stephanos Leandrou**, Demetris Lamnisos, Panicos A. Kyriacos, Stephanie Constanti, Constantinos S. Pattichis, Comparison of 1.5T and 3T MRI hippocampus texture features in the assessment of Alzheimer's disease. Biomedical Signal Processing and Control, volume 62: 102098 September 2020. DOI: https://doi.org/10.1016/j.bspc.2020.102098

Conference Publications

1. **Leandrou S.**, Petroudi, S., Kyriacou, P. A., Reyes-Aldasoro, C. C. & Pattichis, C. S. An overview of quantitative magnetic resonance imaging analysis studies in the assessment of Alzheimer's disease. March 2016 - IFMBE Proceedings, volume 57, pp. 281-286. DOI: 10.1007/978-3-319-32703-7_56

2. **Leandrou S.**, Ioannis Mamais, Styliani Petroudi, Constantino Carlos Reyes-Aldasoro, Panayiotis A Kyriacou, Constantinos S Pattichis. Hippocampal and entorhinal cortex volume changes in Alzheimer's disease patients and mild cognitive impairment subjects. March 2018 - IEEE EMBS International Conference on Biomedical & Health Informatics (BHI), pp. 235-238, DOI: 10.1109/BHI.2018.8333412

3. Kleo G. Achilleos, **Stephanos Leandrou**, Nicoletta Prentzas, Panayiotis A. Kyriacou, Antonis C. Kakas and Constantinos S. Pattichis. Extracting Explainable Assessments of Alzheimer's disease via Machine Learning on brain MRI imaging data. 2020 IEEE 20th International Conference on Bioinformatics and Bioengineering (BIBE) DOI: 10.1109/BIBE50027.2020.00175

4. E. Prodromou, **S. Leandrou**, E. Schiza, K. Neocleous, M. Matsangidou, C.S. Pattichis. A Multi-User virtual reality application for visualization and analysis in medical imaging. 2020 IEEE 20th International Conference on Bioinformatics and Bioengineering (BIBE) DOI: 10.1109/BIBE50027.2020.00135

Conference Presentations

1. **Leandrou S.**, I. Mamais, D. Lamnisos, S. Petroudi, Member IEEE, PA, Kyriacou, SM-IEEE, Constantino Carlos Reyes- Aldassoro, SM-IEEE, C.S. Pattichis, SM-IEEE. The Role of Imaging in the Age of Precision Medicine for the Accurate Assessment of Alzheimer's Disease, **RSNA 2018, Chicago, Illinois**.

2. **Leandrou S.**, I. Mamais, Petroudi, S., Kyriacou, P. A., Reyes-Aldasoro, C. C. & Pattichis, C. S. Quantitative MRI in the Assessment of Alzheimer's Disease: A Volume Analysis of Normal, Mild Cognitive Impairment and Alzheimer's Disease Subjects, **RSNA 2017, Chicago, Illinois.**

3. **Leandrou S.**, I. Mamais, Petroudi, S., Kyriacou, P. A., Reyes-Aldasoro, C. C. & Pattichis, C. S. The role of imaging in Alzheimer's disease, in 2017, **4th Cypriot-Hellenic conference of Radiology, Nicosia, Cyprus**

Acknowledgements

I would like to express my sincere thanks to Prof. Panicos Kyriacou for giving me the opportunity to conduct this research, but also for his useful comments and support during my studies.

Furthermore, I would like to thank my supervisor, Prof. Constantinos Pattichis for the patient guidance, encouragement and advice he has provided. I have been extremely lucky to have the opportunity to work with Prof. Pattichis on such an exciting field of medical image processing. I would like to thank him for his motivation, courage and enthusiasm through the journey of my PhD project.

Besides my advisors, I would like to thank Dr. Carlos Reyes Aldasoro and Dr. Styliani Petroudi for their insightful comments and encouragement. Without they precious support at the beginning of this journey it would not be difficult to conduct this research.

1

Introduction

1.1 Overview

Alzheimer's disease (AD) is the most common type of dementia that affects memory, thinking and behavior in elderly people. It represents almost 80% of dementia cases. Usually, age of 65 and older, is the greatest known risk factor, however, early-onset AD was noticed also in patients under the age of 65 [1]. By 2050, one new case of AD is expected to develop every 33 seconds [2]. Unfortunately, even nowadays, there is no cure to halt the progressive neurodegeneration of AD, but only to slow the worsening of dementia symptoms. Usually these symptoms include disorientation, confusion and behavior changes, whereas, in advance subjects there is difficulty in speaking, walking even swallowing, therefore, these subjects require 24/7 care.

The diagnosis of the disease relies on clinical and neuropsychological tests [3], [4] which evaluate memory and language abilities. Therefore, a subject is categorized as a patient with "probable" AD and only post-mortem material will confirm the disease. The motivation of this research, derives from a major disadvantage of clinical assessment, where structural changes within the brain occur several years before the first clinical symptoms appear [5], [6]. As a consequence, when a patient is diagnosed with AD by using only clinical and psychometric or cognitive assessment, the brain tissue has already undergone widespread and irreversible synaptic loss [7]. Most importantly, Mild Cognitive Impairment (MCI) which is the pre-dementia stage cannot be

identified easily by cognitive tests, as these subjects do not have major memory problems which will affect their daily routine, therefore they cannot be detected.

Problem statement: Due to the fact that only histological confirmation at post-mortem biopsy will identify the disease, there is a great interest in the role of neuroimaging biomarkers, especially of those derive from structural Magnetic Resonance Imaging (MRI). Although amyloid markers such as cerebrospinal fluid (CSF) Amyloid β ($A\beta_{1-42}$) and Aβ Positron Emission Tomography (PET) could detect changes in an earlier stage of the disease, both techniques begin to plateau at the MCI stage where the disease becomes evident [8]. Furthermore, PET studies are not accessible for all subjects, due to several factors such as cost, radiopharmaceutical limitations (availability, targeting amyloid or tau proteins) and most importantly, the exposure to ionizing radiation.

On the other hand, structural MRI changes become more pronounced in the MCI stage, which is the most critical stage of the disease because an MCI subject might convert to AD. However, the human vision cannot identify these subtle changes and computational analysis is required. Although it is well known that Neurofibrillary Tangles (NFTs), are a fundamental neuropathological hallmark of AD which affect and damage the neuronal tissue and cause dementia, however, these plaques cannot be detected with the conventional MRI methods such as volumetry.

Motivation: Texture analysis is a method not usually used in the assessment of AD and studies the statistical properties of the image intensities. The ability to detect dementia-specific textural patterns in the brain tissue and to discriminate these from the texture of normal healthy brain tissue may provide a valuable and complementary MRI-based biomarker of the disease. Moreover, it is likely that an MRI marker based on texture will be able to detect in an

earlier stage the disease than markers that target larger scale changes in the brain, such as atrophy. The establishment of such biomarkers, will allow the identification of MCI individuals in an earlier stage thus, these subjects will have the opportunity to prevent the conversion to AD.

Most extensively used MRI measurements include Region Of Interest (ROI) volume measurements such as hippocampal and cortex volume or whole-brain atrophy measurements. Although hippocampus represents the most established ROI used in the assessment of AD, the earlier involvement of the entorhinal cortex was proved by many studies. Furthermore, although volumetry represents the most commonly used method to date for the assessment of AD, the study by Sørensen et al [9], found that hippocampal texture was superior to volume reduction for the disease prediction. Therefore, it is hypothesized that through the earlier involvement of entorhinal cortex and by using texture analysis, it is likely to detect microscopic alterations of the disease before atrophy spreads and perhaps these represent changes due to NFTs and Aβ plaques.

1.2 Aims and Objectives

Many studies have been investigating the complex heterogeneity of AD, trying to understand how the disease initiates and from which region of the brain. Although only post mortem biopsy will confirm the disease, imaging biomarkers are currently being used for its early detection. In the literature there are several structural quantitative imaging methods used and each one of them provides different information regarding the disease. Many methods, evaluate the volume of specific structures or regions and seek for atrophy, other methods use the brain cortex thickness and other texture characteristics of the image.

The **first aim** of the present thesis was to review the literature and evaluate the regions of the brain successively affected by the disease (Chapter 2). Also, in

Chapter 2 a review to the state-of-the-art research in precision medicine is made to specifically highlight the fundamental challenges in the emerging fields of radiomics and radiogenomics and their value in AD. The **second aim** was to evaluate the MRI methods used in quantitative imaging. Therefore a comparison of the several MR structural methods derived from volume, thickness, voxel based morphometry (VBM) and texture were performed to assess their performance in detecting and predicting the disease (Chapter 3).

Currently, in both literature and clinical practice, two types of MRI field strengths are being used, the 1.5 Tesla (T) and 3T. Some studies have compared how the magnetic field strength could influence quantitative volumetric imaging. However, no study has evaluated before, how texture features are affected by a stronger magnetic field. Therefore, the **third aim** of this thesis was to evaluate how the MRI magnetic field strength could affect texture features in their ability to classify AD subjects in comparison with volumetric and thickness features (Chapter 5).

In the literature, most of the studies have been using hippocampus in their analysis, because it is highly associated with AD as is the region responsible for declarative memory. However, entorhinal cortex, is recognized as a region severely affected by AD pathology and is reported to be the most heavily damaged cortex in AD. Furthermore, entorhinal cortex atrophy is predicted to occur prior to hippocampal damage and is one of the earliest signs of disease manifestation. However, no study used extracted entorhinal cortex texture features before in the assessment of AD. Therefore, the **fourth aim** of this thesis is to evaluate the diagnostic and predictive ability of entorhinal cortex texture features in the assessment of AD (Chapter 6).

1.3 Contribution (Novelty)

Through a literature review this thesis will evaluate and detect the brain regions successively being affected by the AD and compare the MR imaging

quantitative methods currently being used for the assessment of AD. The findings of the literature review will determine the regions affected in the initial stages and the methods to be used for further analysis.

The first novelty of this research is the fact that there is no published study that compared texture features extracted from both 1.5T and 3T MR field strengths as most of the studies have been using volumetric measures. For this comparison the hippocampus which is the most frequently used ROI for the assessment of AD will be used. Specifically, it will be evaluated, if hippocampal texture features extracted from 1.5T and 3T images are statistically different and if a stronger magnetic field could provide better results in the classification of subjects.

The second novelty of this research is the fact that although entorhinal cortex is the region being affected in the very early stages of the disease, even before hippocampus, no study has used texture analysis on this region before. Textural features were used before but on ROIs that are affected in a later stage, therefore, it will be evaluated if entorhinal cortex texture features extracted from T1-weighted MR images could be used as a new biomarker for the assessment of AD and perhaps provide an earlier detection of the disease, especially of the MCI subjects.

1.4 Thesis Structure

Chapter 2 describes the pathophysiology of AD and the areas of the brain which are affected in an early stage. Then, chapter 2 concentrates on the diagnosis of the disease describing the main method used which is the neuropsychological assessment and its major disadvantages. Apart from the cognitive tests, this chapter also refers to the fluid biomarkers currently being used in the diagnosis of the disease and it ends with the imaging biomarkers such as from PET and MRI.

Chapter 3 describes the use of medical imaging and the necessity of quantitative imaging in the assessment of AD. Specifically, it tabulates the methods that are currently being used with structural MRI such as: : i) Voxel-based Morphometry (VBM), ii) volumetric measurements in specific ROIs, iii) cortical thickness measurements, iv) shape analysis and v) texture analysis. The aforementioned methods are being used in both classification and prediction of the disease and this chapter describes both their advantages and disadvantages.

Chapter 4 describes the pre-processing methods and tools used for the data preparation of this research.

Chapter 5 compares hippocampal texture features extracted from both 1.5T and 3T MRI systems of AD subjects. It is hypothesized that higher magnetic fields will provide better differentiation between the texture characteristics of the NC, MCI and AD subjects.

Chapter 6 represents the main chapter of the thesis and it refers to texture analysis of the entorhinal cortex and compares it with the "gold standard" method, which is the hippocampal volumetry in both classification and prediction of AD.

Chapter 7 describes the major conclusions, contributions and the future scope of this work.

2

The Alzheimer's Disease

2.1 Introduction

Alzheimer's disease (AD) represents the most common form of dementia and one of the major causes of disability in later life. Alois Alzheimer (Figure 1) first described it in 1907 [10] and as a neurodegenerative disorder, it is characterized by loss of cognitive functions. Other common types include vascular dementia, Lewy body dementia and frontotemporal dementia (FTLD) [11]. In the UK alone, there are over 850.000 people with dementia and this number is projected to rise to 1.6 million by 2040. This year, approximately 225.000 people will develop dementia, that's one every three minutes (www.alzheimers.org.uk). In 2019 Alzheimer's Disease International (ADI) estimates that there are over 50 million people living with dementia globally, a figure set to increase to 152 million by 2050 [12].

Figure 1: Alois Alzheimer (1864-1915)

Unfortunately, due to the complex neuropathology of the disease there is no cure for it, apart from the treatment taken to slow its progressive manifestation.

Furthermore, there is no definitive diagnosis as only post-mortem biopsy will confirm the disease, thus, a patient is classified with probable AD. However, by using specific imaging techniques, it is now feasible to detect AD several years before clinical symptoms arise and perhaps modifying treatment could be more beneficial. Advances in medical imaging, genetics, bio-specimen and clinical data give this opportunity to the research community especially when the aforementioned data are combined.

This chapter will concentrate on the pathophysiology of AD, the methods currently being used in the assessment of AD and the biomarkers that have been used in the literature and to improve the diagnosis of a probable AD subject.

2.2 The disease physiology

There are still many unsolved issues regarding the pathophysiology of this highly heterogeneous disease and the exact pathogenesis is not yet fully understood. However, the greatest risk factors for AD are age (over 65), family history and the presence of Apolipoprotein e4 (ApoE4) gene [13]. According to Braak and Braak [14], the most evident change is the progressive deposition of abnormal proteins $A\beta_{(1-42)}$, that trigger the formation of senile plaques and NFTs, which affect and damage the neuronal tissue and cause dementia (Figure 2). The analysis of CSF showed that $A\beta_{(1-42)}$ concentration was less in AD subjects rather than in NC [7-8].

It seems that Aβ oligomers in the brain seem to be responsible for that reduced levels of $A\beta_{(1-42)}$ [15]. Ultimately, it is these Aβ oligomers that become large Aβ fibrils that concentrate to form insoluble deposits in extracellular space, including diffuse plaques and dense-core plaques.

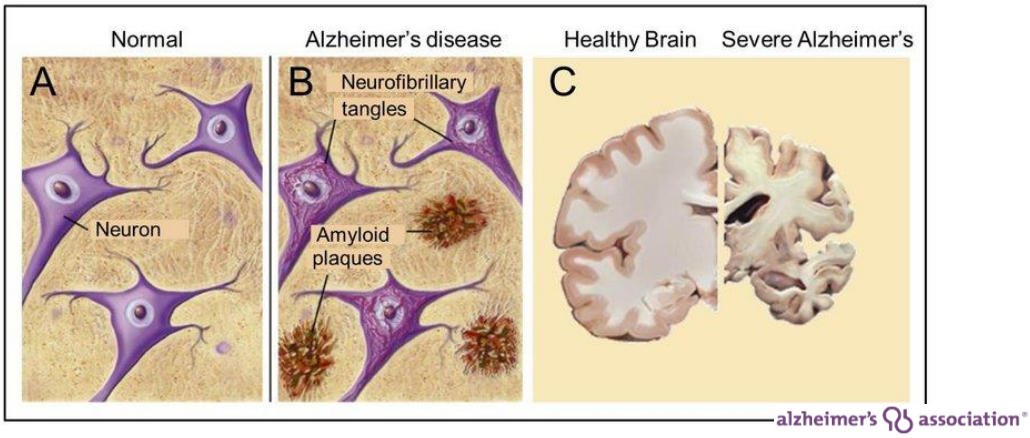

Figure 2: AD hallmarks: a) tissue-level representation, showing the presence of amyloid (senile) plaques and neurofibrillary tangles; b) late-stage AD brain, showing marked shrinkage in comparison with a healthy brain.

According to Metaxas and Kempf [16], "NFTs are a fundamental neuropathological hallmark of AD and have been characterized by loss of cytoskeletal microtubules and tubulin-associated proteins. Although the exact molecular mechanisms linking the loss of cytoskeletal elements to NFT development remain unclear, signal transduction pathways involving protein phosphorylation and de-phosphorylation are likely to play a main role in the formation of neurofibrillary lesions".

In the Braak staging system [5] it was shown that NFTs appear initially in the trans-entorhinal region of the temporal lobe, spreading to limbic areas such as the hippocampus, the amygdala and the parahippocampal gyrus [17]–[19], and ultimately affecting large areas of the neocortex. However, although these patterns of pathology spread through the brain for a long protracted pre-clinical stage (~10-15 years) [20], when first clinical symptoms become apparent, there is already an inevitable progression of atrophy. Atrophy initially affects the Medial Temporal Lobe (MTL) (Figure 3) [21]–[23] a region which includes anatomically related structures that are essential for declarative memory [18]. With the disease progression, these regions lose neuronal tissue with consequent brain atrophy [24].

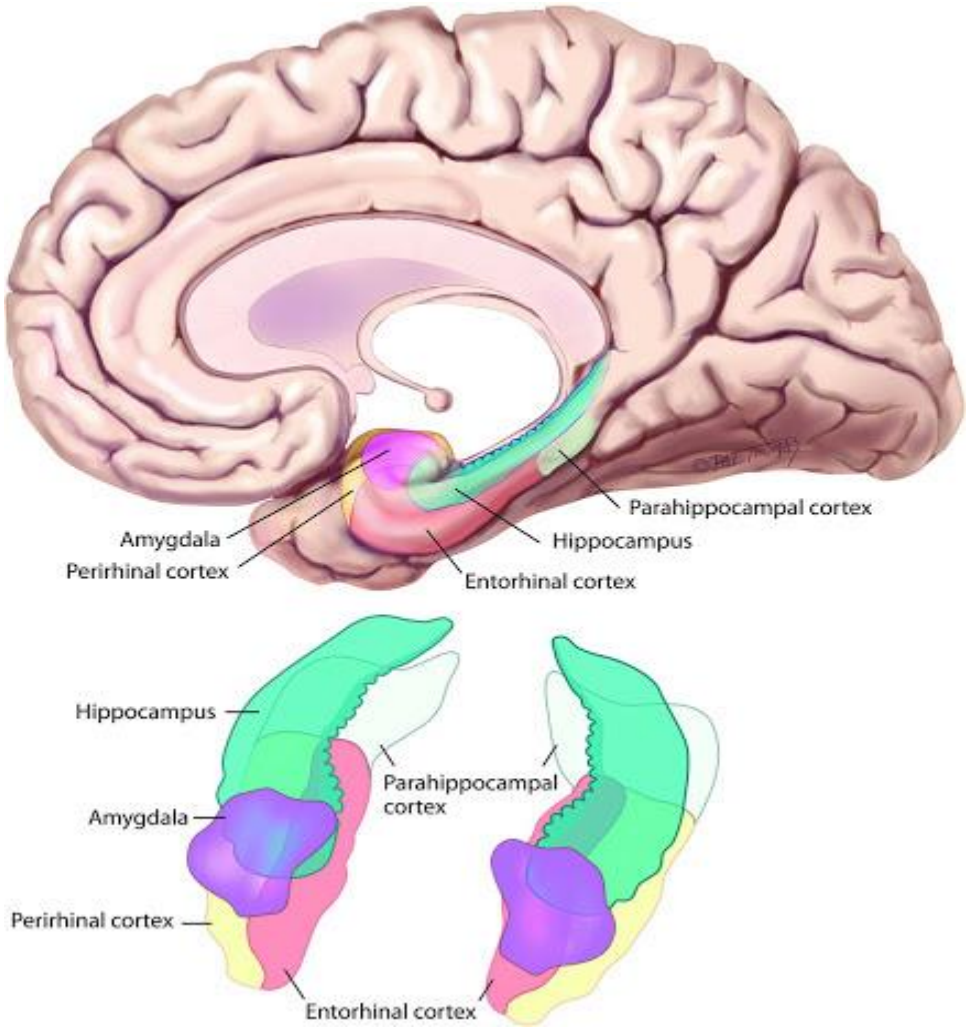

Figure 3: The medial temporal lobe: It consists of the hippocampal formation (blue-green) superiorly and the parahippocampal gyrus inferiorly. The entorhinal (brown) and perirhinal (yellow) cortices form the medial and lateral components, respectively, of the anterior portion of the parahippocampal gyrus, while the parahippocampal cortex (off-white) forms the posterior portion. Figure adapted from Purves, et al. 2008 [25].

Within MTL, entorhinal cortex, is recognized as a region severely affected by AD pathology and is reported to be the most heavily damaged cortex in AD [26]. Entorhinal cortex atrophy is predicted to occur prior to hippocampal damage and is one of the earliest signs of disease manifestation. The rate of atrophy in the entorhinal cortex correlates with severity of cognitive symptoms [27] and is considered predictive of conversion from MCI to AD [28].

2.4 Clinical Symptoms

Clinically, AD affects memory, language, and other cognitive skills and eventually leads to an inability of everyday activities. In the early stages, the most common symptom is difficulty in remembering recent events, while advanced AD patients often suffer from loss of the ability to take care of themselves, communicate with others or even recognize their family members. Eventually these subjects require day-to-day support and personal care. As the condition of the patient worsens with the disease progression, eventually it leads to death. In a majority of cases (>95%) the onset of AD is sporadic, and is usually classified by its age of onset (>65 years). On the other hand, 1-5% of cases exhibit an earlier onset, typically in the late 40s or early 50s (so-called early-onset AD). These predominate two forms of AD are clinically indistinguishable; however, early-onset AD is generally more severe and is associated with a rapid rate of progression. Figure 4 shows a theoretical timeline for the progression of AD.

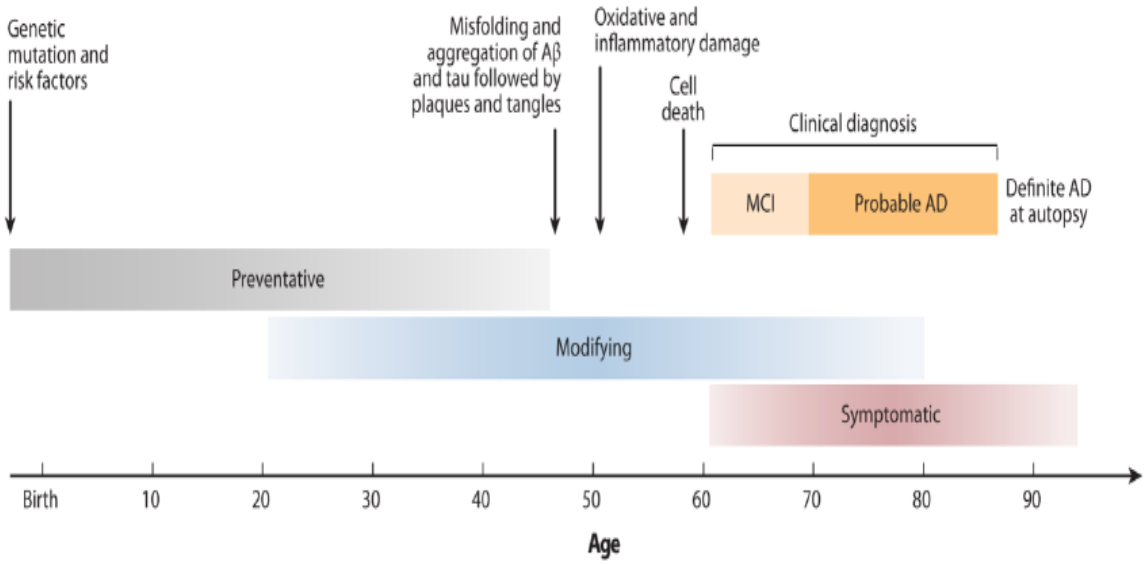

Figure 4: This figure shows a theoretical timeline for the progression of AD-related neuropathology and clinical changes, with changes in amyloid and tau pathology occurring years before the onset of AD. The grey, blue, and red shaded bars reflect time points at which different types of potential interventions may be beneficial (grey, preventative; blue, disease modifying; red, symptomatic). Figure adapted from Shaw et al., 2007 [29].

2.5 Disease Diagnosis

According to the National Institute on Aging (NIA) and the Alzheimer's Association, the disease progression consists of three stages: the pre-clinical stage, the pre-dementia stage called MCI and the AD or dementia stage. MCI represents the transitional stage between normal ageing and AD, and MCI subjects experience memory impairment as the most prominent feature. These subjects may have decreased memory function beyond the normal level based on a given person's age and education; however, they do not fulfill the criteria for dementia, as their cognitive function is comparable to NC subjects. Most of the MCI subjects will remain stable even after 10 years of follow-up [30] and only a small percent (10%-15%) will progress to AD [31]. Distinguishing MCI subjects is of great importance and much effort has been put into identifying the MCI subjects that will eventually convert to AD.

The diagnosis of the disease still remains probable and only post-mortem biopsy will confirm AD as it reveals deposits of Aβ plaque deposition and NFTs in the brain tissue [32]. Thus, clinical diagnosis for ''probable AD'' cannot be given until the patient have affected memory and cognitive skills and unfortunately, by that time the brain tissue will already undergone widespread and irreversible synaptic loss [7].

2.6 Cognitive tests

Nowadays, the diagnosis of AD is based on the clinical features of the disease, with a presence of a memory disorder and an impairment in at least one other cognitive domain, both of which interfere with social function or activities of daily living. Mini Mental State examination (MMSE) [3] (see Table 1 in Appendix A) and Clinical Dementia Rating (CDR) [4] are two of the most commonly used tests in clinical practice for the assessment of AD.

2.7 MMSE and CDR scores

MMSE consists of a series of clinical and psychometric assessment through neuropsychological tests, which assess language and memory abilities, and the ability of solving problems. The maximum MMSE score is 30 points. A score less than 12 indicates severe dementia, 13 to 20 recommends moderate dementia, 20 to 24 suggests mild dementia and 24 to 30 represents NC [3].

In parallel, CDR is used to describe memory, orientation, judgment, and problem solving, home and hobbies and personal care. A score of 0, represents normal controls, 0.5, very mild dementia, 1, mild dementia, 2, moderate dementia and 3, severe dementia [4].

Unfortunately, cognitive assessment is not objective as they might be affected from external factors, e.g. from the psychological condition of the patient. This leads to a large variability in the definition especially of the MCI subjects. Thus, the research community has driven a search for diagnostic imaging markers. The revised criteria for the diagnosis of AD were proposed in 2007 by the National Institute of Neurological Disorders and Stroke–Alzheimer Disease and Related Disorders working group [33]. According to these criteria, the clinical assessment should include at least one supportive feature: (i) MTL atrophy as seen in structural MRI, (ii) Temporoparietal hypometabolism as seen in PET, due to neuronal death the brain is not absorbing the 18^{F}-FDG radiotracer, (iii) Positivity on amyloid imaging as seen in PET and iv) Abnormal neuronal CSF markers (tau and/or Aβ).

2.8 Fluid Biomarkers in AD

In medicine, a biomarker or a "biological marker" represents an indicator of a particular disease or state which can be reproduced and measured accurately. Furthermore, in order to identify a good biomarker with diagnostic utility it must be sensitive, specific, and easy to administer to patient populations.

Especially in the case of AD, where biopsy is unavailable and the diagnosis of the disease is made postmortem, diagnostic biomarkers are very important. Furthermore, apart from AD which is the most common form of dementia, an ideal biomarker should be able to distinguish other forms of dementia such as Lewy-body dementia, vascular dementia. Although significant advances in neuroimaging techniques could provide both anatomical, functional and metabolic information regarding the disease physiology, CSF and plasma studies represent a more direct and convenient means to study the disease progression.

2.9 Core Cerebrospinal Fluid Biomarkers

Biochemical biomarkers of the disease derived from CSF, a fluid which occupies the subarachnoid space. Lumbar puncture is an invasive procedure to collect CSF, therefore, it stands as a major drawback in this *in vivo* method. CSF biomarkers are related to the three main pathological changes that occur in the brain: Aβ deposition into extracellular Aβ plaques, intracellular formation of NFTs and neuronal loss [34].

There are three major proteins constituents of AD pathology which are the leading diagnostic and prognostic biomarkers of the disease. These are (1) $A\beta_{(1-42)}$, (2) Total Tau (T-tau), and (3) phosphorylated tau (P-tau) derived by enzyme-linked immunosorbent assays (ELISA's). However, CSF sample is required, therefore, the patient has to go through the invasive lumbar puncture procedure for CSF collection. So far, there are no studies reporting biomarkers in peripheral blood and perhaps this could be a new field of research.

Compared to other body fluids, CSF is considered an important source for AD biomarkers as it is in direct contact with the extracellular space of the brain and as a result it allows the evaluation of chemical changes occur in the brain. There are 42 amino acids in the β-amyloid peptide which are highly insoluble and aggregates into extracellular Aβ deposits in the brain of AD subjects. As a

result, there is a decrease of $A\beta_{(1-42)}$ (~40%) concentrations in the CSF of AD subjects [35]. On the other hand, P-tau and T-tau concentrations increase in the cytosol of neurons where there are attached to microtubules. In AD subjects, tau and p-tau proteins are detached from microtubules and they accumulated into NFT. During this process, these proteins are also released into extracellular space and they are detected in higher concentrations in the CSF sample [36]. Therefore elevated levels of p-Tau in AD can be exploited as a predictive biomarker.

The combination of $A\beta_{(1-42)}$, T-tau, and P-tau provides high diagnostic power in the classification of AD with sensitivity and specificity reaching 92% and 89%, respectively [37].

2.10 Genetic Risk Factors

- *The following text is part of a journal paper by Panayides et al., 2018 - (Radiogenomics for Precision Medicine With A Big Data Analytics Perspective," IEEE J Biomed Health Informatics, volume 23, Issue 5, pp. 2063-2079, December 2018. DOI:* 10.1109/JBHI.2018.2879381*)*

Genetic data have been essential in understanding the complex pathophysiology of AD. According to **Error! Reference source not found.** the presence of mutations in amyloid precursor protein (APP), presenilin 1 (*PSEN1*) or presenilin 2 (*PSEN2*) can determine the early development of the disease. Furthermore, APOE is included in the well-established genes for AD. The APOE gene is found in human body as three polymorphic alleles: ε2, ε3 and ε4 with a worldwide frequency of 8.4%, 77.9% and 13.7%, respectively. However, in an AD patient the ε4 allele could increase up to ~40% **Error! Reference source not found.**. Today, APOE gene represents the strongest major genetic risk for both early-onset AD (EOAD) (<65 years) and late-onset AD (LOAD) (≥65 years), the latter representing the majority of cases, with ε4 allele being the most descriptive factor **Error! Reference source not found.**.

Research relying on genome wide association studies (GWAS) and whole exome and whole genome sequencing data, have identified a significant number of genes that are correlated to AD. GWAS investigate single nucleotide polymorphisms (SNPs) throughout the genome to identify genetic variants of a disease which might lead to a more precise therapy. In **Error! Reference source not found.**, nine additional genes /loci have been identified for LOAD, namely CR1, BIN1, CLU, PICALM, MS4A4/MS4A6E, CD2AP, CD33, EPHA1 and ABCA7. A comprehensive overview of GWAS in AD appears in **Error! Reference source not found.**. Furthermore, quantitative MCI phenotypes for genetic or genome-wide association studies using data from the Alzheimer's Disease Neuroimaging Initiative (ADNI) database [38] (published 2009-2012) are summarized in **Error! Reference source not found.**.

Typically, AD studies investigate imaging biomarkers, and in particular longitudinal structural MRI data studies are the most frequent. For a review on quantitative MRI brain studies in MCI and AD, the reader is referred to **Error! Reference source not found.**. However, the combination of several AD biomarkers, such as MRI scans, PiB scans, and measurements of CSF Aβ and tau or APOE allele status, significantly add predictive value to the clinical diagnosis and the evaluation of the treatment efficacy. Towards this direction, a brief overview of emerging radiogenomics methods for the assessment of AD is provided next, and tabulated in Table 2.

In **Error! Reference source not found.**, 742 ADNI participants were examined to map the 3D profile of the MTL volume differences. It was found that rs10845840 SNP located in GRIN2B gene, was significantly associated with greater atrophy of the temporal lobe bilaterally. In addition, Enhancing Neuro Imaging Genetics through Meta-Analysis (ENIGMA's) first project **Error! Reference source not found.** was a GWAS study trying to identify the genome associated with hippocampal volume. Hippocampal formation is the most

frequently used biomarker for the assessment of AD as is the structure responsible for learning and memory. It was found that, intergenic variant rs7294919 was associated with hippocampal volume and rs10784502 with intracranial volume. Similarly, GWAS on 33,536 individuals (the largest study up to date) from the ENIGMA database was performed in **Error! Reference source not found.**. They discovered 4 novel loci associated with hippocampal volume, three of them lie within genes (ASTN2, DPP4 and MAST4) and the fourth is found 200 kb upstream of the sonic hedgehog. Hippocampal subfield analysis was also performed and it was shown that a locus within the MSRB3 gene might could affect the dentate gyrus, subiculum, CA1 and fissure.

In **Error! Reference source not found.**, they used a Bayesian method to identify indirect genetic associations between AD and NC using image phenotypes. Associations between imaging and disease phenotype were captured simultaneously with the correlation from genetic variants and image features in a probabilistic model. In their model brain regions not associated with AD were not included even if they were strongly modulated by genetics. In addition to the APOE variants, more SNPs are suggested for further investigation (see table 2).

In **Error! Reference source not found. Error! Reference source not found. Error! Reference source not found.**, the authors showed that the combination of imaging, genetics and neuropsychological tests could provide better accuracy in the prediction to AD conversion compared to single modality classifiers. Combined CSF, MRI, PET and genomics were used in **Error! Reference source not found.** to investigate the shapes of trajectories of AD biomarkers as a function of MMSE, demonstrating that a sigmoidal shape over time is followed. Brain metabolism and gray matter (GM) density combined with GWAS to identify the genetic influences on NC, MCI and AD subjects was

investigated in **Error! Reference source not found.** and Key findings linked most gene's effects with the disease stage.

APOEs is the strongest genetic predictor of AD and toward this direction, the study in **Error! Reference source not found.** revealed that specific alleles in APOE ε4 carriers, correlated with a more severe cortical thickness and MTL atrophy. Moreover, APOE ε4 carriers who had a high Aβ PET imaging, were more affected by cognitive decline as depicted in **Error! Reference source not found.**, **Error! Reference source not found.**. Their results were correlated with **Error! Reference source not found.** where subjects with negative β- amyloid peptide scan had less temporoparietal hypometabolism, less severe MTL atrophy, and low APOE ε4 gene. In a longitudinal study **Error! Reference source not found.** the authors followed a whole brain approach using MRI and PET and showed that ε4 allele carriers had faster rates of cortical loss especially in the area of MTL, and increased longitudinal accumulation of amyloid-β pathology on their cortex. The study suggested that APOE gene influences on AD could be detected in middle age. Similarly, longitudinal MRI and PET also used in **Error! Reference source not found.** and APOE ε4 was strongly related to baseline Aβ and to greater memory decline and hippocampal atrophy in Aβ+ subjects.

Moreover, in **Error! Reference source not found.**, it was shown that lower baseline FDG PET can predict subsequent cognitive decline while APOE ε4 allele was more frequent in AD compared to MCI and NC subjects. A reduction in glucose metabolism was also seen in APOE ε4 allele carriers in AD-signature ROIs in **Error! Reference source not found.**. The author in **Error! Reference source not found.**, compared baseline regional cerebral metabolic rate for glucose (CMRgI) using FDG PET in mildly affected AD subjects and 142 amnestic MCI subjects to those from NC. As expected, compared to NC, AD and amnestic MCI subjects had significantly lower CMRgI bilaterally (in

posterior cingulate, precuneus, parietotemporal and frontal cortex) which was correlated with MMSE scores and APOE ε4 allele. The results were correlated with the study in **Error! Reference source not found.**.

Diffusion tensor imaging (DTI) is a MRI technique that allows the assessment of the microstructural integrity of White Matter (WM) based on fractional anisotropy (FA) and mean diffusivity. It was found that the microstructural integrity of WM tends to follow an anterior to posterior path with MCI and AD subjects having more damage in posterior regions **Error! Reference source not found.**. Furthermore, the authors in **Error! Reference source not found.** used DTI to measure FA and revealed a reduction in cingulum fibers in the parahippocampal and posterior cingulate regions of MCI and AD subjects. In **Error! Reference source not found.**, structural MRI and DTI was used to assess the cortical GM thickness and fractional anisotropy. Their analysis indicated that *RORA, NARG2*, and *ADAM10* influences GM thickness and WM-FA values. In **Error! Reference source not found.**, DTI-MRI and neurite orientation dispersion and density imaging (NODDI) with tract-based spatial statistics was used to investigate APOE ε4 modulation of WM damage in subjects with young onset AD. Interestingly, different WM changes in pre-symptomatic stages of AD were detected".

Table 1: ADNI-Based Radiogenomics Studies in Mild Cognitive Impairment and Alzheimer's disease

STUDY	GENETIC & IMAGING DATA	BIOSTATISICAL METHODS	DESCRIPTION/ KNOWLEDGE ADVANCEMENT
2010- **Error! Reference source not found.**	GWAS, sMRI	Regression analysis, Permutation test	SNP (rs10845840) located in GRIN2B gene, was significantly associated with the atrophy of both temporal lobes
2012- **Error! Reference source not found.**	GWAS, sMRI	Fixed-effects, Random-effects, Haplotype analysis	Intergenic variant rs7294919 associated with hippocampal volume, an HMGA2 locus rs10784502 associated with intracranial volume, and a suggestive association with total brain volume at rs10494373 within DDR2
2017- **Error! Reference source not found.**	GWAS, sMRI	Regression coefficients, Mixed-effects models, Quantile–Quantile plots	Four novel genome wide loci (rs11979341, rs7020341, rs2268894 and rs2289881) were associated with hippocampal volume
2016- **Error! Reference source not found.**	GWAS ,sMRI	Pearson correlation, Logistic regression, sRRR regression, T- test	Left entorhinal cortex average thickness, was associated with APOE variants, and SNPs such as re59776273, rs113814152, rs79079416 and rs147030865 are suggested for further analysis Left hippocampal volume was associated with APOE variant and rs293169 SNP
2016- **Error! Reference source not found.**	APOE, Cognitive evaluation, sMRI, FDG PET, AV45-PET	ANOVA, Chi-square test, *t*-tests	The combination of imaging, genetics and/or cognitive biomarkers better predicts MCI to AD conversion phenotype. This combination provided a 87% accuracy in the prediction of the disease compared to 76% of glucose PET as a single biomarker
2014- **Error! Reference source not found.**	Plasma proteins and sMRI	Parallel independent component analysis, Pearson correlation coefficients	This combination can provide a better prognosis and prediction of the disease. Specifically, VBM and TBM where combined with the changes in BMP6, Eselectin, MMP10 and NrCAM. In the classification of the disease a 93% sensitivity and 92% specificity was achieved. In the prediction from MCI to AD a 94% accuracy was reached
2016- **Error! Reference source**	Cognitive evaluation, sMRI, APOE and TOMM40, CSF, plasma	Receiver operating characteristic analysis	The combination of specific plasma markers and CSF only provided 80% accuracy, 88% sensitivity and 70% specificity in predicting progression from MCI to AD

not found.			
2012-**Error! Reference source not found.**[a]	APOE, Cognitive evaluation, PET, FDG PET, sMRI, CSF	Linear mixed effect models, Concordance correlation coefficient	Each biomarker follows a sigmoid shaped trajectory and is affected by interactions with age and APOE status
2016-**Error! Reference source not found.**	GWAS, sMRI, FDG-PET	Linear regression analysis, *t*-tests/ Chi-square tests with two-sided P-values	Gray matter density: No genetic influence in NC. In MCI subjects the SLC24A4/RIN3 rs10498633 and ZCWPW1 rs1476679 genes showed significant effects. Furthermore, ABCA7 rs3752246, EPHA1 rs11771145, and INPP5Drs35349669 genes were associated for AD patients.Brain metabolism: Significant associations were only seen in NC groups for SLC24A4/RIN3rs10498533, NME8 rs2718058, and CD2AP rs9349407 genes
2012-**Error! Reference source not found.**	APOE, sMRI	Logistic regression analysis, Independent-sample *t*-tests	In APOE ε4 carriers, the V and A alleles (I405V and C-629A) of the cholesteryl ester transfer protein gene were associated with greater baseline cortical thickness and less 12-month atrophy in the MTL
2014-**Error! Reference source not found.**[b]	Neuropsychological evaluation, APOE, β-amyloid (Ab) imaging	Linear regression analysis, Wilcoxon rank sum tests	There is a strong correlation between Aβ and APOE ε4 in cognitive decline. Greater cognitive decline was present in high Aβ/APOE ε4+ participants compared to all other groups (low Aβ/APOE ε4-, low Aβ/APOE e4+, and high Aβ/APOE e4-)
2018-**Error! Reference source not found.**[c]	Neuropsychological evaluation, APOE, β-amyloid (Ab) imaging	ANOVA	Memory decline in β-amyloid–positive adults may accelerate with older age and that this increase in acceleration may be associated with the APOE ε4 allele
2017-**Error! Reference source not found.**	APOE, sMRI, FDG-PET, CSF	Linear models or Logistic regression analysis	MTL atrophy was less severe in subjects who had a negative β-amyloid. This was correlated with the patient's disproportionately low APOE ε4 and disproportionately high APOE ε2 carrier prevalence
2018-**Error! Reference source not found.**	APOE, sMRI, β-amyloid (Ab) imaging	MCMC Bayesian & GB convergence analyses	APOE ε4 carriers had increased longitudinal accumulation of amyloid-β pathology and more atrophy in the area of MTL
2018-**Error! Reference source not found.**	APOE, β-amyloid (Ab) imaging	Polygenic risk scores	APOE ε4 linked to greater memory decline and hippocampal atrophy in Aβ+ subjects
2011-**Error! Reference source not found.**	APOE, FDG-PET	ANOVA and post-hoc two-sample *t*-tests	Longitudinal FDG-PET is associated with concurrent cognitive decline. AD subjects had higher frequency of the APOE ε4 allele gene compared to MCI and NC subjects
2014-**Error! Reference source not found.**	APOE, FDG-PET	Linear regression, Wald tests, *t*-test	APOE ε4 carriers had significant declines in FDG ratio
2009-**Error! Reference source not found.**	APOE, FDG-PET	*t*-test, Linear regression analysis	Lower CMRgl correlated with APOE ε4 allele where AD and amnestic MCI groups had higher proportion of subjects with one or two copies of the APOE ε4 allele
2012-**Error! Reference source not found.**	APOE, FDG PET- MRI	Univariate analyses	High APOE ε4 gene subjects were associated with lower CMRgl and lower GM volume
2011-**Error! Reference source**	GWAS, sMRI, DTI	Correlation analysis	A potentially significant association observed for the rs2456930 polymorphism reported as a significant GWAS finding in AD. RORA, NARG2, and ADAM10 influence GM thickness and WM-FA values

not found.			
2017-**Error! Reference source not found.**	APOE, sMRI (DTI and NODDY)	Fisher's exact test, *t*-test, Wilcoxon rank sum test	Subjects with the APOE ε4 gene had more widespread WM disturbance whereas in non ε4 allele carriers the disruption was more focal

[a]Database(s): ADRC: Mayo Alzheimer's Disease research center; MCSA: Mayo Clinic study of aging; AIBL: Australian Imaging, Biomarkers and Lifestyle; HABS: Harvard Aging Brain Study; ADNI: Alzheimer's Disease Neuroimaging Initiative; MCI: Mild Cognitive Impairment; AD: Alzheimer's disease; sMRI: structural MRI; VBM: Voxel Based Morphometry; TBM: Tensor Based Imaging; CSF: Cerebrospinal fluid; FDG-PET: Fluorodeoxy glucose- Positron Emission Tomography; AV45-PET (florbetapir); rs-fcMRI: resting state functional connectivity MRI; TOMM40: Translocase of Outer Mitochondrial Membrane 40 homolog; NODDI: Neurite Orientation Dispersion and Density Imaging; GWAS: Genome-wide Association Studies; ANOVA: Analysis of Variance; MCMC: Markov Chain Monte Carlo, GB: Gelman-Rubin convergence; sRRR: Bonferroni correction Row-sparse reduced-rank regression

2.11 Chapter main findings

1. The disease diagnosis still remains probable and only post mortem biopsy will identify it.
2. Clinical assessment and cognitive tests will reveal the disease after structural changes have occurred within the brain.
3. MTL is the region whereas the disease initiates and more specifically entorhinal cortex is the first region affected followed by the hippocampus, the amygdala and the parahippocampal gyrus.
4. Research relying on genome wide association studies (GWAS) and whole exome and whole genome sequencing data, have identified a significant number of genes that are correlated to AD.

3

Quantitative MRI in AD Detection

3.1 Abstract

This chapter represents a review of the literature where structural MRI quantitative methods used in the assessment of AD are presented. Most of the studies reviewed in this chapter, have been concentrating in the MTL of the brain where the disease initiates. Within MTL entorhinal cortex is affected in an earlier stage compared to hippocampus, however, the majority of the studies have been using hippocampus perhaps due to the fact that hippocampus is responsible for long-term memory. Furthermore, hippocampal measurements are more feasible due to hippocampus shape and size which allows its easier segmentation compared to other regions.

Additionally this chapter will discuss the advantages and disadvantages of the several MR quantitative methods used in AD and determine which method is better to be used in the several stages of the disease. Furthermore, it will evaluate the accuracy, sensitivity and specificity of these methods in the classification of NC from MCI and AD subjects and which one offers better prediction possibilities.

As structural changes in the early stages of the disease, initiate from the MTL and entorhinal cortex and hippocampus are the main ROIs used in the assessment of AD, this chapter will conclude which of the two ROIs is better to be used in the assessment of AD and in which stage.

This chapter concludes that in the earlier stages of the disease the entorhinal cortex is better to be used for both classification and prediction of AD. It was seen that the limited number of research articles that used texture analysis, had better results compared to other quantitative methods, probably because it detects subtle neurodegenerative changes better compared to the other methods. In the more advanced stages of the disease, where atrophy is more widely developed within MTL and the rest of the cortex, volume measurements could provide equal results to texture. Undoubtedly, entorhinal cortex is the region to be preferred when comes to the prediction of the disease. Although texture analysis seem to provide equal and even better results compare to other quantitative methods, there is lack of research regarding its use in the assessment of AD.

3.2 Introduction

Neuroimaging biomarkers have transformed the assessment of neurodegenerative diseases as they can detect structural changes before the manifestation of the clinical symptoms. Imaging biomarkers represent a non-invasive method to assess AD. Two main categories are currently being used: (1) molecular techniques, such as from PET, where metabolically changes within brain can be captured and (2) structural methods, such as from MRI, where structural changes of the brain cortex can be detected.

Although, nuclear medicine techniques are beyond the scope of this thesis, a brief review of these methods follows.

3.3 Molecular Neuroimaging in AD

PET is a sensitive neuroimaging technique were radionuclide isotopes are injected intravenous and according to the tracer used it allows the assessment of molecular biology and neuropathology of the disease. In contrast with MRI were structural changes are detected, PET imaging allows the *in vivo* assessment of brain function. In PET imaging, there are several radionuclide compounds that are currently used in AD in order to measure:

1. the metabolic and neurochemical processes of the brain such as FDG,
2. amyloid Aβ pathology imaging
3. Tau PET where cerebral tau burden is assessed.

3.4 ^{18}F-fluorodeoxyglucose (18F-FDG) PET

^{18}F-FDG PET was the most widely used tracer for measuring brain function of neuronal activity at the tissue level. Decreased uptake of ^{18}F-FDG and therefore, hypometabolism of the brain has been associated with AD and it follows a characteristic topographic pattern which affects the medial parietal and lateral temporoparietal cortex [39]. PET FDG captures this cerebral metabolic rates of glucose (CMRgIc) within the neurons and provides support to differential diagnosis. Therefore, ^{18}F-FDG PET has been included in the diagnostic criteria of AD [33]. Interestingly, MCI subjects revealed a pattern of hypometabolism in the posterior cingulate and hippocampus [40]. In other studies, hypometabolism in these areas was also found to predict subsequent clinical conversion to probable AD [41] though distinguishing MCI converters from non-converters has been less successful than structural MRI measurements [42].

3.5 PET amyloid imaging - 11C- PiB "Pittsburgh compound B"

Recent developments of molecular imaging have allowed, *in vivo*, amyloid deposits in the brain by using PET. 11C-PiB is the most commonly used *in vivo*

amyloid PET tracer [43] and a study by Nordberg et al., 2013 [44] showed that AD subjects had higher [^{11}C]PIB retention in the neocortical and subcortical brain regions compared to NC, where MCI subjects had intermediate retention (Figure 5). Interestingly, none of the MCI PIB-negative patients converted to AD, and thus PIB negativity had a 100% negative predictive value for progression to AD [44]. Furthermore, MCI ApoE ε4 carriers had also higher [11C]PIB retention compared to MCI ApoE ε4 non carriers [44]–[46]. However, due to amyloid deposition rate which is increased in the early signs of the disease and before any signs become more specific, it might be difficult to identify the disease severity. Jack et al., 2013 [47] revealed that some MCI cases reached a plateau, therefore, it has been suggested that amyloid rate might not be the most accurate method to be used in the prediction of conversion from MCI to AD. Furthermore, it is currently debated whether cognitively normal subjects with a positive amyloid-PET scan represent prodromal AD cases who will eventually develop AD dementia or rather will remain stable [48], [49].

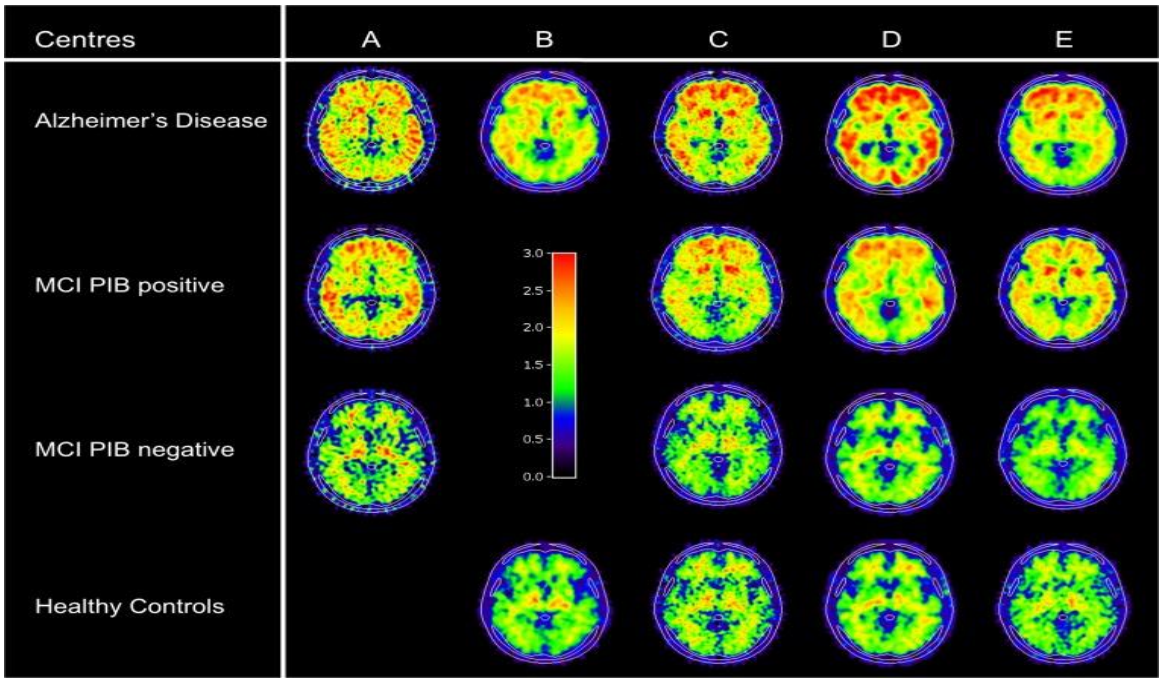

Figure 5: Representative PET scans of healthy controls, patients with MCI and patients with AD. Figure adapted from Nordberg et al., 2012.

Limitations of amyloid PET include the fact that it cannot distinguish specific AD syndromes [50], [51], as most studies show a non-specific pattern of amyloid burden distributed throughout the entire cortex across diseases [52], [53]. However, it was shown that it can give slightly better results from 18-FDG [54]. Perhaps, the most important limitation of amyloid PET is the fact that amyloid positivity dramatically increases with age in cognitively normal individuals and in non-AD subjects, especially after 70 years of age [55], [56].

3.6 Tau PET - tau PET agent (18)F-AV-1451

The Tau protein is predominantly found in brain cells, the neurons, and it has been associated with several brain diseases. In the case of AD is well known that due to abnormal tau protein, neurofibrillary tangles are accumulated and spread through the brain. In contrast with beta amyloid accumulation which is completed at an earlier stage (MCI?), tau accumulation continues throughout the disease progression. As these neurofibrillary tangles are spread they cause "dysfunction" of a structure called synapse, which allows the nerve cells to communicate together through electrical or chemical signals. Due to the fact that tau protein is constantly builds up with the disease progression, tau PET imaging could serve as an in vivo biomarker for the evaluation of AD-related tau pathology and monitoring disease progression [57]. Recent studies suggested that tau PET was able to recapitulate the neuropathological Braak staging [58], therefore, the introduction of tau-PET method has set new boundaries in the evaluation of AD, whereas amyloid PET remains controversial. However, there are several areas of criticisms regarding tau PET as well, which are beyond the scope of this research, therefore the reader is referred to [59], [60].

3.7 Structural Neuroimaging - MRI

MRI is a non- invasive imaging modality, which provides high spatial resolution images. This modality uses strong magnetic fields and radiofrequency (RF) pulses in order to produce the images in comparison with others techniques which use ionized radiation. Although the first MR images were acquired in 1976, MRI was approved for clinical use almost 10 years later [61]. MRI was mainly used to image anatomical changes due to cancerous tumors and neurological disorders such as brain atrophy related to Alzheimer's disease.

Due to its high spatial resolution (~1mm) and contrast between the tissues which derives through the various sequences such as T1-weighted imaging (WI), T2-WI, Fluid Attenuation Inversion Recovery (FLAIR) and others one can observe the different tissues within the brain. The gray matter (GM), also called *cortex*, is layer of 2-3mm thickness and corresponds to the synapses and neuronal cell bodies, neuropil, glial cells and capillaries. The white matter (WM) corresponds to the *myelinated axons* of the neurons and is found deep into the brain. Brain is surrounded by CSF which surrounds the brain and separates is from the skull (see Figure 6).

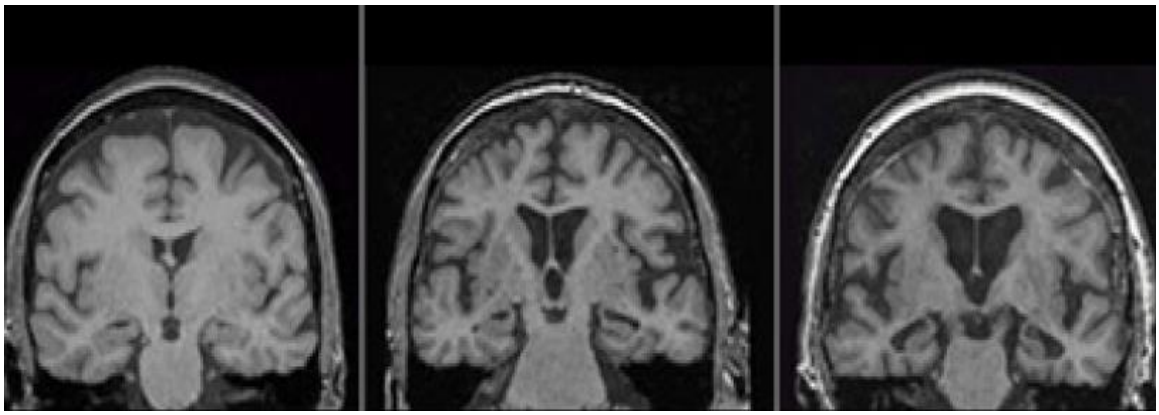

Figure 6: T1-WI image in coronal plane showing the GM, WM (light gray) and CSF (dark) between the skull and the brain in Normal, MCI and AD subject

Currently, in the literature, the pathophysiological process of AD initiates several years before the clinical symptoms arise and most of the literature is

searching for diagnostic imaging markers especially of those derived from quantitative T1-WI MRI. It represents a widely established method for regional and global brain volumes *in-vivo* and its importance in the assessment of AD was underlined by its inclusion in the new diagnostic criteria [33]. Structural MRI uses a no-ionizing radiation, which makes it suitable for longitudinal investigation. However, in the case of structural MRI, radiologists cannot perceive subtle changes of neurodegeneration with "naked" eye, and even if they could, they could never predict the conversion from MCI to AD.

A theoretical representation of the biomarker trajectories during different stages of AD pathogenesis can be seen in Figure 7 and Table 2. This illustration demonstrates that some markers may be more useful for detecting the pathological changes in AD during different stages of development. For instance, some markers may be useful for early diagnosis, whereas others may have more prognostic potential in tracking disease progression. Amyloid markers (CSF $A\beta_{(1-42)}$ and $A\beta$ PET) represent the earliest detectable changes in AD, but begin to plateau at the MCI stage. Functional and metabolic markers (FDG-PET measurements of hypometabolism and functional MRI methods) become abnormal at the MCI stage and progressively change well into the dementia stage. Changes on structural MRI become abnormal during the MCI stage, often following a temporal pattern of changes that correspond to tau pathology in the brain. Most extensively used measurements included hippocampal and entorhinal volume, as well as measurements of whole-brain atrophy.

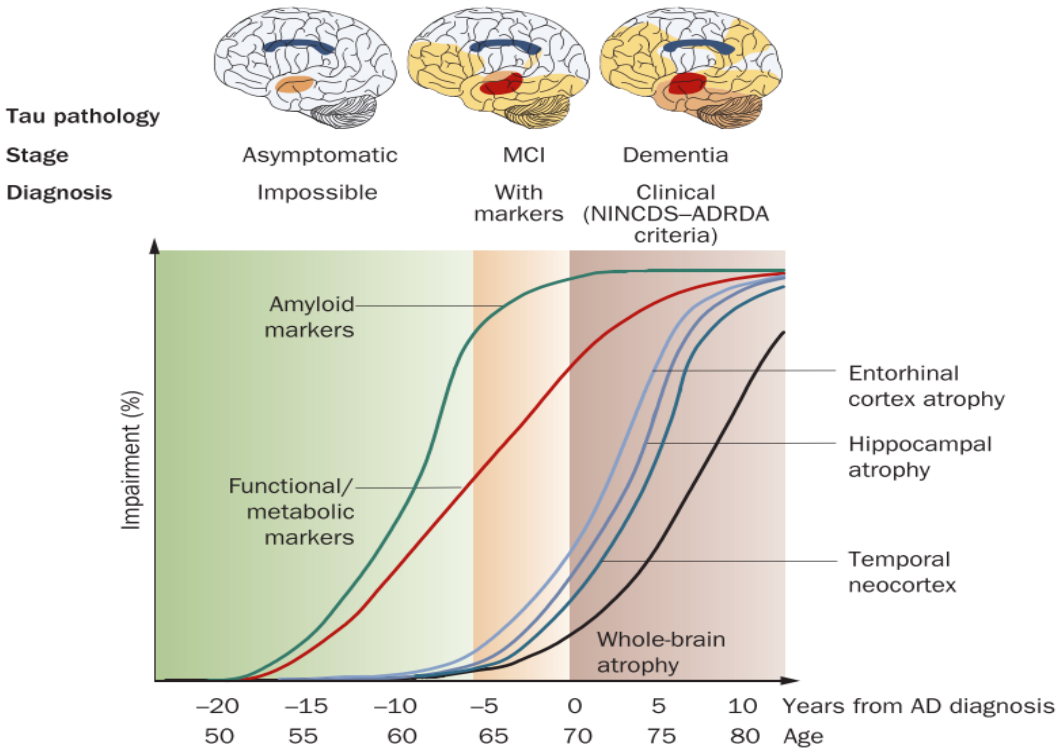

Figure 7: Dynamic biomarker trajectories of AD pathophysiology. Figure adapted from Frisoni et al [8]. Abbreviations: AD, Alzheimer's Disease; MCI, Mild Cognitive Impairment; NINCDS-ADRDA, National Institute of Neurological and Communicative Disorders and Stroke-Alzheimer's Disease and Related Disorders Association

Table 2: Overview of the different biomarkers based on the neuropathological changes in AD

Pathological change	Biomarker category	Biomarker(s)
Aβ deposition = early marker	Biochemical (CSF) Molecular imaging	CSF Aβ1-42 or Aβ1-42/Aβ1-40 PET with amyloid-specific probes
NFT formation	Biochemical (CSF)	CSF P-tau181
Neuronal injury = downstream	Biochemical (CSF)	CSF T-Tau 18F-FDG PET MTL atrophy on MRI

Abbreviations: Aβ amyloid-β, Aβ 1-42 β-amyloid peptide of 42 amino acids, CSF cerebrospinal fluid, FDG fluorodeoxyglucose, HCV hippocampal volume, MTL medial temporal lobe, MRI magnetic resonance imaging, PET positron emission tomography, P-tau 181 phosphorylated tau at threonine 181, SPECT single photon emission computed tomography, T-tau total tau protein. Table adapted from Niemantsverdriet, et al., 2017 [35].

MRI-derived biomarkers of AD are an active research area, which can reveal the cerebral atrophy and can be applied to measure *in-vivo* cortical changes.

The following section explores the several quantitative MR methods and advanced pattern analysis techniques used in the assessment of AD such as: i) VBM which describes global changes or atrophy of the deep cerebral structures, ii) volumetric measurements in specific ROIs, iii) cortical thickness measurements, iv) shape analysis and v) texture analysis. Volumetry remains the most popular technique to assess AD especially in the area of MTL [17], [62]–[64]. Apart from the MTL, other studies chose to assess the whole brain [65], [66], although the cortex is affected in later stage [5]. Furthermore, multimethod studies [67]–[69] combine biomarkers for the better understanding of the disease pathophysiology.

3.8 Quantitative MRI Brain Studies in Mild Cognitive Impairment and Alzheimer's disease: A Methodological Review

The following text is part of a journal paper (Quantitative MRI Brain Studies in Mild Cognitive Impairment and Alzheimer's disease: A Methodological Review) published in: 2018 IEEE Reviews in Biomedical Engineering - DOI: 10.1109/RBME.2018.2796598

3.8.1 Introduction

As a consequence of the AD, structural changes initiate within the MTL of the brain [22], a region which includes anatomically related structures that are essential for declarative memory [18]. Many post mortem studies [5], [14], [70] have implicated entorhinal cortex and the transentorhinal region as early sites of involvement in MCI and in AD subjects. It was shown that the degenerative process, initiates from the entorhinal cortex, followed by the hippocampus, the amygdala and the parahippocampal gyrus [17]–[19]. With the disease progression, these regions lose neuronal tissue with consequent brain atrophy [24].

A definite diagnosis of AD relies on histological confirmation at post-mortem biopsy [33] and brain inaccessibility has driven a search for diagnostic imaging

markers. Imaging, plays an important role in improving our understanding of AD, as it can provide an image of the brain of living patient which are affected by AD. Furthermore, imaging biomarkers, can be used for differential diagnosis due to the uncertainty of clinical tests in differentiating other subtypes of dementia such as FTLD [71], [72]. The entorhinal cortex and the hippocampus (Figure 8), are the two most common ROIs used in both in vivo and post-mortem investigations on the pathophysiology in AD. However, a visual qualitative assessment of MRI is not enough to estimate the rate of the tissue loss in the areas affected by the disease, and quantitative measures are essential for the assessment of the disease. Furthermore, the human eye cannot perceive the minimum degree of atrophy and without quantitative measurements, image evaluation is subjective. On the other hand, by using only MMSE tests, MCI, which represents a transitional period between normal ageing and clinical probable AD, cannot be easily identified through cognitive tests, mainly because these subjects do not have severe memory problems [33]. As the size of the MRI datasets increases and manual tracing is much more time consuming, Computer-Aided Diagnosis (CAD) systems can outline the areas of interest, usually by automated or semi-automated techniques, and can provide quantitative measurements.

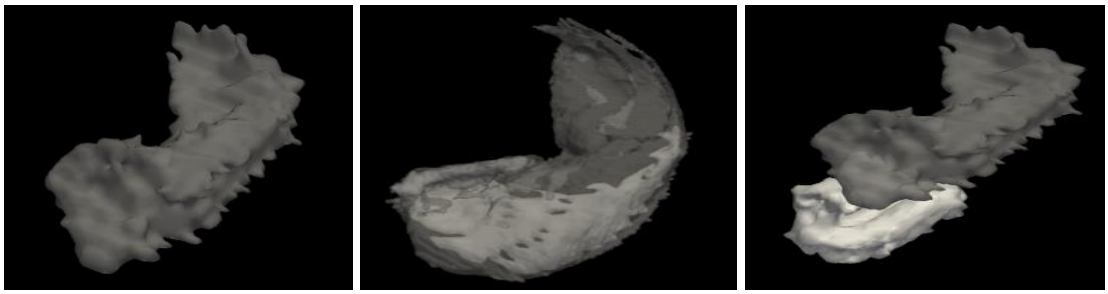

(a) (b) (c)

Figure 8: Hippocampus and entorhinal cortex. (a) The hippocampus. (b) The CA1 area within the hippocampus. (c) The entorhinal cortex with the hippocampus.

This review describes the overall results, including accuracy, specificity, and sensitivity of the image-processing methods that assess AD as observed in structural MRI. Additionally, it describes the effectiveness of these methods in

the prediction of conversion from MCI to AD. The rest of this review is organized as follows: Section 3.3 presents the CAD system pipeline and Section 3.4 the Classification methods. Sections 3.5 and 3.6 describes the use of CAD systems in the diagnosis and prognosis of the disease, respectively. Section 3.7 concludes which methods and structures are suggested for both diagnosis and prognosis of AD.

3.8.2 Computed-aided Diagnosis System Pipeline

The objective of CAD systems is to assist the radiologist in the interpretation of medical images as a supporting tool. Furthermore, CAD provide quantitative information for ROIs to produce accurate and complete pathology reports. In medical image analysis, the following steps: (i) image acquisition and pre-processing, (ii) ROI segmentation, (iii) feature extraction, (iv) classification and (v) interpretation, are usually carried out to provide quantitative measurements of biomedical images. Medical image analysis steps and techniques used for the development of CAD systems for the assessment of dementia, are analyzed in this section.

3.8.3 Datasets and Preprocessing

In AD research, many investigators obtain their data from online databases (Table 3). These databases provide researchers with study data to define the progression of AD. One of the most comprehensive databases is the ADNI database [38], an ongoing, longitudinal, multicenter study. The ADNI was launched in 2003 as a public-private partnership, led by Principal Investigator Michael W. Weiner, MD. The primary goal of ADNI has been to test whether serial MRI, PET, other biological markers, and clinical and neuropsychological assessment can be combined to measure the progression of MCI and early AD. The ADNI image processing pipeline includes post-acquisition correction of gradient warping (Gradwarp) [73], B1 non-uniformity correction [74]

depending on the scanner and coil type, and phantom based scaling correction [75]. For up-to-date information, see www.adni-info.org. Apart from ADNI, (see Table 3) the Australian Imaging Biomarker and Lifestyle flagship study of aging (AIBL) (http://aibl.csiro.au), has already enrolled 1100 participants and collected over 4.5 years' worth of longitudinal data. The Open Access Series of Imaging Studies (OASIS) [76] provides data to be used in the determination of diagnostic markers for the assessment of AD and the data are divided in 2 sets. The cross-sectional MRI data in young, middle aged, non-demented and demented older adults and the longitudinal MRI data in non-demented and demented older adults. AddNeuroMed [77] is a cross European, public/private consortium developed for AD biomarker discovery. It combines modalities and it uses animal models in biomarker research.

Furthermore, two large dementia challenges where research groups could test and compare their algorithms in the AD assessment are the CADDEMENTIA **[78]** (http://caddementia.grand-challenge.org) and the Alzheimer's Disease Bid Data (ADBD) DREAM challenge (http://dreamchallenges.org).

Table 3: Open Source Imaging Data for Aging

Name	Subjects	Data
Alzheimer's Disease Neuroimaging Initiative (ADNI) http://adni.loni.usc.edu/	483 NC, 300 eMCI, 300 lMCI, 550 MCI, 350 AD	Clinical and cognitive assessments, MRI, PET, Genetic, Biospecimen
Australian Imaging Biomarker and Lifestyle flagship (AIBL) https://aibl.csiro.au/	768 NC, 133 MCI, 211 AD	Clinical and cognitive assessments, MRI, PET, Biospecimen, Dietary/lifestyle assessment
Open Access Series of Imaging Studies (OASIS) http://www.oasis-brains.org/	73 NC, 14 ADc, 64 AD	MRI
AddNeuroMed https://consortiapedia.fastercures.org/consortia/anm/	232 NC, 225 MCI, 259 AD	Clinical and cognitive assessments, Blood, MRI

Abbreviations: NC: Normal Controls; eMCI: early Mild Cognitive Impairment; lMCI: Late Mild Cognitive Impairment; MCI: Mild Cognitive Impairment; AD: Alzheimer's disease; ADc: Subjects who converted to AD; MRI: Magnetic Resonance Imaging; PET: Positron Emission Tomography

3.8.4 Region of Interest / Segmentation

The role of segmentation in medical imaging is to separate an image into regions to study anatomical structures, to identify ROIs or to measure the volume of a tissue. For the automatic segmentation of gray matter (GM), white matter (WM) and CSF from MR images, three methodologies have been proposed: (i) statistical-based segmentation methods, (ii) learning-based segmentation methods and (iii) atlas-based segmentation methods. Atlas based segmentation methods are the most frequently used in medical image segmentation. In atlas-based segmentation, an intensity template is registered non-rigidly to a target image and the resulting transformation is used to propagate the tissue class or anatomical structure labels of the template into the space of the target image [79]. The study by Babalola et al. [80] compared atlas-based and model based segmentation techniques and was tested on 270 subjects. The two atlas-based methods, classifier fusion and labelling (CFL) and expectation-maximization segmentation (EMS) using a dynamic brain atlas, performed significantly better than the model based methods, profile active

appearance models and Bayesian appearance models (BAM). Factors that affect accuracy in multi-atlas segmentation are presented in [79].

Based on the aforementioned segmentation methods, several software "pipelined" image analysis packages for automated brain tissue segmentation have been developed (Table 4). These packages usually contain skull stripping, intensity non-uniformity correction and automated segmentation. FreeSurfer [Martinos Center for Biomedical Imaging, Harvard-MIT, Boston USA] [81] is an open source software suite for processing and analyzing brain MRI images. It represents one of the most commonly used software in image analysis and it segments MRI scans automatically using a Bayesian approach [82]. Morey et al. [83] compared automated segmentation methods and hand tracing of the hippocampus and it was shown that Freesurfer is preferable compared to FSL/FIRST [Functional MRI Brain - FMRIB Software Library, abbreviated as FSL - FMRIB Integrated Registration and Segmentation Tool, Oxford University, Oxford UK] [84]. The Statistical Parameter Mapping (SPM) software (Wellcome Trust Centre for Neuroimaging, Institute of Neurology, UCL, London UKis a freely available suite of MATLAB used for segmentation, normalization, registration, volume measurements and other useful image analysis steps.

The LONI Pipeline [85] is a graphical workflow environment which allows grid utilization and provides a significant library of computational tools. It was built to be used in complex neuroimaging analysis which requires deep knowledge about the input/output requirements of algorithms. The LONI Pipeline could be used to design, execute, validate, and deliver complex heterogeneous computational protocols.

Table 4: Selected Brain Segmentation Software Packages

Name	Description	Studies
FreeSurfer	Open source software suite for processing and analyzing (human) brain MRI images https://surfer.nmr.mgh.harvard.edu/	[67], [81], [83], [86], [86]–[90]
Statistical Parameter Mapping (SPM)	MATLAB software package implementing statistical methods for analysis of functional and structural neuroimaging http://www.fil.ion.ucl.ac.uk/spm/	[65], [91]–[100]
LONI Pipeline	Includes workflows that take advantage of all widely used tools available in neuroimaging, genomics, bioinformatics, etc. http://pipeline.loni.usc.edu/	[85], [87], [101]–[103]

3.8.5 Feature Extraction

Thus, through feature extraction it is possible to retrieve important data that can assist the characterization of a pathology. Feature extraction methodologies analyze objects or images to extract the most prominent features that are representative of the various classes of objects.

Table 5 lists selected methods that are currently used in the assessment of AD as described in [67], where these methods were compared. According to Cuingnet et al. [67], these approaches can be divided into three categories, depending on the type of features extracted from the MRI: (i) Voxel-based if the features derive from GM, WM or CSF, (ii) Vertex-based if the features derive from the cortical surface such as thickness measurements and (iii) ROI-based if the features are derived from ROIs. However, apart from the hippocampus, it should be noted that the entorhinal cortex is also a structure currently used by many studies for the assessment of AD. In this review, structural MRI features derived from Voxel Based Morphometry (VBM), cortical thickness, volume, shape and texture are described.

In the assessment of AD, VBM has the advantage examining the whole brain and not a particular structure. Specifically, it detects differences in the local composition between different brain tissue types such as GM and WM [104]. First, the brain images are segmented into their three main tissue components, GM, WM and CSF and then are spatially normalized to the same stereotactic

space. This allows different brains to be compared directly through a voxel-wise statistical analysis over the entire brain. For technical and methodological information about VBM the reader is referred to [105]. Nowadays, VBM is used to examine the whole volume of the brain and to detect differences or similarities in images for two populations [106]. Furthermore, it is also used to calculate cortical thickness changes on the entire cortex. A limitation of thickness measurements is that they cannot detect changes on subcortical structures such as WM or CSF therefore it is only used to detect the regional distribution of cortical atrophy. In general, some of the limitations of VBM include systematic registration errors during spatial normalization [107] and difficulties in detecting WM changes in T1 MRI sequences or pathologies that are not common in the majority of a population [108].

Volumetric techniques are used to measure the volume of a structure; however, a major weakness of volume analysis is that the thickness or shape of a structure might change before its volume. According to [109] global hippocampal volumetry might not be always sensitive enough to follow changes within a single population, which may reflect conversion from a healthy state or disease progression. In differential diagnosis, VBM showed higher accuracy from volume measurements, in the ability to differentiate AD from FTLD [71], [72].

Shape analysis, is used in digital geometric models of surfaces and/or volumes of objects-of-interest in order to detect similarities or differences between the objects [110]. It examines the shape of a structure which gives not only more sensitivity to follow the progression of the atrophy, but also allows its evaluation in different subfields. Among the many techniques [110] used to obtain shape features of the human brain, Corresponding Spherical Harmonic Description (SPHARM), deformation-based morphometry and deformable models are the methods mainly used, mainly due to alignment factors.

Texture is an indistinct concept often attributed to human perception of

variation of the colour/intensity of a surface, quantifying properties such as smoothness, coarseness and regularity. It could be argued that texture refers to the spatial and statistical relationship of pixel values in an ROI. The early stage of AD is associated with small-scale changes in terms of Neurofibrillary Tangles (NFT's) and amyloid-β (Aβ) plaque deposition [32]. According to Castellano et al. [111] these small-scale changes, are able to form certain textural patterns in MRI images recognizable by extracting texture descriptors from the image. In AD, texture analysis is less used than the other methods. However, the information provided by texture analysis cannot be visible through volume and shape properties [91], thus, it may have the advantage of detecting earlier, microscopic alterations [111]. Broadly, the approaches used to describe texture features in neuro MRI can be split into syntactic, statistical and spectral [112].

Statistical based approaches (Table 6), are mostly used and they represent the texture indirectly by non-deterministic properties that prescribe the distributions and relationships between grey levels of an image [112]. According to Kovalev et al. [113] 3D texture features contain more spatial information, higher sensitivity and specificity compared to 2D techniques. 3D texture features include the use of Law filters [114], Run Length Matrix (RLMs) [115], sub-band [116], [117], Gaussian-Markov Random Fields (GMRF) and a combination of co-occurrence matrices and Gabor filters [116]. For a review on 3D texture, the reader is referred to [118].

Table 5: Summary of Structural MRI Features Based on [67]

Category	Subcategory	Tissue	Description	Studies
Voxel based	Direct	GM GM+WM+CSF	Probability maps of voxels of the tissue directly as features in the classification	[92] [93]
	STAND-score	GM, WM, and CSF tissue probabilities	Selection steps and a sequence of feature aggregation is used to reduce dimensionality.	
	Atlas based	Mean tissue probabilities	Uses labelled atlas to group the voxels into anatomical regions	
	COMPARE	GM GM+WM+CSF	Creates homogeneously discriminative regions, in which the voxel values are aggregated to form the features of the classification	
Cortical Thickness	Direct	-	Consists cortical thickness values at every vertex directly as features	[92] [86], [119] [86]
	Atlas based	-	Vertices are grouped into anatomical regions using an atlas	
	ROI	Hippocampus, entorhinal cortex, supramarginal gyrus	Measures the cortical thickness in specific areas	
Volume and Shape	Hippocampus and Entorhinal cortex	-	Discriminative power of the hippocampus and entorhinal cortex only	[16], [39], [40], [49]– [53] [41], [54]– [56]

Abbreviations: STAND: Structural Abnormality Index; ROI: Region of Interest; GM: Gray Matter; WM: White Matter; CSF: Cerebrospinal Fluid

Table 6: Selected 2D Texture Features in the Evaluation of MCI and AD

Category	Subcategory	Tissue	Description	Features	Studies
Statistical	1st order gray-level	-	Contain information related to the gray-level distribution of an image.	Variance, Skewness, Kyrtosis, Mean, Gradient	[128]
	2nd order Co-occurrence matrix (GLCM)	Whole Brain, Hippocampus, Entorhinal cortex	Describe how often 2 pixels with different values appear in the field of view separated by a distance d in direction θ (0°, 45°, 90° and 135°)	Angular second moment, Contrast, Correlation, Sum of squares, Inverse different moment, Sum average, Sum variance, Sum entropy, Entropy, Difference variance, Information measures of correlation.	[9], [91], [129]– [135]
	2nd order Run-length matrix (RLM)	-	Contain information about spatial relationships between groups of pixels having similar gray level values.	Short runs emphasis, Long runs emphasis, Gray-level non-uniformity, Run-length non-uniformity, Run percentage	[130], [134]– [136]

3.8.6 Classification methods

Classification is used for the identification of patterns features of interest into the classes they belong. Moreover, machine-learning techniques have the potential to classify MR features without requiring a priori hypotheses from where this information may be coded in the images [137]. When classifiers are used, image samples are divided into two sets, training and testing [138]. The most popular statistical techniques used in CAD, include Discriminant Analysis (DA), Logistic Regression (LR), neural networks and Support Vector Machine (SVM). These techniques are presented in Table 7.

When the sample size is large, linear DA and LR have similar results, whereas in smaller samples DA performs better. Furthermore, DA is faster compared to LR. Regardless of the data distribution, LR performs well, and it should be used as the first choice to classify data [139]. On the other hand, DA is preferred when the variables are categorized and as long the assumptions are met. Furthermore, DA is preferred when the number of categories is big enough to let the estimated mean and variance be close to the population values of the continuous explanatory variables [139].

SVMs were developed by Vapnik [140] and they represent pattern recognition algorithms, based on training, testing and performance evaluation. Compared to DA which is a more generative method as it focuses on all data points whereas, SVMs are more discriminative as they concentrate on the points that are difficult to classify. They can be used when the data have an unknown distribution [141] and one of their strongest advantages is that they provide excellent results in pattern recognition and good generalization performance. Furthermore, they offer a possibility to train generalizable, nonlinear classifiers in high-dimensional spaces using a small training set [142].

Neural networks can be used as an alternative to LR. ANNs benefit from the availability of multiple training algorithms, they require less statistical training

and they perform well in predicting medical outcomes. Limitations of ANNs include computational load, restricted potential to unmistakably detect possible causal relationships and overfitting suffering [143].

Table 7: Classification Techniques Used in CAD MCI and AD Systems

Classifier	Description	Studies
Discriminant Analysis [142] [144]	Predict classification in a group based on continues variables	[62], [63], [86], [119], [121], [129], [145]
Logistic Regression [146]	It examines relationships between a categorical Y and a continuous X variable	[9], [147]
Neural Networks	Fit nonlinear models using nodes and layers. Could be very good predictors	[130]
Support Vector Machines [140], [148]	Supervised, multivariate learning methods used for classification, as well as regression	[66], [87], [91]–[93], [95], [96], [127]

3.8.7 Computer aided Systems for the Diagnosis of AD

Table 8 tabulates CAD systems for the classification of MCI and AD. Quantitative MRI studies tabulated below are based on amyloid, volume, thickness, shape and texture analysis that are described in the following subsections. For each study the main author, ROI, data type, number of subjects and classification accuracy, sensitivity, and specificity are given.

3.8.8 Quantitative MRI studies based on VBM

VBM describes global changes or atrophy of deep cerebral structures. Evans et al. [149] revealed a mean Standard Deviation (SD) whole brain loss at 1.5% per year in AD patients compared to 0.5% per year in NC. On the other hand, MCI subjects had an intermediate rate of 1.1% loss per year. Interestingly in this study it was noticed that MCI patients who converted to AD had brain atrophy twice more than the MCI patients who did not progress to AD.

Busatto et al. [150] used a fully automated VBM technique to evaluate GM abnormalities over the entire area of the temporal lobe in the classification of NC subjects from AD patients. Their results confirmed the findings of previous

ROI-based studies [17], [151], [152], where significant GM loss was detected bilaterally in the MTL region in AD patients. The entorhinal cortex was found to be the primary region where the neurodegenerative changes initiate in the earliest stages of AD.

Karas et al. [89] used VBM and apart from the earlier findings in the atrophy of the hippocampus, they demonstrated global reduced GM volume including the cerebellum, medial thalamus and head of the caudate nucleus as well of the cingulum, in AD patients. Their findings collated with the histopathological staging of Braak et al. [5], [153]. Another study by Karas et al. [154] analyzed the patterns of GM loss in order to examine what characterizes MCI and what determines the differences with AD by using VBM methods. Apart from quantifying the extent of GM loss between MCI subjects and AD patients, the authors wanted to investigate if the hippocampal volume still changes in patients who converted to AD. The results of the study showed that MCI patients had GM loss in the MTL area, where the parietal and cingulate cortices were areas more related to AD patients. Whitwell et al. [97] compared the pattern of GM loss in MCI patients who progressed to AD within a fixed time of period (18 months from baseline scan), with the subjects who remained stable. Compared to NC, the subjects that progressed to AD, had bilateral GM loss in specific regions of the brain. Interestingly, the non-progressed MCI patients had no areas of GM loss when compared to the NC. Thus, VBM method might not be the most sensitive technique for the classification of normal and MCI patients. However, when the two groups (stable and progressed MCI) were directly compared, the progressed group showed more GM atrophy.

Klöppel et al. [92] used a voxel based SVM approach to analyze the gray matter of NC and AD patients through modeling two different anatomical areas: in the first model they used data from the whole brain and on the second they

used data from a hippocampus-centered ROI. Their method reached an accuracy of 90% when evaluated on 20 NC and 20 AD subjects.

3.8.9 Quantitative MRI studies based on volume analysis

Several studies, used hippocampal volumetric measurements and confirmed that hippocampal atrophy, can constitute a useful diagnostic biomarker. The studies that used AD patients and NC from the ADNI database, reported that the hippocampal volumes were varying between 1600 mm^3 [155] and 3000 mm^3 [156]. According to the study by Schuff et al. [155], the hippocampal loss was accelerated by 26.5 ± 4.5 $mm^3/year^2$ in AD and 12.1 ± 3.2 $mm^3/year^2$ in MCI, equivalent to −1.6 ± 0.2%/$year^2$ and 0.6 ± 0.2%/$year^2$, respectively, relative to baseline volume.

One of the first studies where MRI was used to investigate if volumetric measurements in MTL could provide information for the classification of NC and AD patients took place in 1997, by Jack et al. [157]. Their study included 126 NC subjects and 94 probable AD patients, where they estimated volume measurements of hippocampus, parahippocampal gyrus, and the amygdala. Their results showed a parallel structure decline with increasing age in control subjects for both women and men and in each case MTL volume in AD patients was significantly smaller compared to NC subjects ($p<.001$). The MTL structure, which performed better for this classification, was the hippocampus. In 2001, Galton et al. [120] confirmed that hippocampal atrophy is a useful diagnostic biomarker and they showed that there was a 50% hippocampal atrophy in AD patients.

In [94], Colliot et al. used hippocampal volume to distinguish NC from MCI and AD patients. The technique used, was previously used by Chupin et al., [158], and it was fully automated where both the hippocampus and amygdala were segmented at the same time. The results of their study revealed significant

hippocampal volume reductions in all groups of patients. Specifically, there was a 32% volume reduction between AD and NC, a 19% reduction between MCI and NC and finally, a 15% reduction between AD and MCI.

Apart from hippocampus, other structures such as entorhinal cortex is used for the assessment of AD. However, because its controversial whether entorhinal cortex or hippocampus is more affected with the disease progression, the study by Juottonen et al. [121], used volumetric MRI on AD patients and NC subjects to investigate which of the two structures was more affected. Both structures had the ability to differentiate AD patients from NC subjects and no essential difference was found between the discriminative power of entorhinal cortex and hippocampal volumes. Specifically, the volume of entorhinal cortex in AD patients was 38% less on the right and 40% less on the left side, compared to NC subjects. Similar pattern of atrophy was noticed on the hippocampal volume where it was 33% less on the right and 35% less on the left side compared to NC subjects. Obviously, in the late states of the disease, both structures have similar atrophy rate.

According to Pennanen et al. [62] the appropriate ROI selection should depend on the classification group. Thus, they investigated which structures of the brain can be used to best classify the three different study groups. Their results showed that entorhinal cortex atrophy was more severe, in comparison with hippocampus volume, in MCI subjects, whereas in AD patients the hippocampal atrophy was more pronounced. Specifically, the best overall classification (66%) between MCI and NC subjects was achieved with entorhinal cortex, whereas the best overall classification (82%) between MCI and AD patients and between NC and AD patients (91%) was achieved with hippocampal volume. Similar to [121] the left hippocampal atrophy appear to be more severe for all the subjects.

3.8.10 Quantitative MRI studies based on thickness analysis

Desikan et al. [86] carried out automated structural measurements of entorhinal cortex and supramarginal gyrus thickness in order to differentiate MCI subjects and AD patients from normal patients. They used baseline volumetric scans from two independent cohorts where images obtained from the OASIS [76] and the ADNI database [159]. Hippocampal volume, entorhinal cortex and supramarginal gyrus thickness indicated an average Area Under Curve (AUC) of 0.91 in the training cohort and an AUC of 0.95 in the validation cohort. It should be mentioned that their results were comparable or even more accurate from nuclear medicine techniques such as Fluorodeoxyglucose (FDG)- PET [40], [160] or amyloid-binding PET studies [161], [162]. Furthermore, discrimination accuracy of MCI subjects in this study was comparable to one prior PET study utilizing a radioactive amyloid and tau protein tracer [162] and two MRI studies [63], [163].

Lerch et al. [145] used an automated method to measure the cortical thickness across the entire brain and detect differences between AD patients and NC. Cortical thickness was declined in many areas of the brain; however, the parahippocampal gyrus and the medial temporal lobes were the areas most affected. Similarly with other studies [62], [121] it was found that the left side of the brain was more severely affected. Therefore, according to this study, cortical atrophy in the early stages of AD is not related only with MTL but with limbic system, the lateral temporal lobes and cortex as well.

3.8.11 Quantitative MRI studies based on shape analysis

Gerardin et al. [96] used hippocampal shape features instead of volume analysis and specifically, SPHARM coefficients were used to model the hippocampal shape. Their results revealed that shape analysis can detect local atrophy on the hippocampus, before it starts losing volume. Therefore, this technique may be more sensitive and in particular at the MCI stage. Shape

analysis can be used to reveal atrophy on local and non-global areas of the hippocampus, and according to the authors, the classification accuracy between AD patients and NC subjects, was superior to studies that used volume analysis where classification accuracy was ranging from 80% to 90%. Furthermore, when MCI patients were involved in volume studies, the discriminative power was even lower, ranging from 60% to 74%. However, these results were reported in volume studies where manual and not automated segmentation was used.

Chetelat et al. [98] conducted a longitudinal study where MCI subjects were followed for 18 months. Their purpose was to project possible atrophy maps onto a 3D surface view of the hippocampus between MCI patients who converted or not to AD, compared to the profile of GM loss across normal aging. Their results showed that atrophy was more significant in converters than in non-converters, and this effect was more marked at follow-up. Interestingly, for both converters and non-converters the hippocampal atrophy was more evident on the superior-lateral part of the hippocampus, called CA1. Histopathological studies [164] also agreed that there was a relatively higher degree of atrophy in that specific hippocampal subfield. Similar results, were observed by Apostolova and colleagues [126]. On the other hand, GM loss with increasing age, was more severe on the inferior part of the hippocampus corresponding to the subiculum, something that was reported by Frisoni et al. [165] as well. Ferrarini et al. [127] used hippocampal shape-based markers in the CA1 region and by using SVMs on either one or both hippocampi, they discriminated AD patients from NC subjects with an overall accuracy of 90%, and stable MCI subjects from MCI converters with 80% accuracy.

3.8.12 Quantitative MRI studies based on texture analysis

Freeborough and Fox [129] used texture analysis for the classification of AD patients from NC. They extracted features by using GLCM for offset angles of 0^o, 45^o, 90^o, and 135^o. From each matrix, they derived 13 features and the mean and range of each feature over the four offset angles were completed. They indicated that texture analysis can reveal significant different values between NC and AD patients.

Zhang et al. [130] used 3D texture features to identify NC from AD patients. Over 100 texture features were extracted from spherical ROIs placed within the area of the hippocampus and the entorhinal cortex, using image histograms, gradients, co-occurrence matrices and RLM. To investigate the impact on the ROI selection, they placed 3D ROIs in three ways. The ROI that performed better included the regions of hippocampus and entorhinal cortex and part of CSF. The selection of a larger ROI which in this case included a part of the CSF, generated a higher classification accuracy. They achieved the highest accuracy mentioned in the literature, maybe due to the fact that they used severely affected AD subjects.

Oliveira et al. [131] applied texture analysis on MCI subjects. In their analysis, they choose to use the thalamus and calossal due to their anatomic heterogeneity which is more suitable for texture analysis. The analysis was carried out separately for the two ROIs using manual segmentation and the MaZda tool [166] to extract the features. According to the authors, this method was more reliable than other techniques [129], [167], [168], where the whole brain texture was analyzed. The objective of their study was to classify NC from amnestic MCI subjects and mild AD patients and through their analysis they revealed differences between the thalamus and corpus callosum which differentiated the two groups of subjects.

Simoes et al. [91] used a whole-brain approach by applying local statistical texture maps for the classification of MCI subjects from NC. Through SVM they achieved a mean accuracy of 87%. However, their sample was small (N=30). In the study by Sørensen et al. [9], the classification capabilities of hippocampal texture were evaluated using Receiver Operating Characteristic (ROC) curves with the corresponding AUC as performance measure. Texture analysis had an AUC of 0.912 in discriminating NC vs AD and 0.764 between NC vs MCI. For the same groups the AUC curves for volume analysis, were 0.909 and 0.784 respectively. To the best of our knowledge, this is the only study that evaluated if there is a correlation between texture and the volume of the hippocampus, in MCI subjects. Regarding prognosis, it was shown that hippocampal texture is superior rather than volume measurements with an AUC of 0.74 vs 0.67, respectively and their results were correlated with FDG-PET.

Table 8: Selected Quantitative MRI Studies in the Classification of MCI and AD Subjects

Study	ROI	Data type	Subjects	Classification	Acc.	Se.	Sp.
Klöppel et al. **[92]**	GM	VBM	20 NC, 20 AD	NC vs AD	90%	85%	95%
Colliot et al. **[94]**	Hip.	Volume	25 NC, 24 MCI, 25 AD	NC vs AD NC vs MCI MCI vs AD	84% 66% 82%	84% 66% 83%	84% 65% 83%
Juottonen et al. **[121]**	Hip. & Erc.	Volume	32 NC, 30 AD	NC vs AD	Hp.: 86% Erc.: 87%	80% 80%	91% 94%
Pennanen et al. **[62]**	Hip. & Erc.	Volume	48 AD, 65 MCI, 59 NC	NC vs AD NC vs MCI MCI vs AD	91% 66% 82%	88 % 66% 81%	93% 65% 83%
Desikan et al. **[86]**	Erc. Supramarginal gyrus	Thickness	49 NC, 48 MCI 94 NC, 57 MCI	NC vs AD	NA	74% 90%	94% 91%
Lerch et al. **[145]**	Entire cortex Parahippocampal Gyrus	Thickness	17 NC, 19 AD	NC vs AD	75% 94%	79% 94%	71% 95%
Gerardin et al. **[96]**	Hip.	Shape	23 NC, 23 MCI 25 AD	NC vs AD NC vs MCI	94% 83%	96% 83%	92% 84%
Ferrarini et al. **[127]**	Hip.	Shape	50 NC, 15 MCI-c, 15 MCI-non-c, 50 AD	NC vs AD MCI vs AD	90% 80%	92% 80%	NA NA
Freeborough and Fox **[129]**	Whole brain	Texture	40 NC, 24 AD	NC vs AD	91%	79%	100%
Zhang et al. **[130]**	Hip., Erc. & CSF	Texture	17 NC, 17 AD	NC vs AD	64% - 96%	NA	NA
Simoes et al. **[91]**	Whole brain	Statistical texture maps	15 NC, 15 MCI	NC vs MCI	87%	85%	95%

Abbreviations: Acc: Accuracy; Se: Sensitivity; Sp: Specificity; AUC: area under curve; NC: Normal Controls; MCI: Mild Cognitive Impairment; MCI-non-c: MCI non-converters; AD: Alzheimer's disease; GM: Gray matter; CSF: Cerebrospinal Fluid; Hip: Hippocampus; Erc: Entorhinal Cortex; VBM: Voxel Based Morphometry

3.8.13 Prediction of conversion from MCI to AD

Recently, the task of predicting conversion from MCI to AD has received a lot of attention, mainly because, nowadays, large multi-center studies, such as the ADNI, provide longitudinal data to the research community. The MCI term was first introduced in the literature by Reisberg et al. [169] in 1988 and two decades later, Farias et al. [31] showed that a 10%-15% rate of MCI subjects will progress to dementia. The biggest challenge in AD assessment is to predict if a patient will develop the disease. The identification of these patients is of great importance as they will be provided earlier with possible preventive pharmaceutical (or nonpharmaceutical) interventions. Currently, many studies investigate the prediction of the conversion from MCI to AD using feature sets similar to the ones used for the classification of subjects. A selection of these studies can be found in Table 9.

3.8.14 Prediction based on VBM

Davatzikos et al. [163] used high-dimensional image analysis and pattern classification methods, and proved that there was a subtle, distributed, structural pattern change in MCI subjects which could be identified and measured before clinical symptoms. Their analysis included a number of MTL structures, the cingulate and parts of the orbitofrontal cortex. Similar to [52] and [109] the CA1 area, appeared to be more affected and it showed more diagnostic accuracy from the total hippocampal volume. In contrast to [62], [121], [122] where lateralized hippocampal atrophy was mainly observed, the study by Davatzikos et al. [163] indicated bilateral hippocampal atrophy. When the results were cross-validated, the analysis showed a 90% predictive power. One more recent study by Davatzikos et al. [99] where VBM was used, a lower classification accuracy (56%) was achieved maybe due to the fact that the SVM was trained on NC and AD patients. In [66], Misra and colleagues used VBM analysis to evaluate the volume of WM and GM in 103 MCI subjects which they

were followed up for 15 months in order to predict which individuals will convert to AD. They evaluated their results via cross-validation and achieved a classification accuracy of 82%. However, the number of progressive MCI patients was low (N=27) thus, the results of this study are not directly comparable to other studies that used the ADNI image set. Plant et al. [65], used 3 different classifiers including SVM, Bayes, and voting feature intervals. When the anterior cingulate gyrus and orbitofrontal cortex were included in the measurements, the best predictive accuracy obtained was 75%. Duchesne et al. [170] used only MTL in their VBM analysis and their results were better compared to other studies (see Table 9) that used the whole brain.

Koikkalainen et al. [171] used Tensor-Based Morphometry (TBM) to classify stable from progressive MCI subjects. They selected ROIs using statistical maps of differences on their test set, and they achieved an overall accuracy of 72%. However, their results may be biased as the training and testing were not completely independent. Chetelat et al. [100] longitudinally assessed (for 18 months) the possible structural changes in MCI patients and then compared these changes between the non-converter and converter subjects. A fully automated VBM analysis was carried out and results were similar to the changes observed by other VBM studies such as [154]. Interestingly, (perhaps due to methodological issues) in contrast with most of the ROI volume studies, they did not detect any hippocampal volume differences between AD and MCI patients, suggesting a plateau has been reached.

3.8.15 Prediction based on volume analysis

Chupin et al. 2009 [95] used an automated segmentation technique of the hippocampus and amygdala and hippocampal volume was calculated to predict the conversion from MCI to AD. An overall classification accuracy of 64% was achieved, indicating that global hippocampal volume evaluation may

not be an accurate measure for prognosis, mainly due to the fact that hippocampal volume is variable in young and older adults, which in turn may have implications on the final results [172].

The study by Tapiola et al. [173] used MCI patients who were followed-up for 34 months to investigate the predictive value of different methods on conversion from MCI to AD. They used MRI-derived volumes of MTL structures, WM lesions, MMSE scores and APOE genotype. Interestingly, their results revealed that only MTL volume was able to predict the patients at high risk for developing the disease. Similar results were observed in the study by deToledo-Morrell et al. [147] where hippocampal and entorhinal cortex volumes were compared to determine which of the two regions could differentiate stable from progressive subjects. Twenty-seven MCI patients were followed after baseline diagnosis for 36 months and 10 of them converted to AD. The results showed that both hippocampus and entorhinal cortex could make the prediction, however, the entorhinal cortex was the best predictor with a rate of 93.5%. However, the study included a very small sample and judged it at high risk of bias for patient selection and index test. Sensitivity and specificity of entorhinal cortex were 0.50 and 1.00 respectively.

Killiany et al. [19] investigated the most frequent ROIs used in volume analysis for the assessment of AD, the hippocampus and the entorhinal cortex. Patients with mild AD at baseline were included as well. The measures between the two ROIs were different for each of the pairwise comparisons between the groups. The entorhinal cortex volume was able to differentiate the subjects that will probably develop the disease with an accuracy of 84%, whereas the hippocampal volume could not. The study suggested that more neuronal changes occur within the entorhinal cortex during the preclinical phase of AD, and as the disease spreads, atrophic changes develop within the hippocampus as well. Similarly to the study by Pennanen et al. [62] the hippocampal volume

loss in MCI subjects was 8% whereas in entorhinal cortex volume loss was almost double.

Devanand et al. [174] measured hippocampal and entorhinal cortex atrophy for the prediction of conversion from MCI to AD. In this large longitudinal study, 163 MCI patients and 63 NC subjects were followed for 5 years. Their results confirmed most of the findings of other studies that used smaller samples [19], [175] where hippocampal and entorhinal cortex had more atrophy in MCI converters to AD compared to NC and MCI non-converters. Specifically, entorhinal cortex volume in converters was 17% lower than in non-converters and 29% lower than in NC. For hippocampal volume, the percentages were 11% and 14% respectively. Interestingly, it was observed that when both regions were used together with cognitive scores, the prediction accuracy was improved to 87.7%. Both hippocampal and entorhinal cortex volumes, contributed to the prediction, however, the entorhinal cortex remained highly significant even after controlling for age and cognitive measures. On the other hand hippocampal volume correlated with cognitive measures and thus, less significant for prediction.

Killiany et al. [63] found that entorhinal cortex and superior temporal sulcus including the anterior cingulate gyrus (which is not yet known at which stage of the disease starts to involve), were the most useful regions for prediction of conversion to AD. These areas were used to determine if quantitative MRI measures at baseline could be used to determine whether subjects in the prodromal phase of the disease could be accurately identified before they develop AD. A discrimination accuracy of 93% between NC and the subjects with memory difficulty who eventually developed the disease was achieved. The discrimination accuracy of the subjects with memory difficulty who did not developed the disease, between the NC and the converters was 85% and

75% respectively. Entorhinal cortex and the superior temporal sulcus ROIs were the best discriminators when NC were included.

3.8.16 Prediction based on thickness analysis

Querbes et al. [119] used baseline normalized thickness index on a large sample of patients for the prediction of conversion from stable MCI to AD and compared it to the predictive values of the main cognitive scores at baseline. Their results showed that subtle structural changes could be detected and used to predict the outcome even 2 years before the clinical symptoms appear with a predictive value of 73%. This study, had the advantage of using a cross validation procedure. However, according to Eskildsen et al, [176] the results of the study, most likely show an overestimated accuracy as some subjects are used both for training and testing. Bakkour et al. [90] investigated the abnormalities of the cortex on patients with questionable AD and tried to detect which neocortical measures were better for early diagnosis and predictive power. A total of 49 questionable AD patients were longitudinally followed-up for 2.5 years and according to their results 20 patients converted to mild AD while 29 remained stable. The MTL cortical thickness achieved the best performance.

In a very similar study [176], patterns of cortical thickness measurements were used for the prediction of AD. It was observed that atrophy patterns differed with the disease progression, thus by learning these differences, the prediction accuracies could be improved. MCI subjects who had scans at 6, 12, 18, 24 and 36 months prior to the diagnosis of AD were selected from the ADNI database and they were grouped into time-homogenous groups of progressive MCI. Then, these patients where compared with MCI subjects who remained stable during their longitudinal study period. Interestingly, it was noted that even at 36 months prior to the AD diagnosis, the hippocampus could not be used for prediction of the disease. On the other hand, the entorhinal cortex was the area

affected first, followed by hippocampus. In other studies, such as [66], [68], [95], [99], [119], the baseline data for analysis were not homogeneous with respect to the "time to conversion", since the progressive MCI patients would convert anytime over the course of 6 months to 4 years follow-up. According to the authors, such heterogeneity may conceal the neurodegenerative processes that could be attributed to the different sub-stages of AD. For example, the pattern of atrophy could differ one year before diagnosis compared to the pattern two years earlier.

The study by Desikan et al. [177] identified MCI patients who converted to AD within two years after baseline with an overall accuracy of 91%. They used automated MRI-based software tools to compute measurements of MTL cortex thickness and volume on 64 ROIs among the two hemispheres of 324 MCI subjects. Furthermore, they compared their results with CSF samples and PET measures and remarkably, they showed that structural MRI could better predict the disease progression. In a comparable study by Vemuri et al. [178] where structural MRI and CSF biomarkers on 399 subjects were used, the results were similar. It was found that the Structural Abnormality Index (STAND) score [93], could predict with higher accuracy the time to conversion, compared to CSF.

3.8.17 Prediction based on shape analysis

Costafreda et al. [87] used an automated procedure to extract 3D hippocampal shape morphology. In their prediction model, only hippocampus was used which, achieved a predictive performance comparable or superior to other studies [65], [66], [170] that employed a multi-region or whole brain approach. This was similar to the accuracy achieved using other predictive models based on non-automated techniques. Similarly to [73] and [131], where morphometric pattern analysis was used, the results were significantly better from studies that

suggested that 3D shape analysis is better for the disease prognosis. Furthermore, this study and others [179]–[181] suggested that hippocampal head atrophy may be an early sign of risk and could be used to predict if a subject will develop the disease.

3.8.18 Multimethod studies

Cuingnet et al. [67] compared most of the aforementioned methods used for classification. They obtained data from the ADNI database and they used volume and shape analysis, VBM and cortical thickness methods to predict the conversion to AD. By using SVM they achieved predictive accuracies between 58%-71%. In a similar pattern, Wolz et al. [68] used baseline scans from the entire MCI population of the ADNI cohort. Several methods were used for prediction obtaining accuracies in the range of 56%-68%. When using the same subject groups with [67], they obtained better classification accuracies.

3.8.19 Prediction using texture features

Sørensen et al. [9], tried to detect the accumulated effects caused by NFTs and Aβ plaques, on the hippocampus as changes in the statistical properties of the images intensities. Furthermore, they tested the capability of hippocampal texture in the detection of early cognitive decline and whether texture analysis could reflect changes in hippocampal glucose metabolism in FDG-PET. Texture appeared to have higher but not significantly different AUC compared to hippocampal volume for the prediction of MCI to AD within 12 months. However, hippocampal texture was significantly better compared to volume, for the prediction of MCI to AD within 24 months, showing an AUC of $p=0.005$ and $p=0.002$ respectively. Interestingly, structural texture changes, correlated to a reduction of glucose metabolism and the function of the hippocampus.

Table 9: Selected Quantitative MRI Studies in the Prediction of Conversion from MCI to AD

Study	ROI	Data type	Follow-up (months)	Converters/Total MCI	Acc.	Se.	Sp.
Davatzikos et al. **[99]**	Whole brain	VBM	0-36	69/239	56%	95%	38%
Misra et al. **[66]**	Whole brain	VBM	0-36	27/103	82%	NA	NA
Plant et al. **[65]**	Whole brain	VBM	0-30	9/24	75%	56%	87%
Duchesne et al. **[170]**	MTL	VBM	0-28	11/31	81%	70%	100%
Koikkalainen et al. **[171]**	Whole brain	TBM	0-36	154/369	72%	77%	71%
Chupin et al. **[95]**	Hip. & Amygdale	Volume	0-18	76/210	64%	60%	65%
deToledo-Morrell et al. **[147]**	Hip. & Erc.	Volume	0-36	10/27	93%	NA	NA
Killiany et al. **[19]**	Erc.	Volume	0-36	13/73	84%	NA	NA
Devanand et al. **[174]**	Hip. & Erc.	Volume	0-36	37/139	88%	83%	NA
Killiany et al. **[63]**	Erc., STS	Volume	0-36	19/79	93%	95%	90%
Querbes et al. **[119]**	Cortex	Thickness	0-24	72/122	73%	75%	69%
Eskildsen et al. **[176]**	Cortex	Thickness	0-36	-	67%-76%	NA	NA
Bakkour et al. **[90]**	Cortex	Thickness	0-30	20/49	NA	83%	65%
Desikan et al. **[177]**	Neocortex	Thickness & Volume	0-36	TC: 60/162 VC: 58/162	AUC: 0.82 AUC: 0.84	74% 87%	84% 66%
Ferrarini et al. **[127]**	Hip.	Volume 3D Shape	0-33	15/30	73% 80%	63% 80%	77% 80%
Costafreda et al. **[87]**	Hip.	3D Shape	0-12	22/103	80%	77%	80%
Cuingnet et al. **[67]**	Whole brain	VBM	-	-	71%	77%	78%
-	Hip.	Atlas based	0-18	76/210	67%	62%	69%
-	Cortex	Thickness	-	-	70%	32%	91%
Wolz et al. **[68]**	Whole brain	TBM	-	-	64%	65%	62%
-	Whole brain	Manifold-based learning	-	-	65%	64%	66%
-	Hip.	Atlas based	0-48	167/405	65%	63%	67%
-	Cortex	Thickness	-	-	56%	63%	45%
-	Combination	Combination	-	-	68%	67%	69%
Sørensen et al. **[9]**	Hip.	Texture Texture & Volume	0-12 0-24	-	AUC: 0.74 AUC: 0.74	NA	NA

Abbreviations: ROI: Region of interest; MCI: Mild Cognitive Impairment; VBM: Voxel Based Morphometry; TBM: Tensor Based Morphometry; Acc: Accuracy; Se: Sensitivity; Sp: Specificity; MTL: Medial Temporal Lobe; Hip.: Hippocampus; Erc.: Entorhinal Cortex; STS: Superior Temporal Sulcus; TC: Training Cohort; VC: Validation Cohort; AUC: Area Under Curve

3.8.20 Results

Cerebral atrophy, as captured in structural MRI, is a promising biomarker in the assessment of early AD. Many studies [17], [62]–[64] proved that MTL is an area which showed atrophy even in the preclinical stage of the disease. Although hippocampal formation might be the most frequently used structure for the assessment of AD, the earlier involvement of the entorhinal cortex was proved by many studies [19], [120], [121], [147], [150], [173], [182].

The necessity of quantitative MRI image processing and visualization, derives from the fact that the human eye cannot perceive the subtle anatomical changes affecting the structures of the brain, thus it detects atrophy after the brain has already undergone irreversible synaptic loss. All the aforementioned studies agree that medical image analysis is essential in the assessment of AD and can be used either for classification between subjects or for the prediction of conversion from MCI to AD.

3.8.21 Classification of MCI and AD versus NC subjects

Comparison of Hippocampus and entorhinal cortex in NC versus AD group: Overall, it appears that both entorhinal cortex and hippocampal volume classification accuracy is comparable in distinguishing NC subjects from AD patients. Both structures have similar reduction in atrophy. Furthermore, for this group, whole brain approaches such as VBM and thickness, remained competitive with hippocampal-based approaches, due to the fact that in the advance stages, atrophy is more widespread.

Shape analysis also gave very good results, comparable to GM VBM for the classification between NC subjects and AD patients. However, the best classification accuracy (96.4%) for this group, was reported by Zhang et al. [130] for texture analysis.

Comparison of hippocampus and entorhinal cortex in NC versus MCI group: Both the hippocampus and entorhinal cortex can be used for the classification of patients between NC and MCI subjects. However, entorhinal cortex can provide better classification as it

deteriorates earlier than hippocampus which is consistent with many studies [5], [32], [70], [124], [173]. According to Gomez-Isla et al. [183] some entorhinal cortex layers can undergo 40% to 60% neuronal depopulation even in the earlier phase of AD. Indeed, the study by Pennanen et al. [62] revealed that the entorhinal cortex degenerated twice more rather than the hippocampus between NC and MCI. Thus, when AD patients are not included in the classification group, entorhinal cortex is the suggested structure to be used. All methods appear to have lower classification accuracy in this group of patients, because in MCI subjects the changes are difficult to be identified. Shape analysis appears to be a better technique compared to volume analysis, with similar results to voxel based methods. However, to the best of our knowledge, the best classification accuracy (87%) mentioned in the literature, between NC and MCI patients was achieved by Simoes et al. using texture features on the whole brain [91].

Comparison of Hippocampus and entorhinal cortex in MCI versus AD group: Both hippocampus and entorhinal cortex have the potential to discriminate MCI subjects from AD patients [123]. The study by Du et al. [62] suggested than the entorhinal cortex does not provide any further advantages for this classification. The study by Pennanen et al. [62] used hippocampal volume, but when they included entorhinal cortex to their model, the overall classification was not improved.

Shape analysis and voxel based morphometry studies appear to have similar results for the classification between AD patients from NC and MCI versus AD. It is suggested that in the advanced stages of the disease, the atrophy is more widespread, thus apart from ROI methods, whole-brain methods should be considered as well.

3.8.22 Prediction of conversion from MCI to AD

Most of the studies [19], [120], [121], [147], [150], [173], [182] have been using quantitative MRI measures within the area of MTL to determine if a subject will develop the disease and the results agree that entorhinal cortex is a better predictor compared to other structures such as

the hippocampus. The best discrimination accuracy between normal and patients with memory difficulty, who eventually developed the disease, was achieved by two volume studies of deToledo-Morrell [147] and Killiany et al. [63], with an overall predictive accuracy of 93.5% and 93% respectively.

In the prediction of progression of the disease, the highest accuracies were achieved when both entorhinal cortex and hippocampus were combined in the analysis. VBM methods and cortical thickness gave lower accuracy compared to the other methods, and, there is 'lack of research' regarding the use of texture analysis in the prediction of progression from MCI to AD.

3.8.23 Conclusion

In conclusion, entorhinal cortex can provide better results in the classification of NC from MCI subjects, as the atrophy is more severe compared to the hippocampus in the early stages of the disease. For the discrimination accuracy of AD patients from NC, and AD patients from MCI subjects, volumetric measurements of the hippocampus seem to be preferred mainly because entorhinal cortex is a very small region that is difficult to delineate when it is atrophied. Furthermore, image artifacts and/or anatomic ambiguities can obscure the boundaries of the entorhinal cortex. However, the hippocampus segmentation is more specific and it provides more robust and accurate results for these two groups. On the other hand, entorhinal cortex is a better predictor of conversion from MCI to AD.

3.9 Chapter main findings

1. *In-vivo* biomarkers derive from imaging such as from PET and structural MRI could detect neurodegenerative changes before the onset of the AD symptoms.
2. Volumetry represents the most frequently used method in the assessment of AD, however, atrophy represents a larger scale change and when it is detected it means that the disease has already affected the brain.

3. The entorhinal cortex is more affected by atrophy in MCI and AD subjects and it should be preferred for a better diagnosis of AD.

4. Although hippocampal formation is the most frequently used structure for the assessment of AD, the earlier involvement of the entorhinal cortex was proved by many studies, both *in-vitro* and *in-vivo*. Furthermore, it was seen that it is more affected by atrophy in MCI and AD subjects and it should be preferred for a better diagnosis of AD.

5. Texture analysis is not used as frequently as the other quantitative methods, however, this method could detect smaller scale changes within the tissue, before they become evident from other larger scale methods such as volumetry, and therefore it could provide an earlier diagnosis of the disease.

4

Materials and Pre-processing Methods

4.1 Introduction

This Chapter describes the database where the data for this research were obtained and all the pre-processing methods and tools used to prepare the final data. The ROIs used in the analysis of this research were chosen after a comprehensive literature review analysis. Two basic regions within MTL were chosen, hippocampus and entorhinal cortex due to their early involvement in AD. However, before the extraction of texture features, a volumetric analysis was made in the aforementioned ROIs in order evaluate if the data were consisted with other studies as well. The results of this analysis can be found below in section 4.2.

The description of the database used in this research is described in section 4.3 along with the patient inclusion criteria. Then, the MRI protocol is described in section 4.4 and the image pre-processing steps in section 4.5. In section 4.6, segmentation algorithm and volumetry is described and finally, the texture features extraction along with their equations in sections 4.7 and 4.8 respectively.

4.2 Structural changes within Medial Temporal Lobe

The following text is part of a conference paper (Hippocampal and Entorhinal cortex volume changes in Alzheimer's disease patients and Mild Cognitive Impairment Subjects) published in: 2018 IEEE EMBS International Conference on Biomedical & Health Informatics (BHI) - ***DOI:*** *10.1109/BHI.2018.8333412*

At the very early stage of the disease there is an inevitable progression of atrophy which initially affects the MTL [22] followed by progressive neocortical damage. The entorhinal cortex and hippocampus are two of the most common ROIs used in both *in vivo* and post mortem investigations for the detection of AD. *In vivo* structural MRI studies [18], [19], seems to agree with post mortem studies [14], [70], and indicate that the degenerative process, initiates from the entorhinal cortex, followed by hippocampus, amygdala and parahippocampal gyrus. With the disease progression, atrophy expands in temporal, parietal and frontal neocortices [184], [185] and as a consequent to the rest of the brain.

The objective of this study was to investigate how the volume of the hippocampus and entorhinal cortex ROIs, are affected in AD and MCI subjects.

4.2.1 MRI Acquisition and Participants

All the subjects had a standardized protocol on 1.5-T MRI units from Siemens Medical Solutions and General Electric Healthcare. MR protocols included high-resolution (typically 1.2×1.25×1.25 mm^3 voxels) volumetric T1-weighted, inversion recovery prepared, structural images obtained in sagittal plane. The data had undergone gradwarp-corrected for (i) distortion due to gradient non-linearity [73], and (ii) corrected for image intensity non-uniformity using N3 [186], and B1 non-uniformity [187] and (iii) scaling-corrected based on phantom measures.

Overall, 218 NC, 349 MCI and 165 AD subjects were included in this study. However, 74 MCI subjects converted within 48 months from their baseline scan to AD thus, MCI converters (MCIc) group was added to the analysis.

4.2.2 Measurements extraction

T1-weighted volumetric 3D sagittal magnetization prepared rapid gradient-echo (MPRAGE) scans were collected for each subject. Volume measures of the hippocampus and entorhinal

cortex were reconstructed using FreeSurfer v5.3 software, Martinos Center for Biomedical Imaging, Harvard-MIT, Boston USA [188]. Freesurfer is based on Surface-based Analysis (SBA) and derives morphometric measures from geometric models of the cortical surface. It uses a probabilistic atlas derived from a manually labeled training set of expert measurements and automatically performs subcortical and cortical segmentation of the brain.

Briefly, the Freesurfer surface-based pipeline stages include: (i) volume registration using MNI305 atlas [189], (ii) voxel intensity allocation and classification as White Matter (WM) or other tissue, (iii) separation of both hemispheres and exclusion of the cerebellum and brain stem, (iv) surface generation (for each hemisphere) by tiling the outside of the WM mass for that hemisphere, (v) this surface is refined to follow the intensity gradients between the WM and GM (this is referred to as the white surface) and (vi) white surface is nudged to follow the intensity gradients between the GM and CSF (pial surface) [190].

The Freesurfer subcortical-based pipeline consists of 5 stages which label subcortical tissues and calculates their volumes. These stages are: (i) affine registration with MNI305, (ii) initial volumetric labeling, (iii) intensity variation correction, (iv) dimensional nonlinear volumetric alignment to the MNI305 atlas, and (v) label atlas is built from a training set. For more details of Freesurfer streams, the reader is referred to [188], [191].

4.2.3 Results

Table 10 tabulates the volume differences between the hippocampus and the entorhinal cortex between the 3 groups (from their baseline scan) through ANOVA statistics. Although there was a difference on the data sample between the groups, all the parameters were assessed before the analysis and none of them was violated. STATA V14 was used and the level of significance was α=0.05.

Table 10: Volumes (mean) (SD)) of entorhinal cortex and hippocampus in baseline scans

Group	N	Left ERC (mm^3)	Right ERC (mm^3)	Left Hip. (mm^3)	Right Hip. (mm^3)
NC	218	1944 (367)	1935 (411)	3290 (435)	3323 (458)
MCI	349	1667 (457)*	1689 (455)*	2873 (501)*	2910 (526)*
AD	165	1437 (406)*†	1438 (441)*†	2549 (502)*	2598 (549)*†

Values in parentheses are SD NC=Normal cognition; MCI=mild cognitive impairment; AD=Alzheimer's disease;
* P<0.001 for MCI Vs NC, and AD Vs NC
† P<0.001 for AD Vs MCI

Table 11 illustrates the percentage of volume reduction of hippocampus and entorhinal cortex between the 3 groups from the baseline scans.

Table 11: Volume reduction (%) of entorhinal cortex and hippocampus between the 3 groups in baseline scans

Group	Left ERC (%)	Right ERC (%)	Left Hip. (%)	Right Hip (%)
AD Vs NC	-26.08*	-25.68*	-22.52*	-21.82*
MCI Vs NC	-14.25*	-12.71*	-12.69*	-12.45*
AD Vs MCI	-13.80*	-14.86*	-11.28*	-10.69*

Abbreviations: NC=Normal cognition; MCI=mild cognitive impairment; AD=Alzheimer's disease; ERC: Entorhinal cortex; Hip.: Hippocampus.
*p<0.05

Figure 9 shows the percentage changes of the mean volumes for the two regions for all subjects. According to Table 10 the mean left entorhinal cortex volume of all NC was 1944 (SD 367) mm^3 and 1936 (SD 411) mm^3 for the right. These values were significantly reduced for the MCI subjects, to 1667 (SD 457) mm^3 and 1689 (SD 455) mm^3 for left and right entorhinal cortex respectively. For the same groups, the hippocampal volumes were reduced from 3290 (SD 435) mm^3 and 3323 (458) mm^3 to 2873 (SD 501) mm^3 and 2910 (SD 526) mm^3 for the left and right hippocampus respectively.

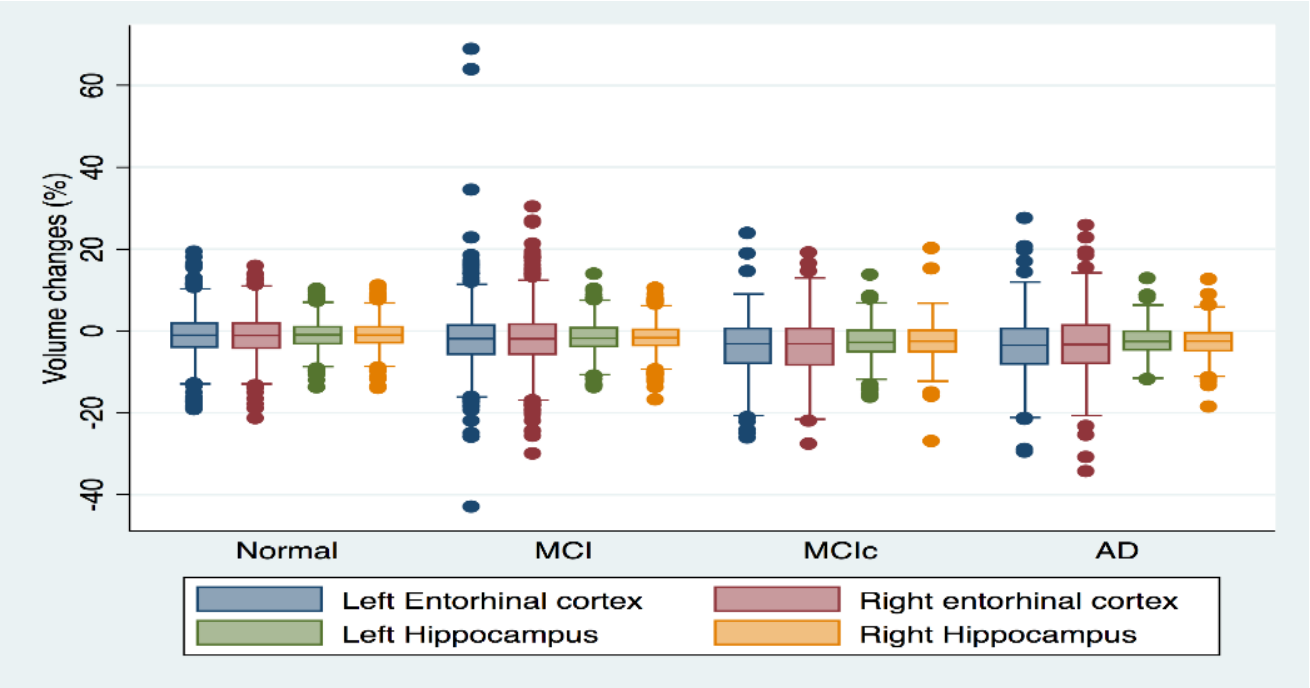

Figure 9: Hippocampal and entorhinal cortex volume changes, between the 4 groups.

Figure 10 represents the longitudinal volume changes between the two structures for the MCI and MCIc groups.

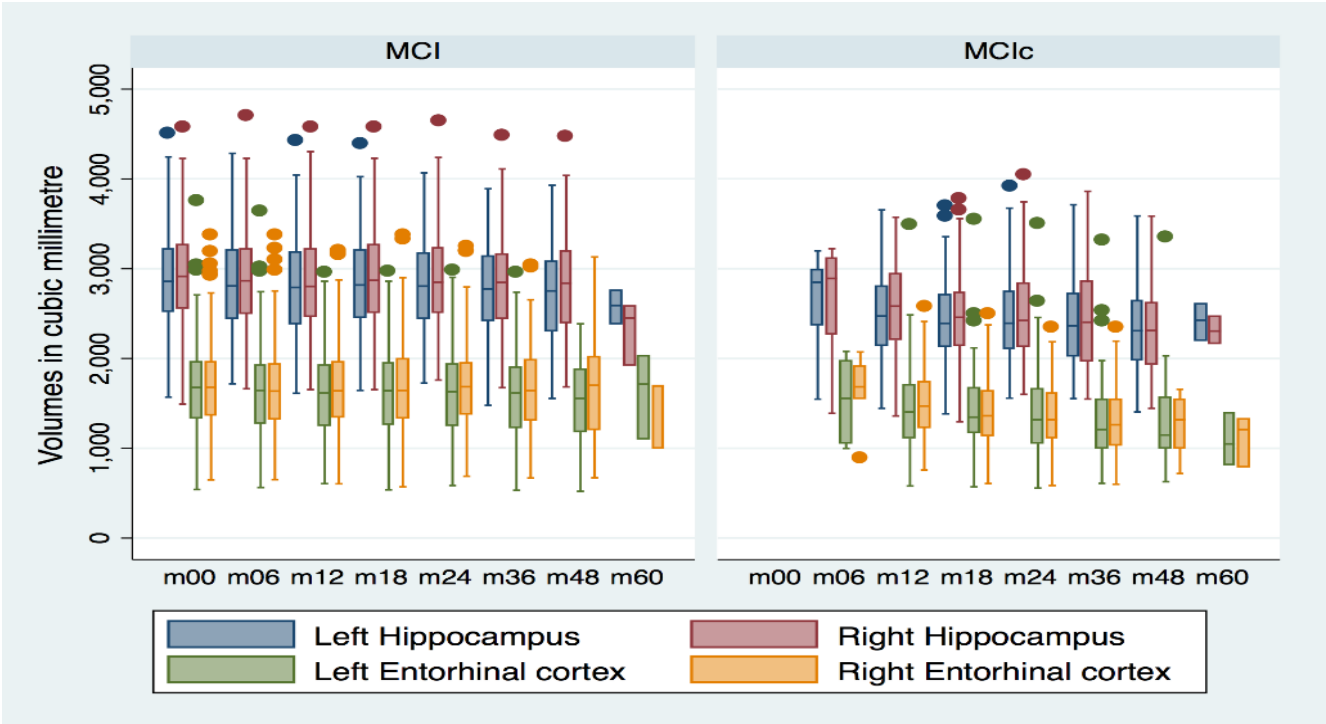

Figure 10: Hippocampal and entorhinal cortex volume changes between MCI and MCIc.

4.2.4 Discussion

From all the biomarkers used in AD, hippocampal atrophy as assessed on high-resolution T1-weighted MRI images is the best established and validated biomarker [152], [192]. Hippocampal measurements are more feasible due to hippocampus shape which allows easier segmentation and thus, it can be evaluated with more accuracy rather than other MTL structures such as entorhinal, perirhinal and parahippocampal cortices [8]. However, the earlier involvement of the entorhinal cortex was proved by many MR quantitative studies [28], [150], [173] and this was correlated with our results where entorhinal cortex was more affected by atrophy rather than the hippocampus.

Juottonen *et al*. [121], used volume measurements on both entorhinal cortex and the hippocampus in NC and AD subjects and both regions had similar results on the classification between NC and AD subjects. Both regions appear to have similar pattern of atrophy. Similar to our results, the entorhinal cortex was more affected rather than the hippocampus in AD patients, however, both structures had similar discriminative power.

Pennanen *et al*. [62] noticed that entorhinal cortex in MCI subjects was the region with the more severe volume loss providing an accuracy of 66% for the classification of NC from MCI subjects. On the other hand, the hippocampus appeared to be more affected in AD subjects which was not correlated with our findings were entorhinal cortex was found to be more affected by atrophy. More severe atrophy of the entorhinal cortex was also reported by Du *et al*. [193].

4.2.5 Study major findings

- Both entorhinal cortex and hippocampal volumes were significantly reduced in MCIc group compared to NC subjects.
- Compared to hippocampus, entorhinal cortex seems to be the region with the more severe volume loss in MCI converters and AD subjects.

- The atrophy rate between entorhinal cortex and hippocampus was correlated for both MCI and MCIc groups.
- Entorhinal cortex was more affected in the MCIc group and it should be preferred more for the disease prognosis.

In conclusion, the entorhinal cortex is more affected by atrophy in MCI and AD subjects and it should be preferred for a better diagnosis of AD. Furthermore, the more severe involvement of the entorhinal cortex could provide a more accurate prediction of the disease.

4.3 The ADNI Database

In the 1990s, the development of structural and functional imaging as provided by MRI and FDG PET respectively, have led to the expansion of knowledge regarding the AD. Many studies after the development of these diagnostic modalities were assessing how the atrophy of medial, basal and lateral temporal lobe and medial parietal cortex as seen in structural MRI could lead to the diagnosis of AD. Other researches were using PET imaging in order to evaluate the deposition of brain Aβ protein or the decreased ^{18}F-FDG uptake in temporo-parietal cortex [194]. Furthermore, many studies were concentrated in biological fluids such as, the cerebrospinal and the changes on its proteins, Aβ and tau [195]. All that knowledge obtained by the many researchers and the methods used for the assessment of the disease led to confusion especially when the methods were compared. That led to the need for the development of a large ongoing, longitudinal, multicenter study in which all these methods and results could be included and compared. A cohort with that concept, could link all these data for further analysis and unite the general scientific community around the globe; to develop technical standards for imaging in longitudinal studies; to determine the optimum methods for acquiring and analysing images; to validate imaging and biomarker data by correlating these with concurrent psychometric and clinical assessments; and to improve methods for clinical trials in MCI and AD [186].

Michael W. Weiner, M.D., Medical Centre and University of California, was the principal investigator for the initiation of a large cohort and in 2005, called the Alzheimer's disease Neuroimaging Initiative (ADNI). The ADNI database (www. http://adni.loni.usc.edu/) was launched by the National Institute on Aging (NIA), the National Institute of Biomedical Imaging and Bioengineering (NIBIB), the Food and Drug Administration (FDA), private pharmaceutical companies and non-profit organizations. The primary goal of ADNI was to recruit NC, MCI and AD subjects to test whether structural MRI, 18F-FDG PET, and other biological markers such as urine, serum and CSF, as well as clinical and neuropsychological assessment can be combined to measure the progression of MCI and early AD. However, to be useful from a clinical point of view, an imaging marker should be effective across sites and scanners. Therefore, the evaluation of this marker should be performed on data acquired over a range of sites and scanners. The ADNI has made such multi-site data publicly available, and thus has enabled the comparison of predictive accuracy of different methods under similar circumstances [196].

4.3.1 The ADNI Standardized datasets: ADNI-1, ADNI-GO and ADNI-2

With numerous researchers working with the same data from the ADNI database, there is the potential for direct comparisons of the various endpoints of brain structures as well as the algorithms and preprocessing steps used to extract these structural measures. To ensure these comparisons are meaningful, ADNI defined standardized datasets that multiple researchers can use for making methodological comparisons, thereby mitigating the risk that some of the observed differences in algorithm performance are an artifact of the use of different input data. In order to ensure meaningful methodological comparisons of structural MRI endpoints, the ADNI MRI-Core [197] recommended that all researchers should be using only image data that have passed the quality control assessments conducted at the Aging and Dementia Imaging

Research Laboratory at the Mayo Clinic (see [186] and http://adni.loni.usc.edu/methods/mri-analysis/adni-standardized-data/).

ADNI-1 launched in 2005 and consists of approximately 200 NC individuals to be followed for 3 years, 400 MCI subjects to be followed for 3 years, and 200 AD patients to be followed for 2 years. All the subjects were scanned with 1.5 T MRI at each time points and half of them with also be scanned with FDG PET. Subjects not assigned to the PET arm of the study were eligible for 3T MRI scanning. Apart from the MR imaging data, ADNI-1 was also consisted of fluid biomarkers such as CSF which was collected from half of the patients. Sampling varied by clinical group: Healthy NC were sampled at 0, 6, 12, 24, and 36 months, subjects with MCI were sampled at 0, 6, 12, 18, 24, and 36 months and AD subjects were sampled at 0, 6, 12, and 24 months [186].

In 2009, toward the end of ADNI-1 study, ADNI-GO (GO stands "Grand Opportunity", a type of stimulus grant from the NIH) was secured in order to continue the original ADNI-1 study for 2 more years with both longitudinal studies of the existing cohort and the enrolment of a new cohort. Specifically, 200 early MCI (eMCI) patients were included to investigate how the biomarkers are related to the early stage of MCI. In ADNI-GO, imaging was performed at 3T using the same sequence (MP-RAGE) and parameters as in ADNI 1. Furthermore, new modalities such as Functional MRI (fMRI) and MR sequences (FLAIR, T2*GRE, DTI) were added into ADNI-GO cohort.

In September 2011, ADNI-2 launched and included the existing ADNI-1 and ADNI-GO cohort plus, 150 elderly controls, 100 eMCI, 150 MCI and 150 AD patients and lasted for 5 years. Scanning protocols for newly enrolled subjects, in both ADNI-GO and ADNI-2 were identical and ADNI-2 exams were acquired exclusively at 3T MRI scanners [186], [197], [198] . ADNI-3 began in 2016 and was done exclusively on 3T scanners. Between 1070-2000 participants were enrolled: approximately 700-800 rollover participants from ADNI2 and 370-1200 newly

enrolled subjects. Clinical, cognitive, imaging, biomarker and genetic characteristics were assessed across three cohorts: Cognitively normal, MCI and mild AD dementia. In addition to all biomarkers used in ADNI 2, in ADNI 3 the researcher is also provided with londitudinal tau PET scans with AV 1451, amyloid PET using Florbetaben, CSF amyloid and tau using a new immunoassay platform, MR 3D ASL perfusion and biology approaches to understand better AD genetics.

4.3.2 Patient inclusion criteria

According to the ADNI inclusion criteria, enrolled subjects were all between 55 and 90 years of age and spoke either English or Spanish. Each subject was willing, able to perform all test procedures described in the protocol and had a study partner able to provide an independent evaluation of functioning. Inclusion criteria for CN were: MMSE scores between 24 and 30; CDR [4] of zero; absence of depression, MCI and dementia. Inclusion criteria for MCI were: MMSE scores between 24 and 30; CDR of 0.5; objective memory loss, measured by education adjusted scores on Wechsler Memory Scale Logical Memory II [199]absence of significant levels of impairment in other cognitive domains; absence of dementia. Inclusion criteria for AD were: MMSE scores between 20-26; CDR of 0.5 or 1.0; NINCDS/ADRDA criteria for probable AD [33], [200]. Detailed description of inclusion/exclusion criteria can be found in the ADNI protocol (https://adni.loni.usc.edu/wp-content/uploads/2017/09/ADNI_D_Procedures_Manual_2.15.17.pdf)

All subjects selected for this study were from standardized data collections (http://adni.loni.usc.edu/methods/mri-tool/mri-analysis/) and specifically from the ADNI-1 Complete 2 and 3 year 1.5 Tesla datasets. All data acquired as part of this study are publicly available (http://adni.loni.usc.edu/). Enrolled subjects were all between 55 and 90 years of age and each subject was willing, able to perform all test procedures described in the protocol and had a study partner able to provide an independent evaluation of functioning.

4.3.3 Cognitive measures

All subjects underwent through clinical and cognitive assessment at the time of baseline scan to determine their diagnosis. Inclusion criteria for NC were: MMSE scores between 24 and 30; CDR of zero; absence of depression, MCI and dementia. Inclusion criteria for MCI were: MMSE scores between 24 and 30; CDR of 0.5; objective memory loss, measured by education adjusted scores on Wechsler Memory Scale Logical Memory II [199], absence of significant levels of impairment in other cognitive domains and absence of dementia. Inclusion criteria for AD were: MMSE scores between 20 and 26; CDR of 0.5 or 1.0; National Institute of Neurological and Communicative Disorders and Stroke and the Alzheimer's Disease and Related Disorders Association (NINCDS/ADRDA) criteria for probable AD [33], [200]. Definitive autopsy-based diagnosis of AD was not possible and detailed description of inclusion/exclusion criteria can be found in the ADNI protocol (http://adni.loni.usc.edu/methods/documents/).

4.4 MRI Protocol

In 2004, the MRI Core and external advisors, met together in order to choose the final protocol to be used for the execution phase of ADNI. The evaluation group selected the 3D MP-RAGE sequence acquired by 1.5T scanners (General Electric Healthcare, Philips Medical Systems or Siemens Medical Solutions) at multiple sites from the ADNI website. The sequence was repeated back-to-back in ADNI-1 to increase the likelihood of acquiring at least one good quality MPRAGE scan and to permit signal averaging if desired. The whole brain was covered without image wrap using voxel size of $1mm^3$ with a maximum of 1.5mm in any one direction. The T1-weighted MP-RAGE sequence provides a high tissue contrast and as a consequence it enables accurate structural neuroimaging analysis. Compared to other sequences, MP-RAGE sequence was found to be of better quality with superior gray/white contrast to noise.

The range of parameters of the sequence were TR = 2400ms, TI = 1000ms, TE = 3.5ms, flip angle = 8°, field of view = 240 × 240mm and 160 sagittal 1.2mm-thick-slices and a 192 × 192 matrix

yielding a voxel resolution of 1.25 × 1.25 × 1.2 mm^3, or 180 sagittal 1.2mm-thick-slices with a 256 × 256 matrix yielding a voxel resolution of 0.94 × 0.94 × 1.2 mm^3 [186].

The ADNI MR protocol fulfills a number of principles that were selected by scientists in the field of MR imaging in order to minimize research burden for the scientists participating in ADNI. The final format of the protocol that was used in the execution phase of ADNI-1 dataset is consisted of:

1. A standard pre-scan and scouting procedure recommended by the manufacturer
2. A sagittal 3D MP-RAGE
3. A sagittal 3D MP-RAGE repeat
4. A sagittal B1-calibration scan (phased array)
5. A sagittal B1-calibration scan (body coil)
6. An axial proton density T2 dual contrast FSE/TSE.

For the implementation of this research, only MP-RAGE sequence was used. Regarding sequences 4 and 5, they are used to correct for B1-intensity variation of the phased array receiver coil. These steps will be described in the Pre-processing section among with the measurements used to monitor the scanner's performance over time. All the subjects had a standardized protocol on 1.5-T MRI units from Siemens Medical Solutions and General Electric Healthcare. MR protocols included high-resolution (typically 1.25×1.25×1.25 mm^3 voxels) T1-weighted volumetric 3D sagittal MPRAGE scans. MRI data acquisition techniques were standardized across different sites according to ADNI protocol (http://adni.loni.usc.edu/methods/documents/mri-protocols/).

4.5 Image Pre-processing

For the implementation of this thesis raw unprocessed 1.5 T T1-weighted MRI images derived from the MP-RAGE sequence were downloaded from the standardized datasets (http://adni.loni.usc.edu/methods/mri-analysis/adni-standardized-data/) of the ADNI

database. MRI scans were kept in raw data form so we have control of what is happening to the data.

4.5.1 Image normalization and inhomogeneity correction

According to Materka, 2004 [201], some of the higher-order texture parameters, especially those derived from the co-occurrence matrix, show correlation to first-order parameters, such as the mean intensity and variance. Therefore, in order to avoid this unwanted phenomenon, prior to feature extraction, image normalization was performed on all images using Freesurfer in two steps, before and after skull stripping.

Correction of non-uniformity artifacts in MRI is recommended as a preprocessing step [202]. A problem that occurs in quantitative texture analysis of MRI is that there are intra-scan and inter-scan image intensity variations due to the MRI instrumentation, therefore, image intensity normalization methods should be applied prior to further image analysis. These (inhomogeneity artifacts), often appear in MRI and they interfere with texture analysis and as a result lead to errors in tissue description. As a result, prior to texture analysis, image spatial non-uniformity was performed as an image preprocessing step to reduce those errors. This step is part of the Freesurfer pipeline (description below in section 4.6.1 and in Figure 11) which conforms the MRI scans to 1 x 1 x 1 mm^3 resolution and corrects image intensity using the non-parametric non-uniform intensity normalization (N3) algorithm [74] which is the most popular method found in texture literature [203], [204].

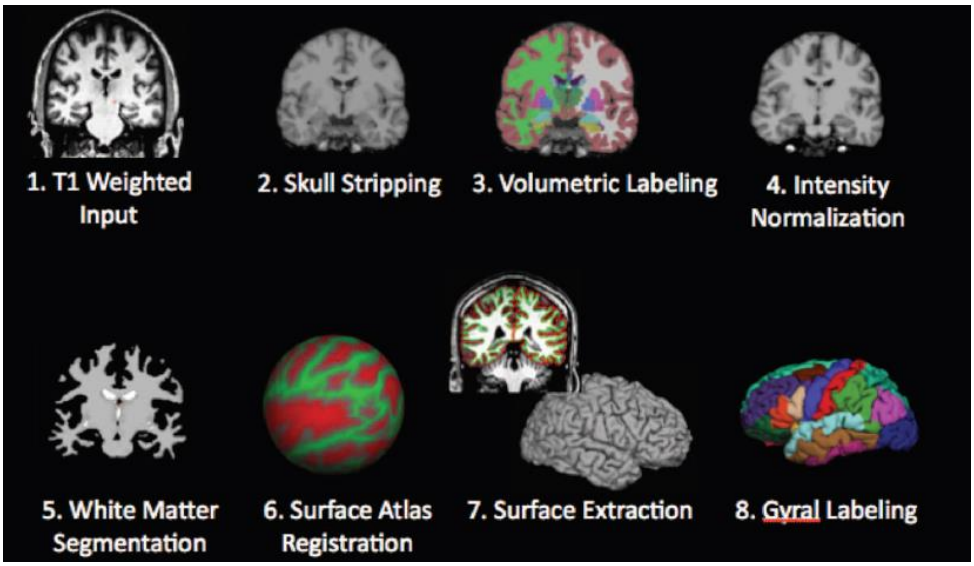

Figure 11: Processing stream overview of the FreeSurfer recon-all function. Image adapted from [205]

4.6 Segmentation algorithm and Volumetry

ROI segmentation was performed using the Freesurfer v6.0 image analysis suite (Massachusetts General Hospital, Boston, MA), which is documented and freely available for download online (https://surfer.nmr.mgh.harvard.edu/) for the study of cortical and subcortical anatomy. Nowadays, Freesurfer is the most commonly used software in quantitative neuroimaging and represents an automated technique which provides segmentation by assigning a neuroanatomical label to each voxel in the MR image volume. A probabilistic atlas is used to produce segmentations with a Bayesian inference algorithm from a manually labelled training set. This probabilistic algorithm can also be used to define curvature information of the cerebral cortex into gyri-based neuroanatomical regions that represent standard measures of cortical thickness and surface area.

4.6.1 The T1-freesurfer-cross-sectional pipeline

The pipeline used in Freesurfer, (http://www.clinica.run/doc/Pipelines/T1_FreeSurfer/), is a wrapper of different tools and the technical details of these procedures were described in prior publications [73], [188], [190], [191], [206], [206]–[212]. The Freesurfer pipeline, conforms the MRI scans to an isotropic voxel size of 1 mm^3, and the MRI intensity was normalized using the

automated N3 algorithm [74] followed by skull stripping and neck removal. Details of these have been discussed in previous publications [188], [191].

In brief, this multistep pipeline includes motion correction, automated Talairach transformation, first normalization of voxel intensities, removal of the skull, linear volumetric registration, intensity normalization [74], nonlinear volumetric registration, volumetric labeling, second normalization of voxel intensities and white matter segmentation. Output includes segmentation and volumes of the most important subcortical structures (see Table 12) and extraction of cortical surfaces, cortical thickness (in mm) estimation and volume (in mm^3), spatial normalization onto the FreeSurfer surface template (FsAverage), and parcellation of cortical regions. FreeSurfer morphometric procedures have been demonstrated to show good test-retest reliability across scanner manufacturers and across field strengths [212], [213]. Cy-Tera supercomputer of the Cyprus Institute was used to run FreeSurfer as each subject required approximately 13 hours of processing.

Table 12: Freesurfer subcortical structures

Lateral ventricle	Putamen	Corpus callosum, posterior part	4th ventricle
Inferior part of the lateral ventricle	Pallidum	Corpus callosum, middle posterior part	5th ventricle (CSF sometimes found in the septum pellucidum)
Cerebellum white matter	Hippocampus	Corpus callosum, central part	Brain stem
Cerebellum cortex	Entorhinal cortex	Corpus callosum, middle anterior part	CSF, White Matter, Gray Matter
Thalamus	Amygdala	Corpus callosum, anterior part	Choroid plexus
Caudate	Accumbens	3rd ventricle	Ventral diencephalon

4.7 Texture feature extraction

Figure 14, shows a schematic view of the proposed texture working hypothesis in AD. NFTs inside the neurons and Aβ plaques between neurons spread throughout the brain, causing neuronal death. Changes in the statistical properties of the image intensities due to the accumulated effect of NFTs and/or Aβ plaques may be reflected as certain textural patterns prior to atrophy.

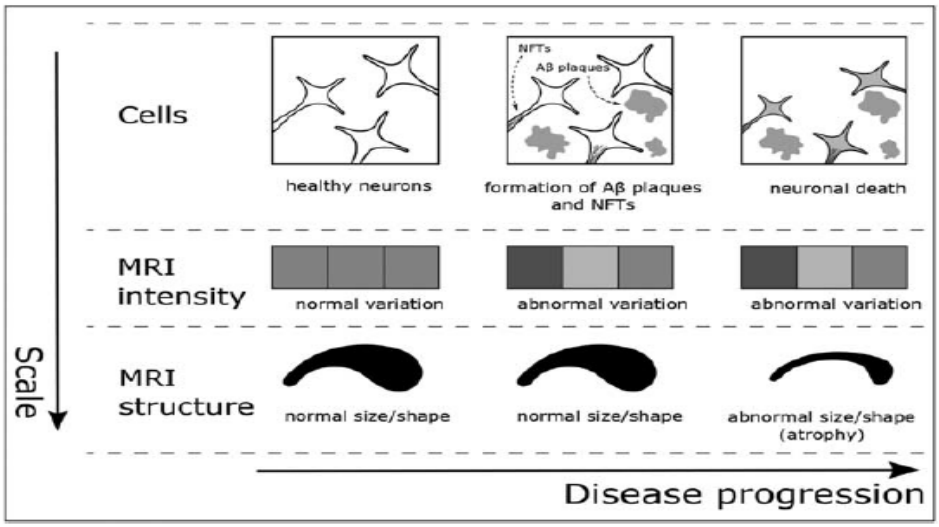

Figure 12: Schematic view of the proposed texture working hypothesis in AD. Image adapted from Cai et al., [214].

Texture features used in this thesis were extracted using GLCM texture method, a way of extracting second order statistical texture features from gray-level images. Texture features were calculated using KNIME Analytics platform [215]. The following Haralick texture features [216] were computed: Angular Second Moment (ASM), Contrast, Corelation, Variance, Sum Average, Sum Variance, Entropy and Cluster shade and their average in four directions (0°, 45°, 90°, 135°) was used (see Figure 13) and the separation distance between pixels was set to 1. This distance was chosen to reflect the degree of correlation between adjacent pixels short range neighborhood connectivity, mainly because the ROIs used were very small (see Figure 13 a, b).

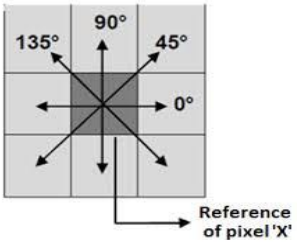

Figure 13: Directionality of GLCM

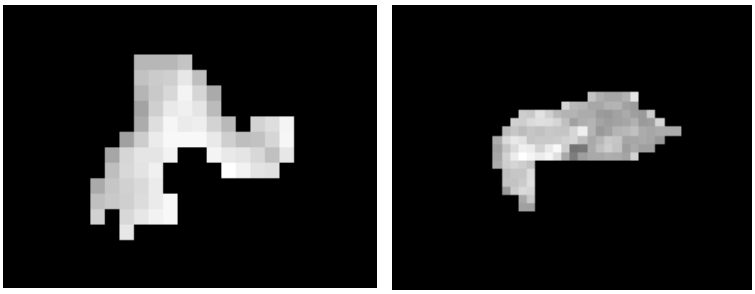

Figure 14 a, b: Entorhinal cortex (a) and the hippocampus (b) in 2D images. Entorhinal cortex measures approximately 14x13 pixels and hippocampus 21x10 pixels

4.7.1 GLCM Texture Features

According to [217] GLCM is a matrix where the number of rows and columns is equal to the number of quantized gray levels, Ng, in the image. The matrix element $p(i, j)$ is the set of second order statistical probability values for changes between gray level i and j at a particular displacement distance (d) and angle (θ). To illustrate this method, suppose an image to be analyzed has Nx columns and Ny rows. The gray level appearing at each pixel is quantized to Ng levels. Let $L_x = \{1, 2, \ldots, N_x\}$ be the columns, $L_y = \{1, 2, \ldots, N_y\}$ be the rows, and $G_x = \{0, 1, \ldots, N_g - 1\}$ be the set of Ng quantized gray levels. The image can be represented as a function that assigns some gray level in G to each pixel or pair of coordinates in $L_y \times L_x$; $L_y \times L_x \rightarrow G$. The texture-context information is specified by the matrix of a relative frequency $C(i, j)$. $C(i, j)$ represents the number of occurrences of gray levels i and j within the window, at a certain (d, θ) pair. The probability measure can be defined as

$$Pro(x) = \{p(i, j) \mid (d, \theta)\},$$

where $p(i, j)$ is defined as

$$p(i,j) = \frac{\mathrm{C(i,\ j)}}{\sum_{i=0}^{Ng-1} \sum_{j=0}^{Ng-1} C(i,j)}$$

The sum in the denominator thus represents the total number of gray level pairs (i, j) within the window and is bounded by an upper limit of $N_g \times N_g$.

The means for the columns and rows of the matrix are, respectively, defined as:

$$u_x = \sum_{i=0}^{N_g-1} \sum_{j=0}^{N_g-1} i.p(i,j)$$

$$u_y = \sum_{i=0}^{N_g-1} \sum_{j=0}^{N_g-1} j.p(i,j)$$

The standard deviations for the columns and rows of the matrix are, respectively, defined as:

$$\sigma_x = \sum_{i=0}^{Ng-1} \sum_{j=0}^{Ng-1} (i-u_x)^2.p(i,j)$$

$$\sigma_y = \sum_{i=0}^{Ng-1} \sum_{j=0}^{Ng-1} (j-u_y)^2.p(i,j)$$

4.7.2 Texture features description

Specifically, in this study, eight textural features were used to quantitatively evaluate textural characteristics of the entorhinal cortex and hippocampus. Most of these features were describe also by Cal et al [214] and can be seen in Table 13.

Angular Second Moment (ASM)

Also known as Uniformity or Energy and measures uniformity of pixel intensity relationships within a region of interest. ASM is high when image has very good uniformity or when pixels are very similar.

$$ASM = \sum_{i=0}^{N_g-1} \sum_{j=0}^{N_g-1} p(i,j)^2$$

Contrast

Contrast measures the quantity of local variations within pixel intensity relationships within an image. If there is a large amount of variation in an image, the contrast will be high.

$$Con = \sum_{k=0}^{N_g-1} k^2 \left\{ \sum_{i=0}^{N_g-1} \sum_{j=0}^{N_g-1} p(i,j) || i-j| = k \right\}$$

Correlation

Correlation measures a potential connection between a pixel and its local neighborhood of pixels, reflecting the image gray level correlation. It indicates local gray-level dependency on the texture image; higher values can be obtained for similar gray-level regions.

$$Cor = \frac{\sum_{i=0}^{N_g-1}\sum_{j=0}^{N_g-1}(ij).p(i,j) - u_x u_y}{\sigma_x \sigma_y}$$

Variance

Variance puts relatively high weights on the elements that differ from the average value of *p (i, j)*. It refers to the gray-level variability of the pixel pairs and is a measurement of heterogeneity. Variance increases when the gray-scale values differ from their means. Unlike contrast, variance has no spatial frequency.

$$Var = \sum_{i=0}^{N_g-1}\sum_{j=0}^{N_g-1}(i-u_x)^2.\ p\,(i,j) + \sum_{i=0}^{N_g-1}\sum_{j=0}^{N_g-1}\left(i-u_y\right)^2.\ p\,(i,j)$$

Sum Variance

Sum average is the variance of normalized grey-tone image and it measures the dispersion (with regard to the mean) of the gray level sum distribution of the image

$$Sum\ Variance = \left[\sum_{\boldsymbol{i=0}}^{\boldsymbol{2N_g-2}} \boldsymbol{i^2 p_{x+y}(i)}\right] - Sum\ Average^2$$

Sum Average

Sum Average is the average of normalized grey-tone image and it measures the mean of the gray level sum distribution of the image.

$$Sum\ Average = \sum_{\boldsymbol{i=0}}^{\boldsymbol{2N_g-2}} \boldsymbol{i\, p_{x+y}\,(i)}$$

Entropy

Entropy measures disorder of pixel intensity relationships within a region of interest. Entropy is the highest when all the probabilities *p(i, j)* are equal, and smaller when the entries in p(i, j)

are unequal. Therefore, a homogeneous image will result in a lower entropy value, while an inhomogeneous (heterogeneous) region will result in a higher entropy value.

$$Ent = -\sum_{i=0}^{N_g-1}\sum_{j=0}^{N_g-1} p(i,j)\log(p(i,j))$$

Cluster shade

Cluster shade is a measure asymmetry in gray-level values. A new "$i + j$" image is created, having a range of integer intensities from 0 to 2 ($N_g - 1$). The u_i + j value is computed and stored for the first neighborhood of the image, and is subsequently updated as the neighborhood is moved by one pixel. When the cluster shade is high, the image is asymmetric.

$$Cluster\ Shade = -\sum_{i=0}^{N_g-1}\sum_{j=0}^{N_g-1} (i + j - u_x - u_y)^3 (p(i,j)$$

Table 13: Gray-level Co-occurrence Matrix Texture Features. Table adapted by Cai et al [214].

GLCM Feature	Qualitative Description
Entropy GLCM	Measures disorder of pixel intensity relationships within a region of interest
Energy GLCM	Measures uniformity of pixel intensity relationships within a region of interest
Contrast	Measures the quantity of local variations within pixel intensity relationships within an image
Correlation	Measures a potential connection between a pixel and its local neighborhood of pixels, reflecting the image gray level correlation
Inverse different moment	Measures the smoothness (homogeneity) of the gray level distribution of the image
Homogeneity	Measure the closeness of distribution in the co-occurrence matrix to the matrix diagonal
Cluster shade	Measure asymmetry in gray-level values

Abbreviations: GLCM: Gray-level Co-Occurrence Matrix.

4.8 Texture feature examples and texture variability

Table 14 tabulates the mean (SD) entorhinal cortex volume and texture features computed for all MRI slides for one subject for each subject category (also illustrated in Figure 16 and Figure 17). As expected, there is a volume reduction between the subjects due to atrophy progression. Higher ASM values were seen for AD subjects and higher values in an image represent pixels with similar values. Indeed, in AD subjects the variation of pixel values is less compared to NC (see Figures 18 and 20). Higher contrast values was also seen for AD subjects and this was also seen on their images (Figure 20). On the other hand, an image with high correlation

represents similar pixel values and as it can be seen in Figure 18, NC subjects had more regions with similar grey levels compared to AD. Sum average and variance seem to be similar between the subjects, whereas, sum variance is higher for NC subjects. Entropy, show information content of an image and higher values, represent more homogeneity. As it can be seen in Table 14, NC subjects have greater values, thus, similar degree of pixel intensity. This is also illustrated in Figure 18.

The mean differences and the statistically significant differences between the groups for the aforementioned texture features and volume, can be found in Table 24 (Chapter 6).

Table 14: Examples of entorhinal cortex measures for one NC, one MCI, one MCIc and one AD subjects. Feature values (Mean ±SD) are given for volume, ASM, contrast, correlation, sum average, entropy, variance and cluster shade.

	NC	MCI	MCIc	AD
Volume (mm^3)	1930 (284)	1720 (384)	1544 (338)	1417 (348)
Correlation	0.51 (0.038)	0.49 (0.046)	0.48 (0.047)	0.46 (0.047)
Contrast	217 (19.2)	224.6 (23.7)	232.0 (24.6)	241.2 (23.3)
Sum Variance	672.3 (33)	660 (37)	657.8 (34)	644.6 (39)
Entropy	3.0 (0.192)	2.94 (0.21)	2.88 (1.18)	2.86 (0.20)
Sum Average	30.8 (3.2)	30.2 (3.2)	29.4 (3.0)	29.3 (3.2)
Variance	222.5 (9.5)	221.4 (9.6)	222.4 (10.3)	222.3 (10.7)
Cluster shade	13136 (9746)	15510 (9314)	10910 (6935)	12127 (8682)
ASM	0.214 (0.045)	0.224 (0.048)	0.231 (0.041)	0.230 (0.049)

In order to identify the most important features, random forests (RF) models with 5000 trees were built to measure the mean Decrease Gini index. Gini Index [218] is an impurity splitting method. It was observed that feature selection based on the Gini index increases the overall performance of the RF models [219]. The 9 most promising features between NC and AD subjects are shown in Figure 15. However, in this study the usefulness of rule extraction in the assessment of AD using decision trees (DT) and RF algorithms for the entorhinal cortex was not investigated. In Figure 15, the decrease Gini index for entorhinal cortex texture features is lower compared to volume, however, the inclusion of MCI subjects could provide different results and this will be study comprehensively in the continuation of this research.

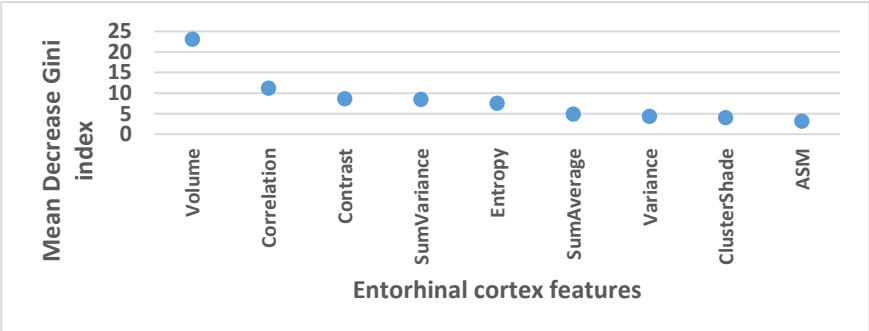

Figure 15: The 9 most promising features.

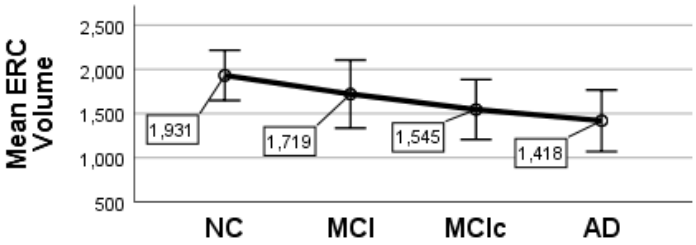

Figure 16: Entorhinal cortex volume (mm³) changes (mean ±SD) between subjects.

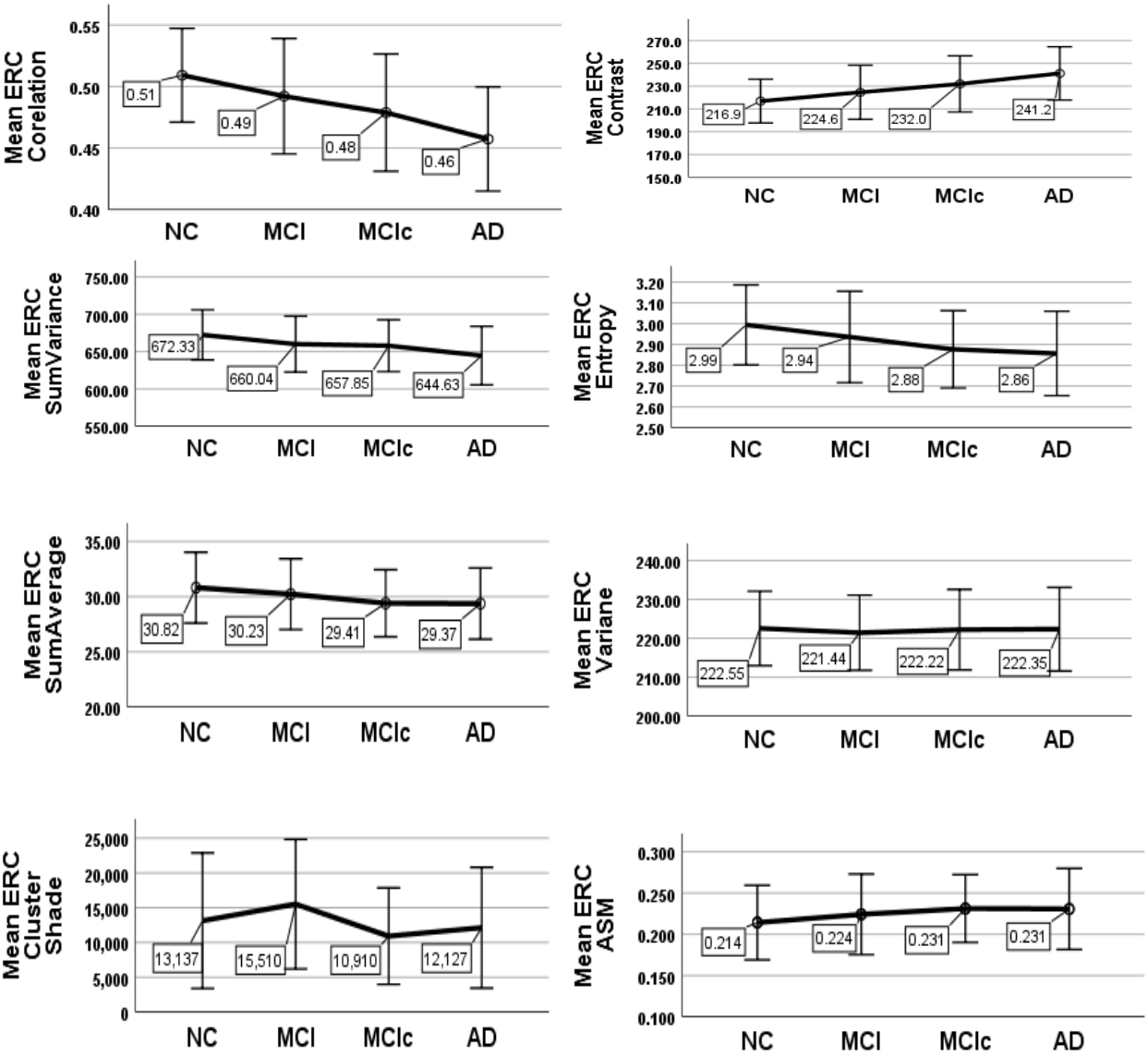

Figure 17: Entorhinal cortex texture features charts (mean ±SD) based on Table 14.

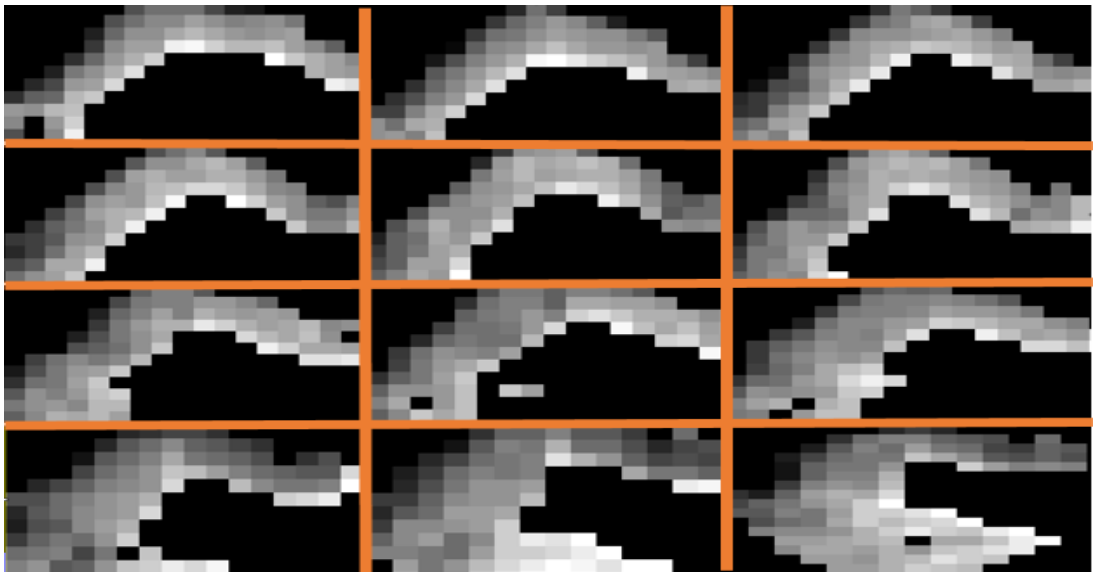

Figure 18: Selected MRI slides (approx. 14x13 pixels) of the entorhinal cortex of an NC subject.

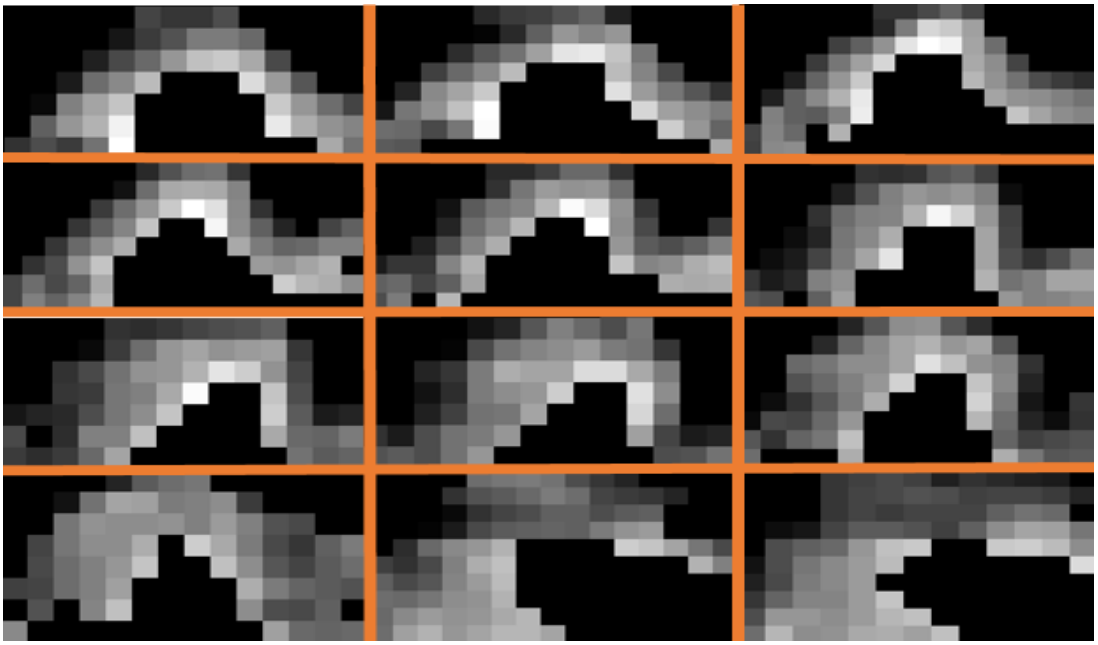

Figure 19: Selected MRI slides (approx. 14x11 pixels) of the entorhinal cortex of an MCI subject.

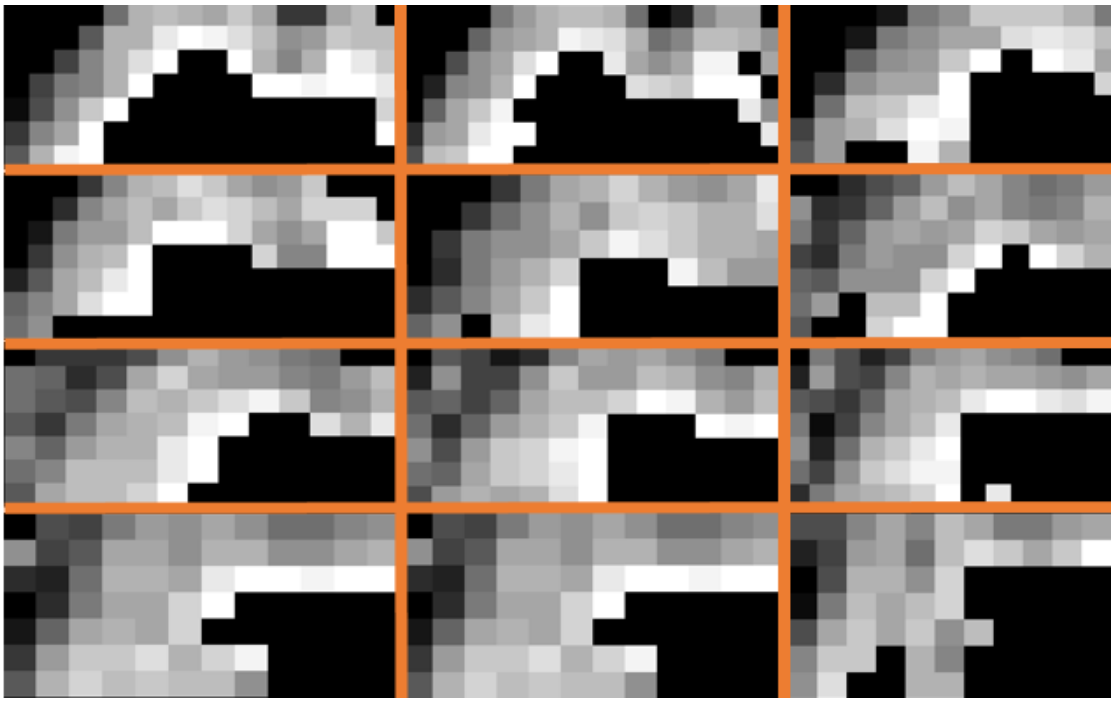

Figure 20: Selected MRI slides (approx. 11x7 pixels) of the entorhinal cortex of an AD subject.

5

Comparison of 1.5T and 3T MRI hippocampus texture features in the assessment of Alzheimer's disease

5.1 Abstract

Many studies evaluated how the MR field strength affects the effectiveness to detect neurodegenerative changes of AD, derived from atrophy or thickness. To the best of our knowledge, no study evaluated before how tissue texture changes are affected by the MR field strength. In this Chapter, hippocampal texture features were extracted from 1.5T and 3T MRI and evaluated how they are affected on stronger magnetic fields.

In the literature, other studies compared the two magnetic fields strength in the assessment of AD, but on volumetric measures [220]. This is the first study that compared texture features extracted from 1.5T and 3T images and we hypothesized that higher magnetic fields will provide better differentiation between the texture characteristics of the NC, MCI and AD subjects mainly due to the higher image quality and resolution provided by stronger magnetic fields MRIs [221].

MR imaging data from 14 NC, 14 with MCI, 11 MCIc and 10 AD subjects scanned at 1.5T and 3T were included. Haralick's texture features were extracted from the hippocampus, along with hippocampal and amygdala volumes and cortical thickness. One-way ANOVA, paired-

samples and Wilcoxon signed t-tests were used to evaluate if there were significant differences between the features.

The results showed that 3T MRI texture features were significantly different for NC vs AD, NC vs MCI and MCI vs AD, whereas, 1.5T for MCI vs AD only. Amygdala and hippocampal volumes, showed significant differences for NC vs AD for both MRI strengths, whereas cortical thickness for MCI vs MCIc for the 3T. Paired sample t-test and Wilcoxon signed-rank test revealed significant differences for Angular Second Moment (ASM), contrast, correlation, variance, sum variance and entropy, the amygdala volume and cortical thickness. Between NC vs MCI, 3T texture revealed higher AUC.

Furthermore, 3T texture revealed significant differences for more features compared to 1.5T, whereas, atrophy and thickness had similar results. As expected, 3T texture changes provided earlier diagnosis compared to 1.5T volume or texture changes.

5.2 Introduction

Theoretically, increasing the magnetic field strength from 1.5T to 3T, roughly doubles the signal-to-noise ratio (SNR), and provides a higher contrast to noise ratio (CNR), per unit scan time, to better differentiate gray/white matter and other tissues. Therefore, the boundaries between grey and white matter are better seen in 3T images and as a result the delineation is easier. However, the higher magnetic field of 3T comes with a cost of increased level of artifacts [221] which might affect the features extracted from the images. However, due to the physical origin of these artifacts, the Radiologic Technologists and MR Physicists manage these artifacts through specific pulse sequences parameters (minimum repetition time or flip angle) and image protocol design. Furthermore, some commercial scanners use corrections for some artifacts such as constant level appearance (CLEAR), phased-array uniformity enhancement (PURE), and prescan-normalization [221]. Furthermore, with stronger fields, the magnetic field inhomogeneity increases as well due to susceptibility increase in spatial

variations [222]. Currently, most MRI studies are conducted at 1.5T [67], [129], [223], [224]; however, some studies investigated a stronger magnetic field, such as from 3T as tabulated in Table 15, investigating whether 3T MRI strength fields can provide better atrophy detection compared to 1.5T [79], [220], [225]–[227]. Overall, 1.5T and 3T scans did not significantly differ in their power to detect neurodegeneration from atrophy.

Table 15: Volumetric studies comparing 1.5T and 3T MRI features in the assessment of AD

Main Author	Region of Interest	Data Type	Subjects	Description
Briellmann *et al.*, 2001, [225]	Hippocampus	Volume	NC	Control hippocampal volume measurements obtained at 1.5T and at 3T were not different.
Chow *et al.*, 2015, [220]	Hippocampus	Volume	NC, MCI, AD	3T images, with their higher contrast and higher signal-to-noise ratio, may enhance the topographic localization of atrophy.
Ho *et al.*, 2010 [226]	Whole brain	Volume	AD, MCI	1.5T and 3T scans did not significantly differ in their power to detect neurodegenerative changes.
Macconald *et al.*, 2014, [227]	Hippocampus	Volume	NC, AD	Hippocampal volume and atrophy rates discriminated well between controls and AD subjects, and there was no evidence of a difference in predictive ability between 1.5T and 3T.
Lötjönen *et al.*, 2011, [79]	Hippocampus	Volume	NC, MCI, AD	When comparing hippocampus volume extracted from 1.5T and 3T images, the absolute value of their difference was low (equal to 3.2%).

Abbreviations: NC: normal controls; MCI: mild cognitive impairment; AD: Alzheimer's disease; T: Tesla.

The main objective of this chapter is to evaluate if smaller scale tissue changes in AD derived from texture are more easily detectable in 3T which could lead to an earlier diagnosis. Specifically, texture features were extracted from the hippocampus of normal NC, MCI and AD subjects in order to evaluate how well each magnetic field strength detects textural differences between these groups. To the best of our knowledge, this is the first study that compared texture features extracted from 1.5T and 3T images for the hippocampus. However, for comparison, we included larger scale changes as well, such as volumetric features derived from hippocampus and amygdala, plus, cortical thickness which also represents a well-known AD biomarker [119], [228]–[230]. In this study, it is hypothesized that through texture features, stronger magnetic fields could provide better differentiation between the aforementioned groups.

The following text is part of a journal paper (Comparison of 1.5T and 3T MRI hippocampus texture features in the assessment of Alzheimer's disease) published in: 2020 Biomedical Signal Processing and Control, August 2020 - DOI: *https://doi.org/10.1016/j.bspc.2020.102098*

5.3 Data Preparation

For the preparation of this article data were obtained from the ADNI database (http://adni.loni.usc.edu/). The ADNI was launched in 2003 as a public-private partnership, led by principal investigator Michael W. Weiner, MD. The primary goal of ADNI was to test whether serial MRI, positron emission tomography (PET), other biological markers and clinical and neuropsychological assessment can be combined to measure the progression of MCI and early AD.

5.3.1 Subjects

Baseline scans of a total of 49 subjects were included in the study (14 NC, 14 MCI, 11 MCIc and 10 AD subjects) who underwent both 1.5T and 3T MR imaging. Inclusion criteria for NC were: MMSE scores between 24 and 30; CDR of zero; absence of depression, MCI and dementia. Detailed description of inclusion/exclusion criteria can be found in the ADNI protocol (adni.loni.usc.edu/methods/documents/).

All the subjects had a standardized protocol on both 1.5T and 3T MRI units from 3 MR imaging vendors (GE Healthcare, Milwaukee, Wisconsin; Philips Healthcare, Best, the Netherlands; or Siemens, Erlangen, Germany) with a standardized protocol developed to evaluate 3D T1-weighted sequences for morphometric analyses. T1-weighted volumetric 3D MPRAGE baseline scans collected for each subject. The 1.5T and 3T scanning protocols used a 3D sagittal volumetric sequence. The typical 1.5T acquisition parameters were TR = 2400 ms, minimum full TE, TI = 1000 ms, flip angle = 8°, FOV = 24 cm, with a 256 × 256 × 170 acquisition matrix in the x-, y-, and z-dimensions, yielding a voxel size of 1.25 × 1.25 × 1.2 mm^3. For 3T scans, the typical parameters were a TR = 2300 ms, minimum full TE, TI = 900 ms, flip angle = 8°, FOV =

26 cm, with a 256 × 256 × 170 acquisition matrix in the x-, y-, and z-dimensions, yielding a voxel size of 1.0 × 1.0 × 1.2 mm^3.

5.3.2 Data Analysis

FreeSurfer v6.0 software (Martinos Center for Biomedical Imaging, Harvard-MIT, Boston USA) [188] was used for the segmentation and volumetric representations of the subcortical brain regions were used in this study (the hippocampus and the amygdala) and the surface-based estimation of cortical thickness. Both intensity and continuity information from the segmentations and deformation procedures are used to produce representations of the cortical borders. Cortical thickness is calculated as the closest distance from the GM/WM boundary to the GM/CSF boundary at each vertex on the tessellated surface [190]. FreeSurfer is currently the most commonly used software for cortical thickness analysis in AD.

Hippocampal texture features were calculated using KNIME Analytics platform [215]. The following Haralick texture features [216] were computed: Angular Second Moment (ASM), Contrast, Correlation, Variance, Sum Average, Sum Variance and Entropy. Their average was calculated in four directions (0°, 45°, 90°, 135°) with the distance between adjacent pixels set to 1.

5.3.3 Statistical Analysis

Baseline score differences for cognitive tests, volume, thickness and texture were examined between the 4 groups through one-way ANOVA and statistical significance was $p< .05$. One-way ANOVA with post hoc Bonferroni correction was also used to examine the between-group differences. Then a paired-samples t-test was used for normally distributed data for a direct comparison between 1.5T versus 3T texture, volume and thickness measures. In the cases where the assumption of normality as assessed by Shapiro-Wilk's test was not met, a Wilcoxon signed-rank test was used. Furthermore, through a logistic regression model receiving operating characteristic (ROC) curves, we determined the performance of both

systems and their ability to distinguish NC from MCI subjects. Statistical analysis was performed with IBM SPSS Statistics Version 24 (IBM Corp. Released 2011. IBM SPSS Statistics for Windows, Version 20.0. Armonk, NY: IBM Corp.)

5.4 Results

5.4.1 Baseline demographics for baseline measures

Baseline demographics including gender, age and MMSE scores are tabulated in Table 16. As expected, the NC subjects had the highest MMSE score compared to the other groups. Furthermore, there were significant differences for sex and MMSE score variables but not for age.

Table 16: Demographics data

Variables at Baseline	NC (n=14)	MCI (n=14)	MCIc (11)	AD (n=10)	*p* value
Sex (M/F)	4/10	10/4	8/3	3/7	.030
Age (mean ± SD)	74.9 (5.2)	71.8 (8.1)	74.4 (6.6)	75.0 (7.5)	.588
MMSE Score (mean ± SD)	29 (1.1)	27 (1.4)	26 (1.4)	23 (2.2)	.000

Abbreviations: NC: normal controls; MCI: mild cognitive impairment; MCIc: MCI converters; AD: Alzheimer's disease; MMSE: mini mental state examination; SD: standard deviation.

In Table 17, features extracted from 1.5T showed no statistical significant differences among the groups, except for hippocampal entropy (p= .035), and hippocampal and amygdala volumes, (p= .004 and p= .006 respectively). On the other hand, features extracted from 3T images, revealed statistical significant differences among all groups for all texture features including hippocampal and amygdala volumes. Cortical thickness was also statistically significant between the groups for both 1.5T and 3T, p= .031 and p= .015 respectively

Table 17: Texture, volumetric and thickness features for the NC, MCI, MCIc and AD groups for 1.5T and 3T MRI systems.

Features	Mean (SD)									
	NC		MCI		MCIc		AD		*p* value	
	1.5T	3T	1.5T	3T	1.5T	3T	1.5T	3T	1.5T	3T
	Hippocampal Texture features									
ASM	.102 (.035)	.070 (.021)	.105 (.043)	.095 (.037)	.105 (.023)	.102 (.024)	.121 (.032)	.112 (.033)	.616	.009
Contrast	166 (20.0)	150 (14.9)	169 (15.0)	173 (9.9)	179 (19.8)	180 (14.0)	180 (19.5)	177 (17.8)	.209	.000
Correlation	.54 (.07)	.46 (.09)	.52 (.083)	.47 (.10)	.54 (.043)	.54 (.03)	.53 (.055)	.54 (.022)	.805	.024
Variance	190 (33.3)	154 (21.6)	184 (25.5)	172 (30.5)	204 (10.3)	189 (22.8)	201 (9.0)	205 (9.1)	.181	.000
Sum Average	41 (4.2)	43 (3.1)	39 (5.3)	41 (5.3)	39 (2.5)	38 (2.3)	38 (4.3)	37 (4.2)	.487	.010
Sum Variance	593 (123)	463 (84)	567 (100)	517 (120)	619 (64)	584 (73)	622 (32)	638 (29)	.466	.000
Entropy	3.7 (.21)	3.9 (.16)	3.7 (.08)	3.7 (.18)	3.7 (.14)	3.7 (.24)	3.5 (.17)	3.6 (.14)	.035	.009
	Volumetric Features (mm^3)									
Hippocampus	3685 (380)	3709 (365)	3388 (598)	3299 (557)	3041 (344)	3217 (684)	3038 (463)	3148 (421)	.004	.040
Amygdala	1461 (163)	1625 (189)	1298 (243)	1364 (288)	1292 (235)	1392 (304)	1113 (146)	1227 (341)	.006	.009
	Thickness (mm)									
Cortex	2.32 (.056)	2.34 (.030)	2.31 (.068)	2.34 (.073)	2.24 (.12)	2.28 (.076)	2.24 (.07)	2.29 (.064)	.031	.015

Abbreviations: SD: standard deviation; NC: normal controls; MCI: mild cognitive impairment; MCIc: MCI converter; AD: Alzheimer's disease; MMSE: mini mental state examination; ASM: Angular second moment.

5.4.2 Between-group comparisons

A one-way ANOVA with post hoc Bonferroni correction was conducted on baseline scans to determine if there were significant texture characteristics differences between the four groups. Subjects were classified into four groups NC vs AD, NC vs MCI and MCI vs AD. Texture features were extracted from the hippocampus and data were normally distributed, as assessed by Shapiro-Wilk's test ($p > .05$) and statistical significance was defined as $p < .05$. There were no outliers in the data, as assessed by boxplot inspection, and all data are presented as mean ± standard deviation (SD).

As seen in Table 18, 1.5T hippocampal texture features, showed significant difference for entropy only in the MCI vs AD group. Furthermore, hippocampal and amygdala volume showed significant differences between NC vs AD group.

On the other hand, 3T hippocampal texture features, revealed significant differences in more cases. Specifically, for NC vs AD group, all texture features (except correlation) showed significant differences. Furthermore, significant differences were also seen for NC vs MCI and MCI vs AD. Similarly to 1.5T, volumetric measures of hippocampus and amygdala showed significant differences between NC vs AD group only, whereas, cortical thickness between MCI vs MCIc subjects for the 3T.

Table 18: Hippocampal texture, volume and thickness differences at 1.5T and 3T MRI systems

	Mean Difference (SE)							
	NC *vs* AD		NC *vs* MCI		MCI *vs* MCIc		MCI *vs* AD	
	1.5T	3T	1.5T	3T	1.5T	3T	1.5T	3T
	Texture features							
ASM	-.018 (.01)	-.0420 (.01)*	-.002 (.01)	-.023 (.01)	.000 (.01)	-.008 (.01)	.016 (.01)	-.018 (.01)
Contrast	-13.40 (7.7)	-26.84 (5.9)*	-2.93 (7.0)	-22.73 (5.5)*	-9.07 (7.5)	-6.71 (5.9)	-10.45 (7.7)	-4.10 (5.8)
Correlation	-.007 (.02)	-.076 (.03)	-.020 (.02)	-.003 (.03)	-.024 (.02)	-.069 (.03)	-.013 (.03)	-.073 (.03)
Variance	-11.3 (10.7)	-50.9 (10.4)*	-5.7 (9.1)	-17.6 (8.9)	-19.8 (10.0)	-17.5 (9.5)	-17.1 (10.7)	-33.3 (10.4)*
Sum Average	-2.78 (1.7)	-5.18 (1.6)*	-1.16 (1.6)	-1.80 (1.5)	-.352 (1.7)	-2.68 (1.6)	-1.61 (1.8)	-3.38 (1.66)
Sum Variance	-28.9 (41.6)	-174.5 (39.5)*	-25.9 (35.4)	-54.3 (33.7)	-51.6 (37.8)	-66.9 (36.0)	-54.9 (41.6)	-120.1 (39.5)*
Entropy	-.135 (.06)	-.274 (.01)*	-.080 (.06)	-.192 (.07)	-.080 (.07)	-.026 (.07)	-.21 (.07)*	-.082 (.080)
	Volumetric Features (mm^3)							
Hippocampus	-646 (193)*	-561 (214)*	-296 (176)	-410 (195)	-347 (200)	-81 (208)	-350 (193)	-150 (214)
Amygdala	-347 (92)*	-398 (115)*	-162 (79)	-261 (105)	-6.0 (83)	-28 (112)	-184 (91)	-136 (115)
	Thickness measures (mm)							
Cortex	-.082 (.03)	-.052 (.02)	-.007 (.032)	-.003 (.024)	-0.70 (.034)	.069 (.025)*	-.070 (.034)	-.056 (.026)

Abbreviations: SE: Standard error; ASM: Angular Second Moment; NC: Normal controls; MCI: Mild cognitive impairment; MCIc: MCI converter; AD: Alzheimer's disease. *. The mean difference is significant at the .05 level

5.4.3 Comparison between 1.5T and 3T MRI

A paired-samples t-test was used to determine whether there was a statistically significant mean difference between the two magnetic fields for both hippocampal texture, volumes and thickness. Data inspection, revealed no extreme outliers, thus, all data were kept in the analysis.

Hippocampal ASM, contrast and sum average, hippocampal and amygdala volume and cortical thickness met the assumption of normality, as assessed by Shapiro-Wilk's test ($p > .05$), therefore, the paired-samples t-test was used. Statistically significant differences between the two systems were seen for hippocampal ASM, amygdala volume and cortical thickness (Table 19). Within diagnostic groups, significant texture differences from paired-samples t-test ($p < .05$) were seen in the NC group for hippocampal ASM ($t = 3.440$, $p = .004$), contrast ($t = 2.284$, $p = .041$) and amygdala volume ($t = 3.873$, $p = .002$). There were no significant differences within the MCI or AD groups.

Table 19: Hippocampal Paired-Sample t-test for normally distributed texture, volume and thickness features between 1.5T and 3T MRI systems

1.5T – 3T	Paired Differences				
	Mean (SD)	95% CI	t	df	Sig.
Texture features					
ASM	.015 (.029)	.007 - .024	3.730	47	.001
Contrast	3.98 (20.75)	-2.17 – 10.15	1.303	45	.199
Sum Average	.93 (4.14)	-2.13 – .270	1.559	47	.126
Volume measures (mm^3)					
Hippocampus	10.8 (188)	-44.4 - 66.1	.396	46	.695
Amygdala	112.5 (171)	61.5 – 163.5	4.47	46	.000
Thickness Measures (mm)					
Cortex	.031 (.076)	.009 - .053	2.862	47	.006

Abbreviations: SD: Standard deviation; CI: Confidence Interval; ASM: Angular Second Moment.

Four of the hippocampal texture features (corelation, variance, sum variance and entropy) violated the assumption of normality, as assessed by Shapiro-Wilk's test (p< .05), therefore, the Wilcoxon signed-rank test was used. As seen in Table 20, there were statistically significant median difference for all four texture features. Within diagnostic groups, statistically significant differences (p< .05) were seen for NC group in all four-texture features: corelation (z= 2.354, p= .019), variance (z= 2.542, p= .011), sum variance (z= 2.542, p= .011) and entropy (z= 2.551, p= .011). In the MCI group only correlation showed statistically significant difference (z= 2.040, p= .041), whereas in the AD group, there was statistically significant difference for variance (z= 2.366, p= .018) and sum variance (z= 2.028, p= .043).

Table 20: Hippocampal Wilcoxon signed-rank test for not-normally distributed texture features between 1.5T and 3T MRI systems

	Medians (Inter Quartile range - IQR)			
	1.5T MRI	3T MRI		
Features	Texture features		z	*p* value
Corelation	.550 (.090)	.526 (.103)	2.98	.003
Variance	201 (23.4)	185 (57.3)	2.27	.023
Sum Variance	622 (113.6)	574 (.207.5)	2.15	.031
Entropy	3.70 (.273)	3.66 (.304)	2.45	.014

5.4.4 Classification modelling

Furthermore, we compared the classification power between the two systems for NC and MCI subjects. We chose this comparison, as MCI subjects do not fulfil the criteria for dementia, as their cognitive function is comparable to NC subjects and we wanted to explore if through 3T images their differentiation would be more pronounced. Specifically, we calculated a binary logistic regression model for each individual texture, volume and cortical thickness variable and by using ROC curves, we determined their AUC (Table 21). The combination model included raw MRI biomarker scores as well as age and gender as covariates.

Table 21: Classification of NC from MCI subjects through textural, volumetric and thickness features extracted from 1.5T and 3T MRI systems

Texture Features	1.5T		3T		*p* value	
	AUC	95% CI	AUC	95% CI	1.5T	3T
Texture features						
ASM	0.806	0.629 - 0.983	0.837	0.691 - 0.982	0.006	0.002
Contrast	0.816	0.652 - 0.981	0.941	0.848 - 1.000	0.004	0.000
Correlation	0.806	0.631 - 0.981	0.816	0.645 - 0.987	0.006	0.004
Variance	0.811	0.638 - 0.985	0.827	0.671 - 0.982	0.005	0.003
Sum Average	0.796	0.621 - 0.970	0.827	0.668 - 0.985	0.008	0.003
Sum Variance	0.816	0.645 - 0.987	0.827	0.673 - 0.980	0.004	0.003
Entropy	0.839	0.683 - 0.996	0.824	0.663 - 0.985	0.004	0.003
Volume measures (mm^3)						
Hippocampus	0.867	0.721 - 1.0	0.893	0.764 - 1.0	0.001	0.000
Amygdala	0.907	0.778 – 1.0	0.918	0.813 – 1.0	0.000	0.000
Thickness measures (mm^2)						
Cortex	0.824	0.658 – 0.990	0.802	0.622 – 0.982	0.004	0.008

Abbreviations: AUC: area under curve; CI: confidence interval; ASM: Angular Second Moment, ICV: Intracranial Volume

Overall, features extracted from both 1.5T and 3T systems were statistically significant for the classification of this group. However, in all cases higher AUC values were seen from features extracted from 3T and ranged between 0.816 - 0.941 compared to 1.5T ranges (0.796 - 0.907).

5.5 Discussion

The main objective of this study was to evaluate whether a higher magnetic field, such as from a 3T MRI, could capture more significant differences on MCI and AD subjects from a 1.5T MRI. Specifically, smaller scale changes derived from hippocampal texture, and larger scale changes

derived from hippocampal and amygdala volume and cortical thickness were extracted from both 1.5T and 3T systems and their values between NC, MCI and AD subjects were compared.

As seen in Table 21, texture features extracted from 3T, revealed statistically significant differences among the groups in more cases compared to 1.5T which showed statistically significant difference only for entropy in MCI *vs* AD group. Similar findings were also reported in the study by Macdonald *et al.*, [227] where it was also documented that the 3T system was able to detect more changes that were not apparent at the 1.5T system. This finding can be attributed to the fact that due to the higher SNR of the 3T images, degenerative changes are more easily detectable [220]. Furthermore, both systems had the same results regarding volumetric measures, revealing statistically significant results for NC *vs* AD group only, for both hippocampus and amygdala. It seems that both hippocampal and amygdala atrophy magnitude is comparable and this was also seen in another study [230]. In general, it seems that both magnetic strengths do not significantly differ in their power to detect atrophy changes and this finding is consistent with the study by Ho *et al*., 2010 [231].

The finding of capturing more statistically significant changes with texture compared to volume, suggests that texture changes occur earlier than atrophy and they can be captured from structural MRI. This finding is also supported by a recent study by Lee *et al*., [232] and Sørensen *et al.*, [9], where it was found that MRI hippocampal texture features predicted progression to AD earlier than hippocampal volume. Probably, this explains the fact that no volumetric changes were seen for the groups where MCI subjects were included as their neurodegeneration is not as advanced as in AD subjects; however, their neurodegenerative changes were captured by texture features.

In the between systems comparison, the paired-samples t-test and Wilcoxon signed-rank test (Table 19 and Table 20) revealed statistically significant differences between 1.5T and 3T, in five of the seven texture features, whereas hippocampal volume did not. No hippocampal volume differences between 1.5T and 3T were also reported by Macdonald *et al*., [227], for both

automated and manual hippocampal segmentations. Similar hippocampal atrophy patterns between the 1.5T and 3T MRI systems were also reported by Chow *et al.,* [220]. Amygdala volume and cortical thickness also revealed statistically significant differences between the two magnetic strengths.

Higher AUC values were seen from the features extracted from the 3T system in the classification of NC from MCI subjects. We investigated specifically this group, as is of great importance to detect accurately MCI subjects instead of AD subjects, in order to provide them with the appropriate cure before converting to AD. Similar to other studies [220], [227], the discriminative ability was similar between the two systems, although, AUCs in 3T were also higher.

In this study, Haralick features generated from the Gray Level Co-occurrence Matrix (GLCM) to determine the group differences were computed. Haralick texture features were also used in both PET [233] and structural MRI [129], [223], [234] studies. One of the first studies that used Haralick features was the study by Freeborough and Fox, 1998 [129] where it was found that MRI texture features could aid in the diagnosis and tracking of the Alzheimers disease. Haralick features were also used in the recent study by Luk., *et al*, (2018) [223] MRI were texture features were extracted from the whole brain and their AUCs ranged between 0.722 – 0.866 in the discrimination between NC and AD subjects. Furthermore, the study by Gao *et al*., 2018 [234] showed that the addition of texture features effectively improved the classification of AD and the prediction of MCI conversion to AD. However, texture is not a frequently used method compared to others such as volumetry, perhaps, due to its difficulty in understanding its concept and terms.

5.6 Limitations

One major limitation of this study is the small sample size. Furthermore, we had access only to 1.5T and 3T data. Nowadays, MRI systems with higher magnetic fields are also available

such as 7T and perhaps they could reveal more statistically significant differences between texture characteristics and superior possibilities for detecting between-group differences. However, higher magnetic fields are more susceptible to chemical shift artifacts, and this could be also an area of research on how this artifact affect quantitative imaging compared to 1.5T. Perhaps, another limitation could be the fact that the ADNI 3T protocol was designed in such way in order the tissue contrast would match the 1.5T scans [235]. This could affect the comparison between the two systems or even the effectiveness of the 3T system. Future studies could include longitudinal analysis between the two systems and evaluate if 3T systems could capture more changes with time.

5.7 Chapter main findings

1. Structural MRI texture features were extracted from both 1.5T and 3T images of NC, MCI and AD subjects. This is the first study in the literature that compared texture features from both 1.5 T and 3 T systems.

2. 3T texture features revealed statistically significant differences for more features compared to 1,5T, whereas for volume and cortical thickness the two systems appear to have similar results.

3. These findings, suggest that 3T images, seem to enhance brain neurodegeneration as captured by texture analysis, perhaps due to higher CNR and SNR provided by stronger magnetic fields.

4. The added value in the literature from this study is the fact that through texture features extracted from a 3T MRI, it is possible to detect even more changes in texture features compared to texture features extracted from a 1.5T, which could lead to an even earlier diagnosis.

6

Assessment of Alzheimer's disease Based on Texture Analysis of the Entorhinal Cortex

6.1 Abstract

This Chapter represents the main part of this PhD where entorhinal cortex texture features were used for the first time in the literature for the assessment of AD in both classification and prediction. Texture analysis was chosen for this research because it could detect smaller scale changes of neurodegeneration compared to other methods such as volumetry which detects larger scale changes. On the other hand, entorhinal cortex deteriorates in an earlier stage, compared to hippocampus, within the disease progression. Therefore, through this chapter it was evaluated if entorhinal cortex texture features could provide better results in both classification and prediction of the disease compare to hippocampal volumetry which is the most frequently used method.

Texture features extracted from 194 NC, 200 MCI, 84 MCI who converted to AD (MCIc) and 130 AD subjects. Receiving operating characteristic (ROC) curves, determined the performance of the various features in discriminating the groups, and a predictive model was used to predict conversion of MCIc subjects to AD. An AUC of 0.872, 0.710, 0.730 and 0.764 was seen between NC vs AD, NC vs MCI, MCI vs MCIc and MCI vs AD subjects, respectively. Including entorhinal cortex volume improved the AUCs to 0.914, 0.740, 0.756 and 0.780, respectively. For the disease prediction, binary logistic regression was applied on

five randomly selected test groups and achieved on average AUC's of 0.760 and 0.764 on the training and validation cohorts, respectively. Entorhinal cortex texture features were significantly different between the four groups and in many cases provided better results compared to other methods such as volumetry.

6.2 Introduction

Due to the aforementioned limitations of cognitive assessment in AD diagnosis, the research community has been actively searching for diagnostic imaging biomarkers especially the ones derived from quantitative T1-weighted MRI. However, radiologists cannot perceive subtle changes of neurodegeneration, especially in the early stages of the disease by the naked eyes observation. Even if they could, without any quantitative measurements, it would be impossible to predict the patient's progress.

Volumetry, remains the most established methods used in the assessment of AD, however, the accumulation of NFTs and Aβ plaques is present prior to atrophy and these plaques could affect image intensity structure and distribution. Texture analysis investigates the statistical properties of the image intensities which might represent changes in MRI image pixel intensity due to NFTs and Aβ plaques. Furthermore, MRI biomarkers based on texture might be able to detect earlier stages of AD than biomarkers that use larger scale changes, such as thickness or atrophy. The establishment of such biomarkers will allow the identification of individuals with MCI at an earlier stage which could lead to a better management of the MCI group targeting in slower progression or even prevention to conversion to AD.

Although hippocampus represents the most established ROI used in the assessment of AD, the earlier involvement of the entorhinal cortex was proved by many studies [19], [120], [121], [147], [150], [173], [182]. In two comprehensive reviews [236], [237] the authors concluded that structural changes in the early stages of the disease are more pronounced in the entorhinal cortex. Table 22 tabulates studies that used entorhinal cortex in the assessment of AD. Furthermore, for the disease prediction, entorhinal cortex provided better predictive

accuracies compared to hippocampus. Although volumetry represents the most commonly used method to date, there is lack of research in the assessment of AD using texture analysis. The study of Sørensen *et al* [9], found that hippocampal texture was superior to volume reduction for the disease prediction. Therefore, we hypothesized that through the earlier involvement of entorhinal cortex and by using texture, it is likely to detect microscopic alterations of the disease before atrophy spreads.

The main objective in this chapter is to determine whether MRI entorhinal cortex texture features could detect early cognitive decline in MCI and AD subjects. In addition, a comparison of entorhinal cortex texture to the gold standard method, hippocampal volume, it is made to evaluate which method could provide the best results. Finally, it is evaluated if entorhinal cortex texture features can be used in the prediction of conversion from MCI to AD.

Table 22: Selected quantitative MRI studies where entorhinal cortex was used for the classification of AD and the prediction of conversion from MCI to AD.

Author	Data type	Classification	ROI	Acc.	Se.	Sp.	Description
Classification Studies							
Juottonen et al. [121]	Volume	NC vs AD	Hip. Erc.	86% 87%	80% 80%	91% 94%	Both hippocampus and entorhinal cortex had the same discriminative power.
Pennanen et al. [62]	Volume	NC vs MCI	Hip. Erc.	60% 66%	57% 65%	62% 70%	Between NC and MCI subjects entorhinal cortex atrophy was more pronounced and provided better classification.
Ryo et al [238]	Volume	SMI vs NC	Hip Erc.	NA	67% 78%	85% 93%	Subjects with SMI had lower Erc. volumes than NC, whereas no differences in Hip. volume were seen
Prediction of conversion from MCI to AD							
Killiany *et al.* [19]	Volume	0 vs 36 months	Hip. Erc.	NA 84%	NA	NA	Entorhinal cortex differentiated MCI subjects that developed AD whereas hippocampus did not.
deToledo-Morrell *et al.* [147]	Volume	0 vs 36 months	Hip. Erc.	NA 93%	NA	NA	Entorhinal cortex provided better predictive accuracy from hippocampus
Devanand *et al.* [174]	Volume	0 vs 36 months	Hip. Erc.	79% 80%	61% 63%	NA	Entorhinal cortex had more atrophy rates than hippocampus for MCIc.
Bakkour *et al.* [90]	Thickness	0 vs 36 months	Cortex	NA	83%	65%	Entorhinal cortex volume may be a better predictor in people with MCI rather than hippocampal volume.
Eskildsen *et al.* [176]	Thickness	0 vs 36 months	Cortex	67%-76%	NA	NA	Longitudinal measures in MCI subjects showed that entorhinal cortex was affected first, followed by hippocampus

Abbreviations: SMI: subjective memory impairment; NC: normal controls; MCI: mild cognitive impairment; MCIc: mild cognitive impairment converter; AD: Alzheimer's disease; ROI: region of interest; Acc.: accuracy; Se: sensitivity; Sp: specificity.

The following text contains part of a journal paper (Assessment of Alzheimer's Disease Based on Texture Analysis of the Entorhinal Cortex) published in: 2020 IEEE Frontiers Aging Neuroscience - DOI: 10.3389/fnagi.2020.00176

6.3 Data Preparation

6.3.1 The Alzheimer's Disease Neuroimaging Initiative

Data were acquired from the ADNI (http://adni.loni.usc.edu/). The ADNI was launched in 2003 by the National Institute on Aging, the National Institute of Biomedical Imaging and Bioengineering, the Food and Drug Administration, private pharmaceutical companies and non-profit organizations as a public-private partnership.

6.3.2 Subjects

All subjects selected for this study were from standardized data collections (see http://adni.loni.usc.edu/methods/mri-analysis/adni-standardized-data/) and specifically from the ADNI-1 Complete 2 and 3 year 1.5 Tesla datasets. All data acquired as part of this study are publicly available (http://www.loni.ucla.edu/ADNI/). Enrolled subjects were all between 55 and 90 years of age and each subject was willing, able to perform all test procedures described in the protocol and had a study partner able to provide an independent evaluation of functioning. Overall, 455 subjects were included in the study: 153 NC (73 males and 80 females), 141 MCI (95 males and 46 females), 77 MCI subjects that converted to AD (MCIc) (43 males and 34 females) and 84 AD (40 males and 44 females).

6.4 Data Analysis

6.4.1 Segmentation Algorithm and Volumetry

ROI segmentation was performed using the Freesurfer image analysis suite (Massachusetts General Hospital, Boston, MA), which is documented and freely available for download online (http://surfer.nmr.mgh.harvard.edu/). The Freesurfer pipeline, conforms the MRI scans to an isotropic voxel size of 1 mm^3, and the MRI intensity of all T1-weighted scans analysed in this thesis was normalized using the non-parametric non-uniform intensity normalization (N3) algorithm of Sled et al. 1998 [74] followed by skull stripping and neck removal. Details of these

have been discussed in previous publications [188], [191]. In brief, this multistep pipeline includes motion correction, automated Talairach transformation, first normalization of voxel intensities, removal of the skull, linear volumetric registration, intensity normalization, nonlinear volumetric registration, volumetric labeling, second normalization of voxel intensities, and white matter segmentation (Figure 21). Output includes segmentation of subcortical structures, extraction of cortical surfaces, cortical thickness estimation, spatial normalization onto the FreeSurfer surface template (FsAverage), and parcellation of cortical regions. Hippocampal and entorhinal cortex volumes were computed using Freesurfer segmentations given that this is an established method. Cy-Tera supercomputer of the Cyprus Institute was used to run FreeSurfer.

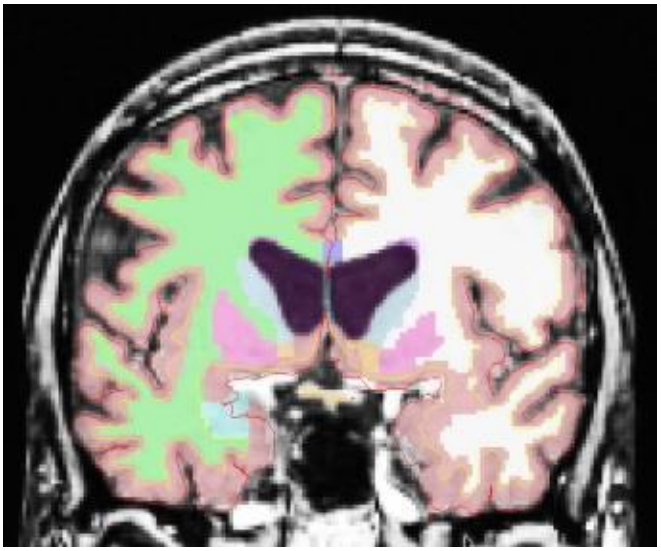

Figure 21: FreeSurfer volumetric segmentations and cortical delineation

Texture features were calculated using KNIME Analytics platform [215]. The following Haralick texture features [216] were computed: Angular Second Moment (ASM), Contrast, Corelation, Variance, Sum Average, Sum Variance, Entropy and Cluster shade and their average in four directions (0°, 45°, 90°, 135°) was used.

6.4.2 Statistical Analysis

Demographic data along with cognitive tests, texture and volume features of subjects at baseline scans were compared with one-way ANOVA to determine statistical differences between the groups (NC, MCI, MCIc, AD). Then, post hoc tests using the Bonferroni correction were applied to determine if there were significant differences in texture features between the groups. There were no outliers in the data, as assessed by inspection of a boxplot.

Texture features and volume were combined as predictor variables in a logistic regression model in order to investigate the potential of combined value of the two MRI biomarkers. Backwards elimination methods was used to select the most suitable variables. Apart from texture and volume, we included age and gender as covariates. Through ROC curves, we determined the performance of the various variables, and their ability to discriminate NC from MCI and AD subjects, as well as to classify the conversion status. The resulting AUC was used to determine the capability for diagnosis. The significance of an AUC was determined using DeLong, Delong and Clarke–Pearson's test [239].

Then, through a repeated measures ANOVA we compared entorhinal cortex and hippocampal volume changes with texture changes within 18 months and evaluated if there were significant texture changes during follow-up period. Data were checked for outliers and normal distribution, as assessed by boxplot and Shapiro-Wilk test ($p > 0.05$). When sphericity was violated, as assessed by Mauchly's test, the Greenhouse-Geisser correction was applied. Then, Post hoc tests using the Bonferroni correction was used to compare the volume and texture changes.

To evaluate the prognostic power of our model, we also used AUC curves on MCI and MCIc subjects. Specifically, the MCI group was randomly divided into both a training set (~70% of the participants) and a trial set (~30%) of the participants. This was iterated 5 times to provide 5 unique training and test groups. The training sets were used to fit two binary logistic regression models: the first model included entorhinal cortex volume, MMSE scores, age and

gender as covariates and the second model had the same features, plus entorhinal cortex texture to determine if the addition of texture based metrics could improve the accuracy. For a more robust prediction model the collinearity between the predictor variables was evaluated and only those for which the collinearity was acceptable were included in the final model. The estimated logistic regression model was then applied to the validation cohorts.

Statistical analysis was performed with IBM SPSS Statistics Version 24 (IBM Corp. Released 2011. IBM SPSS Statistics for Windows, Version 20.0. Armonk, NY: IBM Corp.) or MedCal Version 19 (MedCalc Software bvba, Ostend, Belgium; https://www.medcalc.org; 2019). The significance level of all statistical test was set at $P < 0.05$.

6.5 Results

Baseline demographics including gender, age, MMSE scores are shown in Table 23. All baseline variables (except the age) were significantly different between the four groups based on one-way ANOVA. Estimations of hippocampal and entorhinal cortex volumes are in cubic millimeter (left and right averaged). As expected, AD patients had smaller volumes than MCI subjects and both had smaller volumes than NC subjects.

Table 23: Baseline demographics, hippocampal and entorhinal cortex volume.

Variables at baseline (mean ± SD)	Diagnosis Group				*P* value
	NC (n=194)	MCI (n=200)	MCI_c (n=84)	AD (n=130)	
Sex (M/F)	96 / 98	127 / 73	49 / 35	60 / 70	.003
Age	76.17 (5.20)	74.74 (7.18)	74.88 (7.30)	76.01 (7.35)	.111
MMSE Score	29 (1.0)	27 (1.82)	26 (1.84)	23 (2.16)	<.001
CDR	0.0 (.00)	0.50 (.04)	0.50 (.00)	0.75 (.25)	<.001
Entorhinal cortex Volume (mm^3)	1930 (284)	17191723 (384)	154410 (338)	1417 (348)	<.001
Hippocampal Volume (mm^3)	3539 (413)	3243 (461)	2941 (461)	2892 (474)	<.001

Abbreviations: NC: normal controls; MCI: mild cognitive impairment; MCIc: mild cognitive impairment converter; AD: Alzheimer's disease; MMSE: mini-mental status examination; CDR: clinical dementia rating; SD: standard deviation.

6.5.1 Between groups differences

A one-way ANOVA was conducted to determine if there were significant texture features between the groups for baseline scans (Table 24). For NC vs AD and NC vs MCI groups, entorhinal cortex revealed statistically significant differences in more features compared to hippocampus. Specifically, hippocampus did not show any significant changes for NC vs MCI group, apart for volume. However, hippocampal texture revealed statistical significant differences in more features between MCI vs MCIc group. Between MCI vs AD, both structures had similar results with entorhinal cortex showing statistically significant differences in the texture features contrast, correlation, sum variance and entropy, whereas hippocampus for the texture features ASM, sum average and entropy.

Table 24: Mean differences at baseline scans for entorhinal cortex and hippocampus

	Mean Difference (SE)							
	Entorhinal cortex				Hippocampus			
Group	NC vs AD	NC vs MCI	MCI vs MCIc	MCI vs AD	NC vs AD	NC vs MCI	MCI vs MCIc	MCI vs AD
Texture Features								
ASM	-.017* (.005)	-.01 (.004)	-.007 (.006)	-.006 (.005)	-.013* (.004)	-.008 (.004)	-.023* (.005)	-.023* (.005)
Contrast	-24.3* (2.60)	-7.73* (2.27)	-7.36 (2.93)	-16.60* (2.60)	-2.0 (2.36)	-3.61 (2.11)	-4.62 (2.70)	-5.60 (2.32)
Corelation	-.051* (.005)	-.017* (.004)	-.013 (.005)	-.034* (.005)	-.0004 (.005)	-.0004 (.005)	-.016 (.007)	-.001 (.005)
Variance	-.201 (1.14)	-1.11 (1.01)	-.780 (1.30)	-.910 (1.14)	-2.40 (2.80)	-4.90 (2.46)	-13.0* (2.20)	-7.30 (2.77)
Sum Average	-1.44* (.365)	-.590 (.324)	-.821 (.414)	-.853 (.361)	-1.64* (.560)	-.823 (.498)	2.40* (.640)	-2.47* (.556)
Sum Variance	-27.70* (4.15)	-12.28* (3.68)	-2.18 (4.80)	-15.41* (4.14)	-6.30 (10.0)	-15.20 (8.80)	-41.0* (11.3)	-21.5 (9.80)
Entropy	-.137* (.023)	-.058* (.020)	-.060 (.026)	-.080* (.023)	-.103* (.028)	-.034 (.024)	-.113* (.030)	-.138* (.026)
Cluster Shade	-471 (350)	-260 (312)	-118* (414)	-730 (342)	-1009 (1038)	-2373 (927)	-4600* (1182)	-3383 (1026)
Volumetric Features								
Volume	-513* (39.1)	-211* (34.8)	-174* (45.0)	-301* (38.7)	-646* (52.4)	-295* (42.7)	-302* (60.0)	-351* (51)

Abbreviations: SE: standard error; ASM: angular second moment; NC: normal controls; MCI: mild cognitive impairment; MCIc: mild cognitive impairment converter; AD: Alzheimer's disease.

* The mean difference is significant at the 0.05 level.

6.5.2 Texture differences between groups – Classification

To determine the classification between the groups, a binary logistic regression model was calculated for each individual variable and by using ROC curves we determined their AUC. The combination model included raw single MRI variable scores as well as age and gender as covariates. In most of the cases all eight texture features revealed significant differences between groups (see Tables 25 to 28). Then, all the variables were combined together and the backward elimination method selected the more important predictor variables.

For NC vs AD group, the AUC for entorhinal cortex texture values ranged from 0.540 to 0.824 (Table 25). When texture features were combined into a single classification model, the AUC reached 0.872 which was similar to hippocampal volume (AUC 0.869) and entorhinal cortex volume (AUC 0.888). When entorhinal cortex texture and volume were combined the AUC reached 0.914.

Table 25: Entorhinal cortex texture and volume in classifying NC vs AD

NC vs AD	ROC Analysis AUC	95% CI	*P* value
Entorhinal cortex			
Texture Features			
ASM	0.592	0,529-.656	.005
Contrast	0.794	0.743-0.845	<.001
Corelation	0.824	0.776-0.872	<.001
Variance	0.524	0.458-0.590	.475
Sum Average	0.620	0.555-0.681	<.001
Sum Variance	0.713	0.653-0.770	<.001
Entropy	0.685	0.625-0.744	<.001
Cluster Shade	0.540	0.475-0.604	.238
Volume and Thickness			
Erc. Volume	0.888	0.847-0.925	<.001
Erc. Thickness	0.809	0.755-0.863	<.001
Features Combination			
Texture (ASM, Correlation, Variance, Sum Average & Cluster shade)	0.872	0.828-0.916	<.001
Texture + Erc. Volume	0.914	0.879-0.950	<.001
Hippocampus			
Hippocampal Volume	0.869	0.827-0.912	<.001

Abbreviations: NC: Normal Controls; AD: Alzheimer's disease; ROC: receiver operating characteristic; AUC: area under curve, CI: confidence interval; ASM: angular second moment; Erc: entorhinal cortex.

Between NC and MCI subjects, features combination showed a lower AUC (0.710) compared to entorhinal and hippocampal volume (Table 26). The entorhinal cortex texture and volume combination raised the AUC to 0.740.

Table 26: Entorhinal cortex texture and volume in classifying NC vs MCI

NC vs MCI	ROC Analysis AUC	95% CI	*P* value
Entorhinal cortex			
Texture Features			
ASM	0.618	0.563-0.674	<.001
Contrast	0.664	0.611-0.718	<.001
Corelation	0.671	0.617-0.725	<.001
Variance	0.604	0.548-0.660	<.001
Sum Average	0.618	0.562-0.674	<.001
Sum Variance	0.641	0.586-0.695	<.001
Entropy	0.632	0.577-0.687	<.001
Cluster Shade	0.608	0.551-0.666	<.001
Volumetric and Thickness			
Erc. Volume	0.735	0.686-0.784	<.001
Erc. Thickness	0.659	0.604-0.713	<.001
Features Combination			
Texture (ASM, Correlation, Variance, Sum Average & Cluster shade)	0.710	0.656-0.762	<.001
Texture & Erc. Volume	0.740	0.689-0.791	<.001
Hippocampus			
Hippocampal Volume	0.762	0.715-0.809	<.001

Abbreviations: NC: normal controls; MCI: mild cognitive impairment; ROC: receiver operating characteristic; AUC: area under curve, CI: confidence interval; ASM: angular second moment; Erc: entorhinal cortex.

Between MCI and MCIc subjects, features combination provided a higher AUC (0.730), compared to entorhinal cortex and hippocampal volume (Table 27). The entorhinal cortex texture and volume combination raised the AUC to 0.756.

Table 27: Entorhinal cortex texture and volume in classifying MCI vs MCIc

MCI vs MCIc	ROC Analysis AUC	95% CI	*P* value
Entorhinal cortex			
Texture Features			
ASM	0.565	0.494-0.637	0.85
Contrast	0.583	0.510-0.657	.028
Corelation	0.580	0.505-0.654	.038
Variance	0.531	0.458-0.604	.037
Sum Average	0.591	0.520-0.662	.036
Sum Variance	0.527	0.451-0.603	.475
Entropy	0.593	0.522-0.662	.014
Cluster Shade	0.696	0.632-0.759	.032
Volume and Thickness			
Erc. Volume	0.642	0.573-0.711	<.001
Erc. Thickness	0.670	0.603-0.737	<.001
Features Combination			
Texture (ASM, Correlation, Variance, Sum Average & Cluster shade)	0.730	0.665-0.795	<.001
Texture & Erc. Volume	0.756	0.692-0.820	<.001
Hippocampus			
Hippocampal Volume	0.685	0.617-0.753	<.001

Abbreviations: MCIc: mild cognitive impairment converter; ROC: receiver operating characteristic; AUC: area under curve, CI: confidence interval; ASM: angular second moment; Erc: entorhinal cortex.

Between MCI and AD subjects, features combination showed a higher AUC of 0.764 compared to entorhinal cortex and hippocampal volume, (Table 28). The entorhinal cortex texture and volume combination raised the AUC to 0.780.

Table 28: Entorhinal cortex texture and volume in classifying MCI vs AD

MCI vs AD	ROC Analysis AUC	95% CI	*P* value
Entorhinal cortex			
Texture Features			
ASM	0.627	0.565-0.690	<.001
Contrast	0.704	0.646-0.763	<.001
Corelation	0.725	0.668-0.783	<.001
Variance	0.624	0.560-0.688	<.001
Sum Average	0.649	0.587-0.711	<.001
Sum Variance	0.658	0.596-0.720	<.001
Entropy	0.656	0.594-0.718	<.001
Cluster Shade	0.645	0.583-0.706	<.001
Volume and Thickness			
Erc. Volume	0.726	0.670-0.781	<.001
Erc. Thickness	0.702	0.642-0.762	<.001
Features Combination			
Texture (ASM, Correlation, Variance, Sum Average & Cluster shade)	0.764	0.710-0.818	<.001
Texture + Erc. Volume	0.780	0.728-0.833	<.001
Hippocampus			
Hippocampal Volume	0.711	0.652-0.771	<.001

Abbreviations: MCI: mild cognitive impairment; AD: Alzheimer's disease; ROC: receiver operating characteristic; AUC: area under curve, CI: confidence interval; ASM: angular second moment; Erc: entorhinal cortex.

6.5.3 Measures between different MRI scan Intervals

A one-way repeated measures ANOVA was conducted to determine whether there were statistically significant differences in entorhinal cortex (texture and volume) over the 18 months observation (baseline, 6, 12 and 18 months). For comparison, hippocampal volume was also included in this analysis. At each time point, a diagnosis was made based on the NINCDS-ADRDA Alzheimer's Criteria to identify conversion of MCI to probable AD and vice versa and only MCI and MCIc subjects were included in this part of the analysis. Specifically, longitudinal data of 141 MCI and 77 MCIc subjects were included in this analysis. The means and standard deviations for volume are presented in Table 29 and for texture in Table 30. We

reported the *F*-statistic from the repeated measures ANOVA test as *F* (df_{time}, df_{error})= *F*-value, *P* = *P*-value.

Table 29: Statistically significant difference in entorhinal cortex and hippocampal volume over a 18-month intervention

Within Subjects Effects	Entorhinal cortex volume Mean (SD) mm^3		Hippocampal volume Mean (SD) mm^3	
	MCI	MCIc	MCI	MCIc
Baseline	1733 (390)	1504 (293)	3263 (483)	2906 (439)
6m	1712 (389)	1449 (278)	3213 (487)	2860 (423)
12m	1693 (393)	1424 (269)	3168 (496)	2819 (432)
18m	1657 (411)	1384 (269)	3129 (487)	2781 (436)
F-ratio (Time)	F(2.837, 383)= 45.62, *P* < .0005	F(3, 186)= 45.06, *P* < .0005	F(2.748, 376)= 41.8, *P* < .0005	F(3, 195)= 21.74, *P* < .0005

Abbreviations: MCI: mild cognitive impairment; MCIc: mild cognitive impairment converters; SD: standard deviation.

For entorhinal cortex volume in both MCI and MCIc subjects, there was a significant effect for time, [F (2.837, 383.0)= 45.62, $P < 0.0005$] and [F(3, 186)= 45.06, $P < 0.0005$], respectively. Furthermore, the mean difference was statistically significant at the 0.05 level between all-time points for both MCI and MCIc subjects with the exception of 12-18 time point for MCIc subjects. Post hoc tests using the Bonferroni correction showed that entorhinal cortex volume in the MCI subjects was reduced by an average of 20 ± 6.9mm^3 6 months after the baseline scan, then by an additional 19 ± 6.0mm^3 between 6-12 month time and 36 ± 6.1mm^3 between 12-18 month time. As expected, the entorhinal cortex degeneration was more pronounce in the MCIc subjects. Their entorhinal cortex volume was reduced by an average of 55 ± 10.5mm^3 6 months after the baseline scan, then by an additional 25 ± 9.5mm^3 between 6-12 month time and 40 ± 10.3mm^3 between 12-18 month time.

For hippocampal volume in both MCI and MCIc subjects, there was significant effect for time, [F (2.748, 376.4)= 41.8, $P < 0.0005$] and [F(3, 195)= 21.74, $P < 0.0005$] respectively. Furthermore, the mean difference was statistically significant at the 0.05 level between all-time points for

both MCI and MCIc subjects with the exception of 12-18 time point for MCIc subjects. Interestingly, hippocampal volume reduction in the MCIc subjects was similar to MCI stable subjects. Specifically, post hoc tests using the Bonferroni correction revealed that hippocampal volume in the MCI subjects was reduced by an average of 49 ± 12.6mm^3 6 months after the baseline scan, then by an additional 45 ± 11.5mm^3 between 6-12 month time and 38 ± 11.3mm^3 between 12-18 month time. Similar pattern was seen in MCIc subjects as well, as hippocampal volume reduction was 45 ± 15.8mm^3 after 6 months from the baseline scan, and then reduced by an additional 40 ± 14.0mm^3 between 6-12 month time and additional 38 ± 16.6mm^3 between 12-18 month time.

Remarkably, repeated measures ANOVA in the entorhinal cortex texture features of MCIc subjects, revealed that there was significant effect for time for all features (except for cluster shade), whereas, in stable MCI subjects, there was significant effect for time only for sum variance and entropy.

Table 30: Statistically significant difference in entorhinal cortex texture over a 18-month intervention

MCI stable	Entorhinal Cortex Texture features - Mean (SD)							
	ASM	Contrast	Corelation	Variance	Sum Average	Sum Variance	Entropy	Cluster shade
Baseline	.226 (.047)	220 (22.38)	.498 (.043)	659.4 (38.0)	220 (9.49)	659 (38.0)	2.92 (.216)	1838 (3218)
6m	.228 (.046)	223 (20.95)	.495 (.041)	659.2 (38.5)	221 (9.90)	659 (38.5)	2.90 (.221)	1198 (2986)
12m	.230 (.047)	223 (19.34)	.494 (.043)	656.0 (38.1)	220 (9.50)	655 (41.9)	2.89 (.212)	1276 (3086)
18m	.234 (.047)	222 (24.71)	.493 (.049)	654.0 (38.1)	219 (10.7)	654 (44.3)	2.89 (.212)	1300 (2989)
F-ratio (Time)	F(3, 417)= 2.45 *P* = 0.620	F(3, 384)= 1.05 *P* = 0.370	F(3, 375)= 1.14 *P* = 0.332	F(3, 411)= 2.17 *P* = 0.09	F(3, 411)= 1.44 *P* = 0.230	F(3, 411)= 2.17 *P* = 0.091	F(3, 414)= 2.65 *P* = 0.048	F(3, 396)= 2.49 *P* = 0.060

MCI converters	ASM	Contrast	Corelation	Variance	Sum Average	Sum Variance	Entropy	Cluster shade
Baseline	.230 (.041)	230 (26.6)	.480 (.046)	655.4 (35.0)	221 (10.5)	655 (35.0)	2.87 (.179)	-296.7 (1860)
6m	.237 (.039)	238 (27.4)	.468 (.043)	650.0 (40.5)	222 (11.4)	650 (40.5)	2.82 (.185)	-388.4 (2363)
12m	.235 (.040)	237 (28.5)	.468 (.047)	647.4 (42.0)	222 (12.0)	637 (42.0)	2.82 (.186)	-385.0 (2394)
18m	.243 (.043)	238 (28.8)	.459 (.047)	637.8 (44.3)	219 (12.7)	647 (44.3)	2.79 (.156)	-557.1 (2032)
F-ratio (Time)	F(2.72, 179.5)= 3.86 *P* = 0.013	F(3, 201)= 5.80 *P* < .0005	F(3, 192)= 6.82 *P* < .0005	F(3, 201)= 7.45 *P* < .0005	F(3, 198)= 3.55 *P* < .0005	F(3, 201)= 7.45 *P* < .0005	F(3, 204)= 7.30 *P* < .0005	F(3, 162)= 0.23 *P* = 0.874

Abbreviations: MCI: mild cognitive impairment; ASM: angular second moment; SD: standard deviation.

6.5.4 Prediction of Conversion to AD within 18 months

To evaluate entorhinal cortex texture in the prediction of conversion from MCI to AD all the MCI subjects, were divided into two categories: the MCI subjects who remained stable and did not convert to AD within 18 months (n=200) versus the MCIc subjects who converted to AD within 18 months (n=84). First, we run a prediction model which included entorhinal cortex volume, MMSE scores and gender with age as covariates. Then, a second model was run where entorhinal cortex texture features (contrast and cluster shade) were included as

well, to evaluate if texture metrics could improve accuracy. The selected variables were also evaluated for collinearity between them and their degree of correlation was acceptable.

Then, the MCI group was divided into a training set (~70) and a trial set (~30%). We randomly generated 5 of these sets, with each training set having a total of n=133 MCI and n=55 MCIc, whereas the trial set had total of n=67 MCI and n=29 MCIc. Independent sample t-test and chi-square analysis showed no statistical difference between the baseline demographics in the training and trial sets in each iteration. For each of the 2 models, 5 binary logistic regression models were determined, corresponding to one for each training set (Table 31). The model including texture performed better and achieved AUCs of 0.795, 0.725, 0.745, 0.786, and 0.750 respectively. Then, the logistic regression coefficients from the final model developed from the training cohorts were applied to the validation cohorts and AUCs of 0.780, 0.780, 0.790, 0.735 and 0.735 were seen.

Table 31: Area under curve in five trials of randomly splitting training (70%) and trial data (30%).

	Entorhinal cortex Volume						Entorhinal cortex Volume and Texture					
	Training Cohort			Validation Cohort			Training Cohort			Validation cohort		
Trial	ROC Analysis AUC	(95% CI)	*P* value	ROC analysis AUC	(95% CI)	*P* value	ROC Analysis AUC	(95% CI)	*P* value	ROC analysis AUC	(95% CI)	*P* value
1	0.760	0.690-0.830	.000	0.700	0.583-0.814	.000	0.795	0.728-0.862	.000	0.780	0.662-0.898	.000
2	0.673	0.595-0.751	.001	0.688	0.573-0.804	.005	0.725	0.649-0.801	.000	0.780	0.674-0.886	.001
3	0.663	0.580-0.746	.04	0.658	0.538-0.778	.005	0.745	0.770-0.820	.000	0.790	0.680-0.903	.001
4	0.662	0.582-0.742	.000	0.635	0.500-0.772	.005	.786	0.712-0.860	.000	0.735	0.621-0.848	.001
5	0.647	0.565-0.730	.001	0.709	0.591-0.827	.003	0.751	0.675-0.827	.000	0.735	0.627-0.843	.001

Abbreviations: ROC: receiver operating characteristic; AUC: area under curve, CI: confidence interval.

6.6 Discussion

The main objective of this study was to evaluate entorhinal cortex texture as a new biomarker of AD from T1-weighted MR images. To the best of our knowledge, this is the first study that used texture analysis on the entorhinal cortex for the assessment of AD. Thus, our results are

not directly compared to the same method and ROI previously used in other AD studies, but mainly to hippocampal volume, which represents the most frequently used method in the assessment of AD. In the analysis, apart from entorhinal cortex texture features, we calculated also its volume and we combined them in a binary logistic regression model which included age and gender as covariates.

For entorhinal cortex, one way-ANOVA showed that contrast, corelation and volume were the features that showed statistical significant differences between all groups and for hippocampus were sum average, cluster shade and volume (see Table 24). For the NC vs MCI group, one way ANOVA showed that were statistically significant differences in more features for the entorhinal cortex compared to hippocampus, whereas, hippocampus showed significant differences in more features between MCI vs MCIc group. Perhaps, these differences are correlated with the fact that entorhinal cortex is the region affected first by the disease [19], [120], [121], [147], [150], [173], [182] whereas, hippocampus is involved in a later stage.

In the literature, entorhinal cortex and hippocampus have shown a significant role in the assessment of AD [236]. Similarly, in the present study results of the ROC curve analysis showed that for the entorhinal cortex there were significant differences between NC subjects and AD patients. Specifically, there were significant texture changes in six texture features (apart from variance and clustershade) and their combination provided an AUC of 0.872 ($P < 0.001$) for the discrimination between NC and AD subjects (Table 25). This was similar to entorhinal cortex or hippocampal volume, which showed an AUC of 0.888 ($P < 0.001$) and 0.869 ($P < 0.001$), respectively. When entorhinal cortex texture features and volume were combined into the same model, the diagnostic result was improved, showing an AUC of 0.914 ($P < 0.001$).

Compared to a study that used hippocampal texture such as from Zhang *et al*., [130] their classification accuracy reached 96.4%. However, their dataset included severely affected AD subjects (MMSE 5.53 ± 4.47 compared to 23±1.9 for the ADNI data in the present study).

Compared to the study of Sørensen *et al.,* [9] which also used the ADNI dataset, their hippocampal texture achieved an AUC of 0.912 in discriminating NC from AD. On the other hand, the study of Luk *et al*., [223] used texture features on the whole brain and the combination of hippocampal texture features and volume provide an AUC of 0.924 which was close to our combined model.

Compared to other ADNI volumetric studies where hippocampus was used, NC subjects were classified from AD patients with AUC levels of 0.750 to 0.887 [240] and 0.810 to 0.895 when hippocampal subfields only were used [241]. This is comparable to our hippocampal volume results (AUC 0.869) and close to entorhinal cortex texture (AUC 0.888). In other studies [94], [121], where both hippocampal and entorhinal cortex volume were used, the classification accuracy ranged between 84%-86%. In the study of Pennanen *et al*., [62] the combination of hippocampal and entorhinal cortex volume provided an accuracy of 91%.

Between NC vs MCI subjects, the combination of entorhinal cortex texture features in the logistic regression model provided an AUC of 0.710 and their combination with entorhinal cortex volume, raised the AUC to 0.740 (Table 26). This is comparable to the AUC (0.764) in the study of Sørensen *et al*. [9] where hippocampal texture was used. In the study of Hwang *et al*., 2016 [242] where voxel based 3DT1W was used on the whole brain, their AUC ranged between 0.682 to 0.713 which was close to our single ROI method. The study by Simoes *et al.* [91] used whole brain texture maps reached a classification accuracy of 87% (Se. 85%, Sp. 95%), however, their analysis was based on 3 Tesla (T) images. Compared to other studies [62], [94] that used hippocampal volume for the discrimination between NC vs MCI, a classification accuracy close to 66% was achieved.

Between MCI and MCIc subjects, the combination of entorhinal cortex texture features and volume provided an AUC of 0.756 whereas entorhinal cortex or hippocampal volume provided lower AUCs of 0.642 and 0.685 respectively (Table 27). Our result for this group was similar to the study of Chincarini *et al*. [243] where texture features were extracted from

defined volumes of interest, mainly from the MTL, and through random forest classifiers they achieved an AUC of 0.740. These findings suggest that the entorhinal cortex texture changes precede neuronal atrophy of the hippocampus which is consistent with the most widely used staging scheme proposed by Braak and Braak in 1991 [5]. Specifically, Stage I is associated with NFTs deposition in the entorhinal-perirhinal cortex and in Stage II, the NFTs become more prominent and the entorhinal cortex is eventually involved. In Stage III, the entorhinal cortex is fully involved whereas between Stage III-IV NFTs appear in the hippocampus. Eventually, in stages V-VI apart from the MTL NFTs are also widely distributed in the isocortex.

Between MCI and AD subjects, the combination of entorhinal cortex features showed better diagnostic capability (AUC of 0.764) compared to entorhinal cortex and hippocampal volume (AUCs of 0.726 and 0.711 respectively). The combination of entorhinal cortex texture and volume raised the AUC to 0.780 (Table 28). For this group, other studies [62], [94], [127] achieved a classification accuracy between 80%-82% using volumetric or shape characteristics of the hippocampus and entorhinal cortex.

In the one-way repeated measures ANOVA, the entorhinal cortex volume reduction was more pronounced in the MCIc subjects whereas, hippocampal volume atrophy rate was similar in both MCI and MCI subjects. Similar finding was seen in the study of Devanand *et al*. [174] where it was shown that entorhinal cortex had more severe atrophy rates, compared to hippocampus, in MCIc subjects. Regarding entorhinal cortex texture features (Table 30) the one-way repeated measures ANOVA showed significant effect for time (for all texture features) in MCIc subjects, whereas, in MCI stable subjects there was no statistically significant difference (apart from entropy). Perhaps, this finding indicates that through entorhinal cortex texture features we could identify MCI subjects that in the future they could develop the disease.

Furthermore, we determined whether entorhinal cortex texture could be used to predict conversion of MCI to AD within 18 months. For the discrimination of stable MCI from MCIc

subjects, our prediction model including entorhinal cortex features, volume, MMSE scores, age and gender performed better rather than volume alone and demonstrated an average AUC of 0.760 in the training cohort and an AUC of 0.764 in the validation cohort. In this study, the combination of texture and volume features improved the prediction of conversion from MCI to AD and this was also the finding as well by two recent studies by Gao et al., [234] and Luk et al., [223]. Compared to other studies that followed their subjects for the same time period, such as from [67], [95] and hippocampal volume was used, the classification accuracy between MCI and MCIc was 67% and 64% respectively. Sørensen *et al*. [9], compared hippocampal volumetry and texture in the differentiation between stable MCIs and MCI converters within 24 months and AUCs of 0.670 and 0.740 respectively, were achieved. In the study from Misra *et al*., [66] where a VBM method on the whole brain was used to consider the conversion within 12 months an accuracy of 81.5% was obtained. In a recent study by Lee et al., [232] texture analysis was also used for the prediction of the disease in subjects from the ADNI database. In their analysis texture of the hippocampus, precuneus and posterior cingulate cortex were included and their model ranged between AUCs of 0.79 to 0.82 whereas, our one structure only analysis ranged between 0.735-0.790.

6.7 Limitations

There are some limitations in the present study. First, the ADNI cohort cannot be generalized to the normal population given the patient recruitment was targeted toward clinical trials in patients with AD. The baseline demographics of these sample patients do not fit with the actual demographics of the broader population. For example, female / male ratio is poor with almost twice as many males as females especially for MCI subjects. Furthermore, ADNI study does not provide postmortem pathological confirmation of the clinical status. Therefore, the stable MCI subjects we selected for the present study although, did not progress to AD within the followed-up period, they might have developed the disease or other types of dementia in a later stage. Therefore, as in any AD study involving *in vivo* data, the diagnosis of the disease

remains probable. Thus, MRI patterns of neurodegeneration found in studies like the present may have uncertainties.

6.8 Chapter main findings

1. This is the first study published in the literature that run texture analysis on the entorhinal cortex for the assessment of AD.

2. Entorhinal cortex texture features (ASM, Contrast, Correlation, Variance, Sum Average, Sum Variance, Entropy, Cluster shade) were used for the classification and prediction of the disease.

3. Entorhinal cortex features revealed significant differences between the four groups (NC vs AD, NC vs MCI, MCI vs MCIc and MCI vs AD). Furthermore, entorhinal cortex texture features provided better results in the classification of NC vs AD, MCI vs MCIc, MCI vs AD subjects compared to hippocampal volume or entorhinal cortex volume and thickness.

4. For the prediction of the disease the inclusion of entorhinal cortex texture and volume along with clinical measures of age, gender and cognitive scores, achieved better results compared to volumetric methods.

5. The aforementioned findings, suggest that the deposition of NFTs in the area of entorhinal cortex may precede the development of atrophy in the hippocampus.

7

Conclusions and Future Scope of Work

7.1 Introduction

Cognitive, clinical and neuroimaging measures have been shown to be sensitive to AD and their efficiency as single biomarkers (or in combination) has been proved by many studies. In this study, structural MRI images from 1.5T and 3T systems were used to extract volumetric, thickness and texture features from the entorhinal cortex and the hippocampus to evaluate and compare their ability in the classification and prediction of the disease.

The key aims of the present thesis were: (1) to evaluate the disease progression and detect the brain structures affected in the earliest stage of AD and to be used in the analysis. Post mortem studies were considered as well to choose the most appropriate structures. Furthermore, the major disadvantages of the clinical, cognitive assessment used to evaluate an MCI or AD patient are also reported (Chapter 2). (2) To evaluate how the two main structures, entorhinal cortex and hippocampus, are dynamically affected by the disease and compare the several quantitative methods used in the assessment of AD derived from structural MRI (Chapter 3). (3) To evaluate how the MR magnetic field strength could affect volumetric, thickness and texture features in their ability to classify MCI and AD from NC subjects (Chapter 5) and (4), to test the diagnostic and predictive ability of entorhinal cortex texture features in the assessment of MCI and AD (Chapter 6).

7.2 Major Conclusions and Contributions

Chapter 3 represents a review of the literature of the assessment of AD based on quantitative MRI. In this Chapter, most of the freely available databases that are currently being used from many investigators are described, along with the most frequently used brain segmentation software packages which are necessary for MR quantitative imaging. In addition, Chapter 3 focuses on the quantitative methods derived from MRI images that are currently being used in the assessment of AD. Overall, the results of 30 studies are tabulated in Tables 8 and 9, where 11 studies investigated the classification of the disease and 19 studies evaluated quantitative MRI role in the prediction of the disease, respectively. All the studies agreed that quantitative MRI is essential in the assessment of AD because of the fact that the human eye cannot perceive the subtle anatomical changes affecting the small structures of the brain as seen in non-quantitative MRI.

The findings of this literature review [244] suggested that in the early stages of the disease methods that evaluate the whole brain, such as VBM, is better to be avoided, as in the early stages neurodegeneration initiates from specific regions within the MTL and more specifically the entorhinal cortex. Whole brain methods, could be used in the more advance stages of the disease where atrophy spreads outside the MTL. Texture analysis appears to be a promising method to assess brain, however, its use is very limited as most of the studies preferred volumetric measures. Perhaps, one reason that texture is not so frequently used, relies on the fact that it is more difficult to perceive its meaning compared to other methods such as volume or thickness which are terms that are daily used by the radiologists to describe several pathologies.

Regarding ROI selection, it is suggested that entorhinal cortex is better to be used in the early stages of the disease as it deteriorates more severely compared to hippocampus, whereas, in the more advanced stages, both structures could be used. However, hippocampus represents the most widely used structure in the assessments of AD, perhaps because it is a larger

structure with more specific boundaries and therefore, it's easier to be segmented and used in quantitative analysis. Furthermore, one other reason that hippocampus is preferred, might be its direct relationship to the clinical manifestation of the disease, meaning that when cognitive assessment will detect the disease, hippocampal atrophy will be detected in structural MRI as well. In conclusion, Chapter 3, suggested that texture analysis is better to be used in the early stages of the disease and entorhinal cortex texture features should be evaluated for the disease prediction and classification. To the best of our knowledge, no study in the literature used this combination before.

In *Chapter 5,* it was evaluated whether hippocampal texture features extracted from 1.5T and 3T images are statistically different and if a stronger magnetic field could provide better results in the classification of subjects. This comparison was also an innovation in this thesis, as apart from studies that compared volumetric measures, e.g. from hippocampus, there was no other study that compared texture features before derived from different magnetic fields.

The between 1.5T and 3T texture features comparison of this work research [245] showed that texture features extracted from 3T revealed statistically significant differences for more features between the groups (NC vs AD, NC vs MCI, MCI vs AD). However, for the larger scale changes such as volume and cortical thickness the two systems appeared to have similar performance which was consistent with previous volumetric studies that used volumetric measures [220], [235]. One explanation for this finding is that due to higher CNR and SNR provided by stronger magnetic fields systems, enable the brain neurodegeneration to be captured more efficiently from texture analysis rather than volume changes which occur in a later stage. Furthermore, in the classification between NC vs MCI group, higher AUC's were achieved for 3T for hippocampal ASM, contrast, correlation, variance, sum average, sum variance, hippocampal and amygdala volume and cortical thickness.

The results from this study suggested that the use of texture analysis on 3T images could lead to the earlier diagnosis compared to texture features extracted from 1.5T. Apparently,

nowadays with even stronger magnetic fields such as 7T or 11T systems it would be interesting to investigate what kind of quantitative information could be captured from texture at these magnetic fields.

To address the literature ''gap'' mentioned in Chapter 3, (no study used before texture analysis on the entorhinal cortex for the assessment of AD) in Chapter 6, entorhinal cortex texture features were extracted and tested if they could be used in the assessment of AD, in both classification and prediction. Although there is a limited number of studies that used texture before in the classification and prediction of AD, this is the first study [246] that extracted texture features from the entorhinal cortex in the assessment of AD.

Specifically, the main objective in Chapter 6, was to evaluate if entorhinal cortex texture features extracted from T1-weighted MR images could be used as a new biomarker for the assessment of AD. Specifically, it was investigated if entorhinal cortex texture changes could provide better results compared to the hippocampal atrophy which remains the "gold standard" method in the assessment of AD. Consistent with a number of previous studies, our results were comparable to studies that used hippocampal texture [9], [242] and volumetric measures from the MTL region [243]. In general, the results showed that the combination of entorhinal cortex texture features provided better results in the classification of NC vs AD, MCI vs MCIc, MCI vs AD subjects compared to hippocampal volume or entorhinal cortex volume and thickness. This finding suggests that entorhinal cortex texture changes precede neuronal atrophy of the hippocampus. Furthermore, it was observed that when entorhinal cortex texture features were combined with its volume, AUCs were improved even more.

For the prediction of the disease the inclusion of entorhinal cortex texture and volume along with clinical measures of age, gender and cognitive scores, achieved better results compared to volumetric methods. Therefore, the combination of several biomarkers can improve results and this is consistent with other studies as well [223].

Concluding, this thesis, evaluated if the magnetic field strength could affect texture features in quantitative imaging. Furthermore, it investigated the usefulness of texture features derived from the entorhinal cortex in the assessment of AD. From a disease classification and prediction perspective, it was shown that (1) texture features could provide more statistically significant differences when extracted from stronger magnetic field MRIs, such as 3T, compared to 1.5T, (2) compared to volumetric studies, entorhinal cortex texture features provide (a) better classification between NC, MCI and AD subjects, (b) better prediction of the conversion from MCI to AD.

7.3 Future Scope of Work

This section suggests a number of topics for future scope of work which arise from both this thesis and from gaps that were found in the literature.

7.3.1 Datasets and longitudinal studies

Perhaps the most popular dataset currently used in the assessment of AD is the ADNI dataset. Other studies have been used from many researches as well, such as the European AddNeuroMed [77] cohort (https://consortiapedia.fastercures.org/consortia/anm/) or the Australian, Imaging, Biomarkers and Lifestyles (AIBL) study (https://aibl.csiro.au/) (see Table 3 in Chapter 3). Open Access Series of Imaging Studies (OASIS) (www.oasis-brains.org.) is also a project aimed at making neuroimaging data sets of brain freely available to all the researchers. In order to have a more representative sample of the general population it is suggested that future studies should combine in their analysis subjects from several datasets for robust validation. Furthermore, standardisation of methods still remain a significant challenge, although international consortia have made substantial progress in this area and provide guidelines for future standardisation efforts.

In AD, perhaps the most important information a physician could be provided with is to know if a subject will eventually develop the disease. Therefore, it is very important to identify

specific MRI diagnostic biomarkers to predict whether MCI subjects will eventually convert to AD patients. Most of the studies have been using baseline MRI data but perhaps the best way to estimate antecedent changes in MCI subjects who might convert to AD is through longitudinal and cross-sectional designs. In this thesis, the longitudinal measures (0-18 months) in Chapter 6 showed that the entorhinal cortex atrophy was more severe in the MCIc subjects compared to MCI, whereas, hippocampal volume was similar between the two groups. Regarding the longitudinal measures of entorhinal cortex, more statistically significant changes were seen for MCIc subjects. Therefore, it seems that differences between these timeline scans were statistically different in more cases for texture compared to volumetric measures. Perhaps the initiation of serial MRI scans at annual or longer intervals to investigate the disease progression will provide further insight in predicting the MCI subjects that will develop the disease.

7.3.2 Core biomarkers and PET Imaging

Interestingly, for the disease progression, morphometric measures derived from structural MRI, can provide similar results with cellular or metabolic markers such as CSF, amyloid Aβ and FDG-PET. This was shown in a systematic and quantitative meta-analysis by Schroeter et al. [247] where 1,351 AD patients and 1,097 NC were involved from 40 studies. The aim of the study was to reveal the prototypical neural correlates of AD and its prodromal stage. The analysis included data from studies that used structural MRI and studies that measured reduction in glucose utilization or in perfusion with PET. It was suggested that atrophy in the (trans-) entorhinal area/hippocampus and hypometabolism / hypoperfusion in the inferior parietal lobules could predict more reliably the progression from amnestic MCI to AD. Although, in a meta-analysis [248], PET was a better disease predictor than MRI. However, there should be enough clinical information to justify irradiation of a subject and this a major drawback for PET imaging. After the first symptoms appear, it was found that the evaluation and predictive accuracy was better using structural based biomarkers [8], [178], [249].

However, other studies [19], [62], [163] revealed that structural MRI can also be used before clinical symptoms appear and in some cases it could be more accurate rather than metabolic markers [8], [177], [178]. Marcus et al. [250], supports that amyloid PET imaging should be performed in subjects with suspected AD because it was shown that Aβ plaques could also appear on non-demented elderly subjects. The presence of Aβ plaques in elderly non-demented subjects was also noticed in the study of Pike et al., [46]. Overall, it seems that the effectiveness of structural MRI compared to PET in predicting MCI conversion to AD is controversial and it should be further investigated.

7.3.3 Potential of workflow environments and Deep learning

Nowadays, medical image analysis has become a computationally rich process due to the additional new challenges e.g. to predict if an MCI subject will convert to an AD patient. These processes include many intricate steps run on increasingly larger datasets with the use of many different tools. Graphical workflow environments such as the KNIME Analytics Platform [215] and the LONI's Pipeline [85], facilitate numerous resources developed at other institutions such as, FSL/Oxford [84] or Freesurfer/Harvard [81] to be used. The combination of these tools can be used to analyze images efficiently and effectively. The advantages and possibilities of such workflow environments have not yet been exploited in neuroradiology routine practice.

Deep learning is the state-of-the-art in medical image analysis that is becoming the methodology of choice in many studies. Deep learning algorithms are based on neural networks of several layers of neurons through which a signal is propagated and can also be used for segmentation, registration, classification and other tasks in the assessment of AD [251]. Deep learning applications such as convolutional neural networks (CNN) or recurrent neural network (RNN) are currently used for the early detection and prediction of AD. According to a 2019 systematic review by Jo, No and Saykin [252], for the classification of the disease, accuracies up to 96% and 84.2% for the MCI conversion to AD were seen. Many

workflows, such as the KNIME Analytics platform [215], incorporates several deep learning workflows to be used according to the user needs.

7.3.4 Extracting Explainable Assessments of Alzheimer's disease via Machine Learning

In a recent study [253] a novel argumentation model for the classification of NC and AD subjects was presented. The objective of this study was to investigate the usefulness of rule extraction in the assessment of AD using decision trees (DT) and RF algorithms and integrating the extracted rules within an argumentation-based reasoning frame-work in order to make the results easy to interpret and explain [253]. The KNIME analytics platform was used as well, and the usefulness of rule extraction was demonstrated in the assessment of AD based on hippocampal MRI texture features. RF models with 5000 trees were built to measure the mean Decrease Gini index in order to identify the most important features. Gini Index [218] is an impurity splitting method. It was observed that feature selection based on the Gini index increases the overall performance of the RF models [219]. The 10 most promising features are shown in Figure 22 and for comparison reasons, the respectively figure for entorhinal cortex features in Figure 23. Clearly volume seems to be the most promising feature, however, the argumentation model was based on NC and AD subjects, and it is expected that there would be a large difference in hippocampal volume between the subjects. Part of our future work will be to investigate the argumentation model to the more difficult classification problem between NC and MCI subjects based on entorhinal cortex.

The positive results of the use of the argumentation based symbolic reasoning for composing and interpreting the rule extraction results was demonstrated (see Table 32).

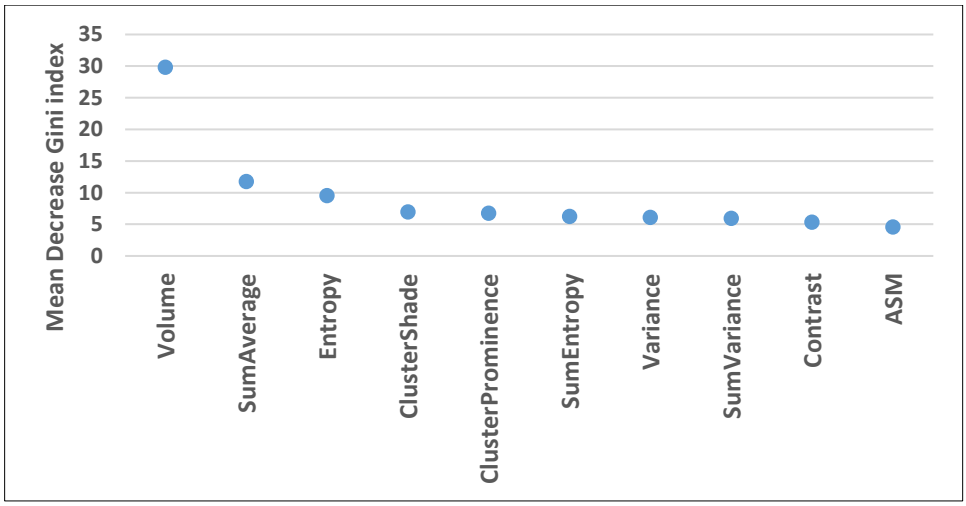

Figure 22: 10 most promising hippocampal features based on mean decrease of the gini index

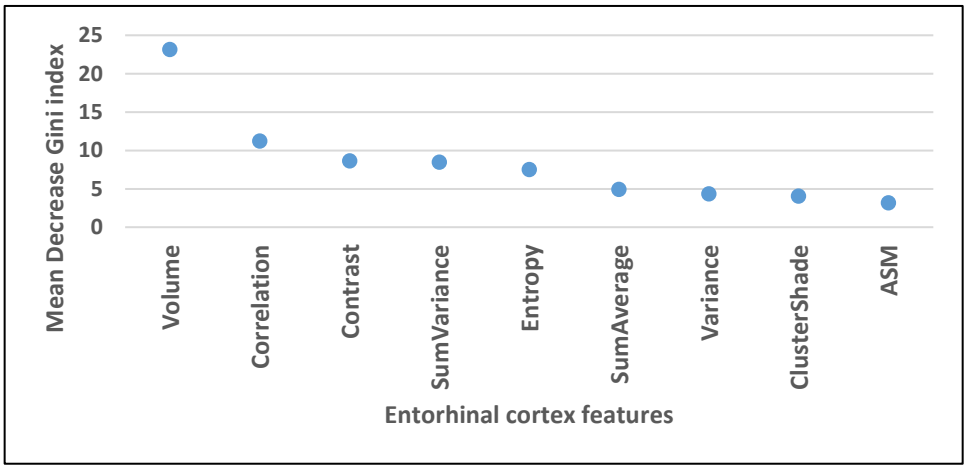

Figure 23: 10 most promising hippocampal features based on mean decrease of the gini index

Table 32: A selection of arguments defined in Gorgias framework

Priority →	Sample Rules from the argumentation model *(in parenthesis: rule no in the model)*	Accuracy	Sensitivity	Specificity
	(r1) If hipVolume >= 2890mm^3 ***return*** subject in NC	84%	96%	51%
	(r2) If hipVolume < 2890mm^3 ***return*** subject in AD	83%	51%	96%
	(r3) If hipVolume<3170mm^3 and hipClusterPRominence<802000 ***return*** subject in AD	87%	28%	98%
	(r5) If hipEntropy >= 3.67 and hipVAriance >= 198 and hipContrast < 194 ***return*** subject in NC	100%	14%	100%
	(r8) If hipSumVariance < 543 and hipSumEntropy < 2.92 ***return*** subject in NC	100%	17%	100%

7.3.4 ROI Investigation and Biomarkers combination

In classification, the most challenging task appears to be the classification between NC and MCI subjects as the classification accuracy of most of the studies is lower compared to other group of subjects. In the study by Davatzikos et al. [163], evaluation of WM areas of the brain both in the temporal lobe and in the superior and middle frontal gyri, appeared to be necessary for the accurate classification of MCI subjects. However, apart from the hippocampus and entorhinal cortex, limited studies have investigated the aforementioned areas. Furthermore, in studies that will be using hippocampus, it would be interesting to evaluate if hippocampal subfields measures could provide similar or perhaps better results than global hippocampal measures. In the study by Khan et al., [241] it was shown that hippocampal subfields were more accurate for predicting MCI conversion to AD. It would be interesting for future studies to evaluate how hippocampal subfields texture could be used for MCI and AD assessment versus to hippocampal subfield volume.

Imaging biomarkers are meaningless if they are not correlated with clinical assessment. The combination of the two provide better predictive accuracy [21], [28], [254]. It is also noted that the are very few studies [67], [68] that combine volume, thickness, shape, intensity, and texture in multivariate assessment of the disease, which in turn may result to better classification and prediction accuracy. This finding was consistent to our results when several variables were combined. In the study by Martinez Torteya et al. [132] the combination of texture-related features together with morphometrical and signal distribution related features improved the conversion to AD (AUC of 0.79). The same is true for the combination of imaging biomarkers derived from structural and functional imaging modalities [160], [255] as well as for the combination of MRI with genomic analysis towards personalized medicine and targeted drugs development.

Although in this thesis texture features were combined along with age, gender and MMSE scores, future studies might include: (1) how the inclusion of other biomarkers such as APOE ε4 or Aβ depositions could benefit the classification or prediction outcome, (2) the correlation of texture features and APOE ε4 or Aβ depositions to MCI and AD subjects. Knowing the heterogeneity of this disease and the meaning of APOE gene, the combination of the aforementioned could provide better results.

7.3.5 The use of texture analysis and other MR sequences

The use of texture analysis, although seems to be promising, is very restricted, when compared to the other methods, regarding the assessment of AD. However, some of the best classification accuracies were achieved with textures features [9], [91], [130] and it should be investigated further in the assessment of AD. Future studies should investigate the potential of texture analysis in other structures of the brain as well. Furthermore, the correlation of MRI texture characteristics and tissue pathology should be investigated. For example, if the accumulation of NFTs is correlated with specific MRI texture features it would be a viable disease biomarker.

Furthermore, in this research it was mentioned that texture features extracted from stronger magnetic fields, can reveal more statistically significant results. Nowadays, there is access to even stronger systems, such as 7T MRIs, which perhaps could reveal even better results.

Furthermore, research on the assessment of AD mainly involves volumetric 3D T1-weighted sequences. However, there are several other MRI strategies such as Diffusion Weighted Imaging (DWI) MRI, and Diffusion Tensor Imaging (DTI) [256], Fluid-attenuated inversion recovery (FLAIR) sequence or gradient echo sequences [257] that might help with the understanding of the disease pathophysiology.

7.3.6 Precision Medicine

Nowadays, precision medicine due to the wealth of today's healthcare big data has become the new trend. Precision medicine is based on quantitative analysis to drive personalized treatment – medication by taking into account individual variability in genes, environment and lifestyle of each person in order to provide a more accurate treatment. At the same time, there is a strong need to bring together all these clinical data, genomics and quantitative imaging features, known as radiomics. The combination of genomics and radiomics is also known as Radiogenomics [258]–[260].

Leading to precision medicine this work proved that quantitative MRI could have a great impact in the assessment, evaluation and treatment of AD leading towards to its better management. Furthermore, research relying on GWAS and whole exome and whole genome sequencing data, have identified a significant number of genes that are correlated to AD [261]. According to Panayides et al [261], radiogenomics could contribute towards enhanced prognosis, diagnosis and treatment in AD. However, this study evaluated only structural imaging techniques, such as MRI, therefore, future studies should use metabolic imaging methods such as PET. Metabolic changes precede structural changes and with the combination of imaging and genetics better accuracy could be provided in the classification and prediction of AD.

7.3.7 Virtual Reality application for visualization and analysis in medical imaging

3D medical imaging provides an invaluable tool to the radiologist in visualizing normal and abnormal tissue and structure for the assessment of disease and treatment planning. Nowadays, 3D reconstruction is more frequently becoming a valuable technique for describing the size and the shape of a pathology which will prepare the doctor prior surgery however, these platforms are only accessible on the scanner's computer or their workstations.

Prodromou et al. [262], developed a multi-user Virtual Reality (VR) application for visualization and analysis in medical imaging which is based on the Unity VR platform that is integrated with the very well-known and popular image Visualization Toolkit– VTK. This application accepts and processes medical images in the form of DICOM, HDR, MHD, SEQ.NRRD and NRRD. This platform was evaluated successfully in the 3D visualization of MRI images of AD subjects acquired from the ADNI database and it was found that the platform could be used by health professionals for teleconsultation or to be used by the health professional and the patient, so that the patient gains a better understanding of the underlying pathophysiology of his/her disease based on medical imaging. Future work could focus in the evaluation such platforms in a more wide spectrum of imaging cases and in the visualization of quantitative imaging features.

References

[1] "2021 Alzheimer's disease facts and figures," *Alzheimer's & Dementia*, vol. 17, no. 3, pp. 327–406, 2021, doi: 10.1002/alz.12328.

[2] Alzheimer's Association, "2016 Alzheimer's disease facts and figures," *Alzheimer's & Dementia*, vol. 12, no. 4, pp. 459–509, Apr. 2016, doi: 10.1016/j.jalz.2016.03.001.

[3] M. F. Folstein, S. E. Folstein, and P. R. McHugh, "'Mini-mental state'. A practical method for grading the cognitive state of patients for the clinician," *J Psychiatr Res*, vol. 12, no. 3, pp. 189–198, Nov. 1975.

[4] J. C. Morris, "The Clinical Dementia Rating (CDR): current version and scoring rules," *Neurology*, vol. 43, no. 11, pp. 2412–2414, Nov. 1993.

[5] H. Braak and E. Braak, "Neuropathological stageing of Alzheimer-related changes," *Acta Neuropathol.*, vol. 82, no. 4, pp. 239–259, 1991.

[6] A. Delacourte *et al.*, "The biochemical pathway of neurofibrillary degeneration in aging and Alzheimer's disease," *Neurology*, vol. 52, no. 6, pp. 1158–1165, Apr. 1999.

[7] C. R. Jack *et al.*, "Hypothetical model of dynamic biomarkers of the Alzheimer's pathological cascade," *Lancet Neurol*, vol. 9, no. 1, pp. 119–128, Jan. 2010, doi: 10.1016/S1474-4422(09)70299-6.

[8] G. B. Frisoni, N. C. Fox, C. R. Jack, P. Scheltens, and P. M. Thompson, "The clinical use of structural MRI in Alzheimer disease," *Nat Rev Neurol*, vol. 6, no. 2, pp. 67–77, Feb. 2010, doi: 10.1038/nrneurol.2009.215.

[9] L. Sørensen *et al.*, "Early detection of Alzheimer's disease using MRI hippocampal texture," *Hum Brain Mapp*, Dec. 2015, doi: 10.1002/hbm.23091.

[10] M. Strassnig and M. Ganguli, "About a Peculiar Disease of the Cerebral Cortex," *Psychiatry (Edgmont)*, vol. 2, no. 9, pp. 30–33, Sep. 2005.

[11] "Alzheimer's Disease and Dementia | Alzheimer's Association." http://www.alz.org/ (accessed May 31, 2016).

[12] A. D. International, "World Alzheimer Report 2019: Attitudes to dementia | Alzheimer's Disease International," Sep. 20, 2019. https://www.alz.co.uk/research/world-report-2019 (accessed Feb. 03, 2020).

[13] R. Guerreiro and J. Bras, "The age factor in Alzheimer's disease," *Genome Med*, vol. 7, Oct. 2015, doi: 10.1186/s13073-015-0232-5.

[14] H. Braak and E. Braak, "Staging of Alzheimer-related cortical destruction," *Int Psychogeriatr*, vol. 9 Suppl 1, pp. 257–261; discussion 269-272, 1997.

[15] K. R. Wildsmith, M. Holley, J. C. Savage, R. Skerrett, and G. E. Landreth, "Evidence for impaired amyloid β clearance in Alzheimer's disease," *Alzheimers Res Ther*, vol. 5, no. 4, p. 33, 2013, doi: 10.1186/alzrt187.

[16] A. Metaxas and S. J. Kempf, "Neurofibrillary tangles in Alzheimer's disease: elucidation of the molecular mechanism by immunohistochemistry and tau protein phospho-proteomics," *Neural Regen Res*, vol. 11, no. 10, pp. 1579–1581, Oct. 2016, doi: 10.4103/1673-5374.193234.

[17] B. C. Dickerson *et al.*, "MRI-derived entorhinal and hippocampal atrophy in incipient and very mild Alzheimer's disease," *Neurobiol. Aging*, vol. 22, no. 5, pp. 747–754, Oct. 2001.

[18] L. R. Squire, C. E. L. Stark, and R. E. Clark, "The medial temporal lobe," *Annu. Rev. Neurosci.*, vol. 27, pp. 279–306, 2004, doi: 10.1146/annurev.neuro.27.070203.144130.

[19] R. J. Killiany *et al.*, "MRI measures of entorhinal cortex vs hippocampus in preclinical AD," *Neurology*, vol. 58, no. 8, pp. 1188–1196, Apr. 2002.

[20] V. L. Villemagne *et al.*, "Amyloid β deposition, neurodegeneration, and cognitive decline in sporadic Alzheimer's disease: a prospective cohort study," *Lancet Neurol*, vol. 12, no. 4, pp. 357–367, Apr. 2013, doi: 10.1016/S1474-4422(13)70044-9.

[21] C. R. Jack *et al.*, “Comparison of Different MRI Brain Atrophy Rate Measures with Clinical Disease Progression in AD,” *Neurology*, vol. 62, no. 4, pp. 591–600, Feb. 2004.
[22] R. I. Scahill, J. M. Schott, J. M. Stevens, M. N. Rossor, and N. C. Fox, “Mapping the evolution of regional atrophy in Alzheimer’s disease: Unbiased analysis of fluid-registered serial MRI,” *Proc Natl Acad Sci U S A*, vol. 99, no. 7, pp. 4703–4707, Apr. 2002, doi: 10.1073/pnas.052587399.
[23] J. R. Petrella, R. E. Coleman, and P. M. Doraiswamy, “Neuroimaging and early diagnosis of Alzheimer disease: a look to the future,” *Radiology*, vol. 226, no. 2, pp. 315–336, Feb. 2003, doi: 10.1148/radiol.2262011600.
[24] J. L. Cummings and G. Cole, “Alzheimer disease,” *JAMA*, vol. 287, no. 18, pp. 2335–2338, May 2002.
[25] A. Baysinger, “Principles of Cognitive Neuroscience,” *Yale J Biol Med*, vol. 88, no. 1, p. 102, Mar. 2015.
[26] G. W. Van Hoesen, B. T. Hyman, and A. R. Damasio, “Entorhinal cortex pathology in Alzheimer’s disease,” *Hippocampus*, vol. 1, no. 1, pp. 1–8, Jan. 1991, doi: 10.1002/hipo.450010102.
[27] X. Li, J. Jiao, S. Shimizu, I. Jibiki, K.-I. Watanabe, and T. Kubota, “Correlations between atrophy of the entorhinal cortex and cognitive function in patients with Alzheimer’s disease and mild cognitive impairment,” *Psychiatry Clin. Neurosci.*, vol. 66, no. 7, pp. 587–593, Dec. 2012, doi: 10.1111/pcn.12002.
[28] D. P. Devanand *et al.*, “Hippocampal and entorhinal atrophy in mild cognitive impairment: prediction of Alzheimer disease,” *Neurology*, vol. 68, no. 11, pp. 828–836, Mar. 2007, doi: 10.1212/01.wnl.0000256697.20968.d7.
[29] L. M. Shaw, M. Korecka, C. M. Clark, V. M.-Y. Lee, and J. Q. Trojanowski, “Biomarkers of neurodegeneration for diagnosis and monitoring therapeutics,” *Nat Rev Drug Discov*, vol. 6, no. 4, pp. 295–303, Apr. 2007, doi: 10.1038/nrd2176.
[30] A. J. Mitchell and M. Shiri-Feshki, “Rate of progression of mild cognitive impairment to dementia--meta-analysis of 41 robust inception cohort studies,” *Acta Psychiatr Scand*, vol. 119, no. 4, pp. 252–265, Apr. 2009, doi: 10.1111/j.1600-0447.2008.01326.x.
[31] S. T. Farias, D. Mungas, B. R. Reed, D. Harvey, and C. DeCarli, “Progression of mild cognitive impairment to dementia in clinic- vs community-based cohorts,” *Arch. Neurol.*, vol. 66, no. 9, pp. 1151–1157, Sep. 2009, doi: 10.1001/archneurol.2009.106.
[32] H. Braak and E. Braak, “Frequency of stages of Alzheimer-related lesions in different age categories,” *Neurobiol. Aging*, vol. 18, no. 4, pp. 351–357, Aug. 1997.
[33] B. Dubois *et al.*, “Research criteria for the diagnosis of Alzheimer’s disease: revising the NINCDS-ADRDA criteria,” *Lancet Neurol*, vol. 6, no. 8, pp. 734–746, Aug. 2007, doi: 10.1016/S1474-4422(07)70178-3.
[34] E. Niemantsverdriet, S. Valckx, M. Bjerke, and S. Engelborghs, “Alzheimer’s disease CSF biomarkers: clinical indications and rational use,” *Acta Neurol Belg*, vol. 117, no. 3, pp. 591–602, Sep. 2017, doi: 10.1007/s13760-017-0816-5.
[35] E. Niemantsverdriet, S. Valckx, M. Bjerke, and S. Engelborghs, “Alzheimer’s disease CSF biomarkers: clinical indications and rational use,” *Acta Neurol Belg*, vol. 117, no. 3, pp. 591–602, Sep. 2017, doi: 10.1007/s13760-017-0816-5.
[36] R. J. L. Kandimalla *et al.*, “CSF p-Tau levels in the prediction of Alzheimer’s disease,” *Biol Open*, vol. 2, no. 11, pp. 1119–1124, 2013, doi: 10.1242/bio.20135447.
[37] K. Sunderland, H. Keselman, J. Algina, L. Lix, and R. Wilcox, “Conventional And Robust Paired And Independent-Samples t Tests: Type I Error And Power Rates,” *Journal of Modern Applied Statistical Methods*, vol. 2, pp. 481–496, Nov. 2003, doi: 10.22237/jmasm/1067646120.

[38] M. W. Weiner *et al.*, “2014 Update of the Alzheimer’s Disease Neuroimaging Initiative: A review of papers published since its inception,” *Alzheimers Dement*, vol. 11, no. 6, pp. e1-120, Jun. 2015, doi: 10.1016/j.jalz.2014.11.001.
[39] X. Y. Zhang, Z. L. Yang, G. M. Lu, G. F. Yang, and L. J. Zhang, “PET/MR Imaging: New Frontier in Alzheimer’s Disease and Other Dementias,” *Front Mol Neurosci*, vol. 10, Nov. 2017, doi: 10.3389/fnmol.2017.00343.
[40] L. Mosconi *et al.*, “Multicenter standardized 18F-FDG PET diagnosis of mild cognitive impairment, Alzheimer’s disease, and other dementias,” *J. Nucl. Med.*, vol. 49, no. 3, pp. 390–398, Mar. 2008, doi: 10.2967/jnumed.107.045385.
[41] A. Drzezga *et al.*, “Prediction of individual clinical outcome in MCI by means of genetic assessment and (18)F-FDG PET,” *J. Nucl. Med.*, vol. 46, no. 10, pp. 1625–1632, Oct. 2005.
[42] D. Zhang, Y. Wang, L. Zhou, H. Yuan, and D. Shen, “Multimodal Classification of Alzheimer’s Disease and Mild Cognitive Impairment,” *Neuroimage*, vol. 55, no. 3, pp. 856–867, Apr. 2011, doi: 10.1016/j.neuroimage.2011.01.008.
[43] P. Bhogal *et al.*, “The common dementias: a pictorial review,” *Eur Radiol*, vol. 23, no. 12, pp. 3405–3417, Dec. 2013, doi: 10.1007/s00330-013-3005-9.
[44] A. Nordberg *et al.*, “A European multicentre PET study of fibrillar amyloid in Alzheimer’s disease,” *Eur J Nucl Med Mol Imaging*, vol. 40, no. 1, pp. 104–114, Jan. 2013, doi: 10.1007/s00259-012-2237-2.
[45] C. C. Rowe *et al.*, “Amyloid imaging results from the Australian Imaging, Biomarkers and Lifestyle (AIBL) study of aging,” *Neurobiol. Aging*, vol. 31, no. 8, pp. 1275–1283, Aug. 2010, doi: 10.1016/j.neurobiolaging.2010.04.007.
[46] K. E. Pike *et al.*, “Beta-amyloid imaging and memory in non-demented individuals: evidence for preclinical Alzheimer’s disease,” *Brain*, vol. 130, no. Pt 11, pp. 2837–2844, Nov. 2007, doi: 10.1093/brain/awm238.
[47] C. R. Jack *et al.*, “Brain β-amyloid load approaches a plateau,” *Neurology*, vol. 80, no. 10, pp. 890–896, Mar. 2013, doi: 10.1212/WNL.0b013e3182840bbe.
[48] K. Herrup, “The case for rejecting the amyloid cascade hypothesis,” *Nature Neuroscience*, vol. 18, no. 6, pp. 794–799, Jun. 2015, doi: 10.1038/nn.4017.
[49] A. Nordberg, “Dementia in 2014. Towards early diagnosis in Alzheimer disease,” *Nat Rev Neurol*, vol. 11, no. 2, pp. 69–70, Feb. 2015, doi: 10.1038/nrneurol.2014.257.
[50] M. Lehmann *et al.*, “Diverging patterns of amyloid deposition and hypometabolism in clinical variants of probable Alzheimer’s disease,” *Brain*, vol. 136, no. Pt 3, pp. 844–858, Mar. 2013, doi: 10.1093/brain/aws327.
[51] J. Dronse *et al.*, “In vivo Patterns of Tau Pathology, Amyloid-β Burden, and Neuronal Dysfunction in Clinical Variants of Alzheimer’s Disease,” *J. Alzheimers Dis.*, vol. 55, no. 2, pp. 465–471, 2017, doi: 10.3233/JAD-160316.
[52] K. Kantarci, “Proton MRS in Mild Cognitive Impairment,” *J Magn Reson Imaging*, vol. 37, no. 4, pp. 770–777, Apr. 2013, doi: 10.1002/jmri.23800.
[53] J.-C. Baron *et al.*, “Diagnostic utility of amyloid PET in cerebral amyloid angiopathy-related symptomatic intracerebral hemorrhage,” *J. Cereb. Blood Flow Metab.*, vol. 34, no. 5, pp. 753–758, May 2014, doi: 10.1038/jcbfm.2014.43.
[54] G. D. Rabinovici *et al.*, “Amyloid vs FDG-PET in the differential diagnosis of AD and FTLD,” *Neurology*, vol. 77, no. 23, pp. 2034–2042, Dec. 2011, doi: 10.1212/WNL.0b013e31823b9c5e.
[55] W. J. Jansen *et al.*, “Prevalence of cerebral amyloid pathology in persons without dementia: a meta-analysis,” *JAMA*, vol. 313, no. 19, pp. 1924–1938, May 2015, doi: 10.1001/jama.2015.4668.

[56] R. Ossenkoppele *et al.*, “Prevalence of amyloid PET positivity in dementia syndromes: a meta-analysis,” *JAMA*, vol. 313, no. 19, pp. 1939–1949, May 2015, doi: 10.1001/jama.2015.4669.
[57] H. Cho *et al.*, “Tau PET in Alzheimer disease and mild cognitive impairment,” *Neurology*, vol. 87, no. 4, pp. 375–383, 26 2016, doi: 10.1212/WNL.0000000000002892.
[58] A. J. Schwarz *et al.*, “Regional profiles of the candidate tau PET ligand 18F-AV-1451 recapitulate key features of Braak histopathological stages,” *Brain*, vol. 139, no. Pt 5, pp. 1539–1550, 2016, doi: 10.1093/brain/aww023.
[59] L. Saint-Aubert, L. Lemoine, K. Chiotis, A. Leuzy, E. Rodriguez-Vieitez, and A. Nordberg, “Tau PET imaging: present and future directions,” *Mol Neurodegener*, vol. 12, no. 1, p. 19, 20 2017, doi: 10.1186/s13024-017-0162-3.
[60] L. Iaccarino, A. Sala, S. P. Caminiti, and D. Perani, “The emerging role of PET imaging in dementia,” *F1000Res*, vol. 6, p. 1830, 2017, doi: 10.12688/f1000research.11603.1.
[61] R. E. Gangarosa, J. E. Minnis, J. Nobbe, D. Praschan, and R. W. Genberg, “Operational safety issues in MRI,” *Magn Reson Imaging*, vol. 5, no. 4, pp. 287–292, 1987.
[62] C. Pennanen *et al.*, “Hippocampus and entorhinal cortex in mild cognitive impairment and early AD,” *Neurobiol. Aging*, vol. 25, no. 3, pp. 303–310, Mar. 2004, doi: 10.1016/S0197-4580(03)00084-8.
[63] R. J. Killiany *et al.*, “Use of structural magnetic resonance imaging to predict who will get Alzheimer’s disease,” *Ann. Neurol.*, vol. 47, no. 4, pp. 430–439, Apr. 2000.
[64] C. R. Jack *et al.*, “Prediction of AD with MRI-Based Hippocampal Volume in Mild Cognitive Impairment,” *Neurology*, vol. 52, no. 7, pp. 1397–1403, Apr. 1999.
[65] C. Plant *et al.*, “Automated detection of brain atrophy patterns based on MRI for the prediction of Alzheimer’s disease,” *Neuroimage*, vol. 50, no. 1, pp. 162–174, Mar. 2010, doi: 10.1016/j.neuroimage.2009.11.046.
[66] C. Misra, Y. Fan, and C. Davatzikos, “Baseline and longitudinal patterns of brain atrophy in MCI patients, and their use in prediction of short-term conversion to AD: Results from ADNI,” *Neuroimage*, vol. 44, no. 4, pp. 1415–1422, Feb. 2009, doi: 10.1016/j.neuroimage.2008.10.031.
[67] R. Cuingnet *et al.*, “Automatic classification of patients with Alzheimer’s disease from structural MRI: A comparison of ten methods using the ADNI database,” *NeuroImage*, vol. 56, no. 2, pp. 766–781, May 2011, doi: 10.1016/j.neuroimage.2010.06.013.
[68] R. Wolz *et al.*, “Multi-Method Analysis of MRI Images in Early Diagnostics of Alzheimer’s Disease,” *PLoS One*, vol. 6, no. 10, Oct. 2011, doi: 10.1371/journal.pone.0025446.
[69] X. Da *et al.*, “Integration and relative value of biomarkers for prediction of MCI to AD progression: spatial patterns of brain atrophy, cognitive scores, APOE genotype and CSF biomarkers,” *Neuroimage Clin*, vol. 4, pp. 164–173, 2014, doi: 10.1016/j.nicl.2013.11.010.
[70] J. H. Kordower *et al.*, “Loss and atrophy of layer II entorhinal cortex neurons in elderly people with mild cognitive impairment,” *Ann. Neurol.*, vol. 49, no. 2, pp. 202–213, Feb. 2001.
[71] M. Á. Muñoz-Ruiz *et al.*, “Structural MRI in frontotemporal dementia: comparisons between hippocampal volumetry, tensor-based morphometry and voxel-based morphometry,” *PLoS ONE*, vol. 7, no. 12, p. e52531, 2012, doi: 10.1371/journal.pone.0052531.
[72] C. Möller *et al.*, “Different patterns of cortical gray matter loss over time in behavioral variant frontotemporal dementia and Alzheimer’s disease,” *Neurobiol. Aging*, vol. 38, pp. 21–31, Feb. 2016, doi: 10.1016/j.neurobiolaging.2015.10.020.

[73] J. Jovicich *et al.*, “Reliability in multi-site structural MRI studies: effects of gradient non-linearity correction on phantom and human data,” *Neuroimage*, vol. 30, no. 2, pp. 436–443, Apr. 2006, doi: 10.1016/j.neuroimage.2005.09.046.
[74] J. G. Sled, A. P. Zijdenbos, and A. C. Evans, “A nonparametric method for automatic correction of intensity nonuniformity in MRI data,” *IEEE Trans Med Imaging*, vol. 17, no. 1, pp. 87–97, Feb. 1998, doi: 10.1109/42.668698.
[75] J. L. Gunter *et al.*, “Measurement of MRI scanner performance with the ADNI phantom,” *Med Phys*, vol. 36, no. 6, pp. 2193–2205, Jun. 2009.
[76] D. S. Marcus, A. F. Fotenos, J. G. Csernansky, J. C. Morris, and R. L. Buckner, “Open Access Series of Imaging Studies (OASIS): Longitudinal MRI Data in Nondemented and Demented Older Adults,” *J Cogn Neurosci*, vol. 22, no. 12, pp. 2677–2684, Dec. 2010, doi: 10.1162/jocn.2009.21407.
[77] S. Lovestone *et al.*, “AddNeuroMed--the European collaboration for the discovery of novel biomarkers for Alzheimer’s disease,” *Ann. N. Y. Acad. Sci.*, vol. 1180, pp. 36–46, Oct. 2009, doi: 10.1111/j.1749-6632.2009.05064.x.
[78] E. E. Bron *et al.*, “Standardized evaluation of algorithms for computer-aided diagnosis of dementia based on structural MRI: the CADDementia challenge,” *Neuroimage*, vol. 111, pp. 562–579, May 2015, doi: 10.1016/j.neuroimage.2015.01.048.
[79] J. Lötjönen *et al.*, “Fast and robust extraction of hippocampus from MR images for diagnostics of Alzheimer’s disease,” *NeuroImage*, vol. 56, no. 1, pp. 185–196, May 2011, doi: 10.1016/j.neuroimage.2011.01.062.
[80] K. O. Babalola *et al.*, “Comparison and evaluation of segmentation techniques for subcortical structures in brain MRI,” *Med Image Comput Comput Assist Interv*, vol. 11, no. Pt 1, pp. 409–416, 2008.
[81] B. Fischl *et al.*, “Automatically Parcellating the Human Cerebral Cortex,” *Cereb. Cortex*, vol. 14, no. 1, pp. 11–22, Jan. 2004, doi: 10.1093/cercor/bhg087.
[82] K. Van Leemput *et al.*, “Automated segmentation of hippocampal subfields from ultra-high resolution in vivo MRI,” *Hippocampus*, vol. 19, no. 6, pp. 549–557, Jun. 2009, doi: 10.1002/hipo.20615.
[83] R. A. Morey *et al.*, “A comparison of automated segmentation and manual tracing for quantifying hippocampal and amygdala volumes,” *Neuroimage*, vol. 45, no. 3, pp. 855–866, Apr. 2009, doi: 10.1016/j.neuroimage.2008.12.033.
[84] S. M. Smith *et al.*, “Advances in functional and structural MR image analysis and implementation as FSL,” *Neuroimage*, vol. 23 Suppl 1, pp. S208-219, 2004, doi: 10.1016/j.neuroimage.2004.07.051.
[85] I. Dinov *et al.*, “Neuroimaging study designs, computational analyses and data provenance using the LONI pipeline,” *PLoS ONE*, vol. 5, no. 9, Sep. 2010, doi: 10.1371/journal.pone.0013070.
[86] R. S. Desikan *et al.*, “Automated MRI measures identify individuals with mild cognitive impairment and Alzheimer’s disease,” *Brain*, vol. 132, no. 8, pp. 2048–2057, Aug. 2009, doi: 10.1093/brain/awp123.
[87] S. G. Costafreda *et al.*, “Automated hippocampal shape analysis predicts the onset of dementia in mild cognitive impairment,” *NeuroImage*, vol. 56, no. 1, pp. 212–219, May 2011, doi: 10.1016/j.neuroimage.2011.01.050.
[88] E. Westman *et al.*, “AddNeuroMed and ADNI: similar patterns of Alzheimer’s atrophy and automated MRI classification accuracy in Europe and North America,” *Neuroimage*, vol. 58, no. 3, pp. 818–828, Oct. 2011, doi: 10.1016/j.neuroimage.2011.06.065.
[89] G. B. Karas *et al.*, “A comprehensive study of gray matter loss in patients with Alzheimer’s disease using optimized voxel-based morphometry,” *Neuroimage*, vol. 18, no. 4, pp. 895–907, Apr. 2003.

[90] A. Bakkour, J. C. Morris, and B. C. Dickerson, “The cortical signature of prodromal AD,” *Neurology*, vol. 72, no. 12, pp. 1048–1055, Mar. 2009, doi: 10.1212/01.wnl.0000340981.97664.2f.
[91] R. Simoes, C. Slump, and A. van Cappellen van Walsum, “Using local texture maps of brain MR images to detect Mild Cognitive Impairment,” in *2012 21st International Conference on Pattern Recognition (ICPR)*, Nov. 2012, pp. 153–156.
[92] S. Klöppel *et al.*, “Automatic classification of MR scans in Alzheimer’s disease,” *Brain*, vol. 131, no. 3, pp. 681–689, Mar. 2008, doi: 10.1093/brain/awm319.
[93] P. Vemuri *et al.*, “Alzheimer’s Disease Diagnosis in Individual Subjects using Structural MR Images: Validation Studies,” *Neuroimage*, vol. 39, no. 3, pp. 1186–1197, Feb. 2008, doi: 10.1016/j.neuroimage.2007.09.073.
[94] O. Colliot *et al.*, “Discrimination between Alzheimer Disease, Mild Cognitive Impairment, and Normal Aging by Using Automated Segmentation of the Hippocampus,” *Radiology*, vol. 248, no. 1, pp. 194–201, Jul. 2008, doi: 10.1148/radiol.2481070876.
[95] M. Chupin *et al.*, “Fully Automatic Hippocampus Segmentation and Classification in Alzheimer’s Disease and Mild Cognitive Impairment Applied on Data from ADNI,” *Hippocampus*, vol. 19, no. 6, pp. 579–587, Jun. 2009, doi: 10.1002/hipo.20626.
[96] E. Gerardin *et al.*, “Multidimensional classification of hippocampal shape features discriminates Alzheimer’s disease and mild cognitive impairment from normal aging,” *Neuroimage*, vol. 47, no. 4, pp. 1476–1486, Oct. 2009, doi: 10.1016/j.neuroimage.2009.05.036.
[97] J. L. Whitwell *et al.*, “MRI patterns of atrophy associated with progression to AD in amnestic mild cognitive impairment,” *Neurology*, vol. 70, no. 7, pp. 512–520, Feb. 2008, doi: 10.1212/01.wnl.0000280575.77437.a2.
[98] G. Chételat *et al.*, “Three-dimensional surface mapping of hippocampal atrophy progression from MCI to AD and over normal aging as assessed using voxel-based morphometry,” *Neuropsychologia*, vol. 46, no. 6, pp. 1721–1731, 2008, doi: 10.1016/j.neuropsychologia.2007.11.037.
[99] C. Davatzikos, P. Bhatt, L. M. Shaw, K. N. Batmanghelich, and J. Q. Trojanowski, “Prediction of MCI to AD conversion, via MRI, CSF biomarkers, pattern classification,” *Neurobiol Aging*, vol. 32, no. 12, p. 2322.e19-2322.e27, Dec. 2011, doi: 10.1016/j.neurobiolaging.2010.05.023.
[100] G. Chételat *et al.*, “Using voxel-based morphometry to map the structural changes associated with rapid conversion in MCI: a longitudinal MRI study,” *Neuroimage*, vol. 27, no. 4, pp. 934–946, Oct. 2005, doi: 10.1016/j.neuroimage.2005.05.015.
[101] I. D. Dinov *et al.*, “Applications of the pipeline environment for visual informatics and genomics computations,” *BMC Bioinformatics*, vol. 12, p. 304, Jul. 2011, doi: 10.1186/1471-2105-12-304.
[102] S. W. Moon *et al.*, “Structural Brain Changes in Early-Onset Alzheimer’s Disease Subjects Using the LONI Pipeline Environment,” *J Neuroimaging*, vol. 25, no. 5, pp. 728–737, Sep. 2015, doi: 10.1111/jon.12252.
[103] M. J. Firbank, R. Barber, E. J. Burton, and J. T. O’Brien, “Validation of a fully automated hippocampal segmentation method on patients with dementia,” *Hum. Brain Mapp.*, vol. 29, no. 12, pp. 1442–1449, Dec. 2008, doi: 10.1002/hbm.20480.
[104] A. Mechelli, C. J. Price, and K. J. F. and J. Ashburner, “Voxel-Based Morphometry of the Human Brain: Methods and Applications,” *Current Medical Imaging Reviews*, May 31, 2005. http://www.eurekaselect.com/60128/article (accessed Nov. 03, 2017).
[105] F. Kurth, C. Gaser, and E. Luders, “A 12-step user guide for analyzing voxel-wise gray matter asymmetries in statistical parametric mapping (SPM),” *Nat Protoc*, vol. 10, no. 2, pp. 293–304, Feb. 2015, doi: 10.1038/nprot.2015.014.

[106] M. Afzali and H. Soltanian-Zadeh, “Comparison of voxel-based morphometry (VBM) and tractography of diffusion tensor MRI (DT-MRI) in temporal lobe epilepsy,” in *2010 18th Iranian Conference on Electrical Engineering*, May 2010, pp. 18–23. doi: 10.1109/IRANIANCEE.2010.5507113.
[107] J. Ashburner and K. J. Friston, “Why voxel-based morphometry should be used,” *Neuroimage*, vol. 14, no. 6, pp. 1238–1243, Dec. 2001, doi: 10.1006/nimg.2001.0961.
[108] S. S. Keller and N. Roberts, “Voxel-based morphometry of temporal lobe epilepsy: an introduction and review of the literature,” *Epilepsia*, vol. 49, no. 5, pp. 741–757, May 2008, doi: 10.1111/j.1528-1167.2007.01485.x.
[109] W. J. P. Henneman *et al.*, “Hippocampal atrophy rates in Alzheimer disease: added value over whole brain volume measures,” *Neurology*, vol. 72, no. 11, pp. 999–1007, Mar. 2009, doi: 10.1212/01.wnl.0000344568.09360.31.
[110] M. J. Nitzken, M. F. Casanova, G. Gimelfarb, T. Inanc, J. M. Zurada, and A. El-Baz, “Shape analysis of the human brain: a brief survey,” *IEEE J Biomed Health Inform*, vol. 18, no. 4, pp. 1337–1354, Jul. 2014, doi: 10.1109/JBHI.2014.2298139.
[111] G. Castellano, L. Bonilha, L. M. Li, and F. Cendes, “Texture analysis of medical images,” *Clinical Radiology*, vol. 59, no. 12, pp. 1061–1069, Dec. 2004, doi: 10.1016/j.crad.2004.07.008.
[112] A. Kassner and R. E. Thornhill, “Texture Analysis: A Review of Neurologic MR Imaging Applications,” *AJNR Am J Neuroradiol*, vol. 31, no. 5, pp. 809–816, May 2010, doi: 10.3174/ajnr.A2061.
[113] V. A. Kovalev, F. Kruggel, H. J. Gertz, and D. Y. von Cramon, “Three-dimensional texture analysis of MRI brain datasets,” *IEEE Trans Med Imaging*, vol. 20, no. 5, pp. 424–433, May 2001, doi: 10.1109/42.925295.
[114] K. Laws, “Textured Image Segmentation,” University of Southern California, 1980.
[115] X. Tang, “Texture information in run-length matrices,” *IEEE Transactions on Image Processing*, vol. 7, no. 11, pp. 1602–1609, Nov. 1998, doi: 10.1109/83.725367.
[116] C. C. Reyes-Aldasoro and A. Bhalerao, “Volumetric texture description and discriminant feature selection for MRI,” *Inf Process Med Imaging*, vol. 18, pp. 282–293, Jul. 2003.
[117] C. C. Reyes Aldasoro and A. Bhalerao, “Volumetric texture segmentation by discriminant feature selection and multiresolution classification,” *IEEE Trans Med Imaging*, vol. 26, no. 1, pp. 1–14, Jan. 2007, doi: 10.1109/TMI.2006.884637.
[118] C. C. Reyes-Aldasoro and A. H. Bhalerao, “Volumetric Texture Analysis in Biomedical Imaging,” in *Biomedical Diagnostics and Clinical Technologies: Applying High-Performance Cluster and Grid Computing*, M. Pereira and M. Freire, Eds. IGI Global, 2011, pp. 200–248. Accessed: Apr. 13, 2015. [Online]. Available: http://eprints.dcs.warwick.ac.uk/747/
[119] O. Querbes *et al.*, “Early diagnosis of Alzheimer’s disease using cortical thickness: impact of cognitive reserve,” *Brain*, vol. 132, no. 8, pp. 2036–2047, Aug. 2009, doi: 10.1093/brain/awp105.
[120] C. Galton *et al.*, “Temporal lobe rating scale: application to Alzheimer’s disease and frontotemporal dementia,” *J Neurol Neurosurg Psychiatry*, vol. 70, no. 2, pp. 165–173, Feb. 2001, doi: 10.1136/jnnp.70.2.165.
[121] K. Juottonen, M. P. Laakso, K. Partanen, and H. Soininen, “Comparative MR analysis of the entorhinal cortex and hippocampus in diagnosing Alzheimer disease,” *AJNR Am J Neuroradiol*, vol. 20, no. 1, pp. 139–144, Jan. 1999.
[122] M. P. Laakso *et al.*, “Hippocampus and entorhinal cortex in frontotemporal dementia and Alzheimer’s disease: a morphometric MRI study,” *Biol. Psychiatry*, vol. 47, no. 12, pp. 1056–1063, Jun. 2000.

[123] Y. Xu *et al.*, “Usefulness of MRI measures of entorhinal cortex versus hippocampus in AD,” *Neurology*, vol. 54, no. 9, pp. 1760–1767, May 2000.
[124] A. T. Du *et al.*, “Magnetic resonance imaging of the entorhinal cortex and hippocampus in mild cognitive impairment and Alzheimer’s disease,” *J Neurol Neurosurg Psychiatry*, vol. 71, no. 4, pp. 441–447, Oct. 2001, doi: 10.1136/jnnp.71.4.441.
[125] G. Chetelat and J.-C. Baron, “Early diagnosis of Alzheimer’s disease: contribution of structural neuroimaging,” *Neuroimage*, vol. 18, no. 2, pp. 525–541, Feb. 2003.
[126] L. G. Apostolova *et al.*, “3D comparison of hippocampal atrophy in amnestic mild cognitive impairment and Alzheimer’s disease,” *Brain*, vol. 129, no. Pt 11, pp. 2867–2873, Nov. 2006, doi: 10.1093/brain/awl274.
[127] L. Ferrarini, G. B. Frisoni, M. Pievani, J. H. C. Reiber, R. Ganzola, and J. Milles, “Morphological hippocampal markers for automated detection of Alzheimer’s disease and mild cognitive impairment converters in magnetic resonance images,” *J. Alzheimers Dis.*, vol. 17, no. 3, pp. 643–659, 2009, doi: 10.3233/JAD-2009-1082.
[128] N. Amoroso, R. Errico, and R. Bellotti, “PRISMA-CAD: Fully automated method for Computer-Aided Diagnosis of Dementia based on structural MRI data.,” presented at the MICCAI 2014, Sep. 2014. Accessed: Dec. 22, 2016. [Online]. Available: https://www.researchgate.net/publication/271442240_PRISMA-CAD_Fully_automated_method_for_Computer-Aided_Diagnosis_of_Dementia_based_on_structural_MRI_data
[129] P. A. Freeborough and N. C. Fox, “MR image texture analysis applied to the diagnosis and tracking of Alzheimer’s disease,” *IEEE Trans Med Imaging*, vol. 17, no. 3, pp. 475–479, Jun. 1998, doi: 10.1109/42.712137.
[130] J. Zhang, C. Yu, G. Jiang, W. Liu, and L. Tong, “3D texture analysis on MRI images of Alzheimer’s disease,” *Brain Imaging And Behavior*, vol. 6, no. 1, pp. 61–69, Mar. 2012, doi: 10.1007/s11682-011-9142-3.
[131] M. S. de Oliveira *et al.*, “MR imaging texture analysis of the corpus callosum and thalamus in amnestic mild cognitive impairment and mild Alzheimer disease,” *AJNR Am J Neuroradiol*, vol. 32, no. 1, pp. 60–66, Jan. 2011, doi: 10.3174/ajnr.A2232.
[132] A. Martinez-Torteya, J. Rodriguez-Rojas, J. M. Celaya-Padilla, J. I. Galván-Tejada, V. Treviño, and J. Tamez-Peña, “Magnetization-prepared rapid acquisition with gradient echo magnetic resonance imaging signal and texture features for the prediction of mild cognitive impairment to Alzheimer’s disease progression,” *J. Med. Imag*, vol. 1, no. 3, pp. 031005–031005, 2014, doi: 10.1117/1.JMI.1.3.031005.
[133] H. Xia, L. Tong, X. Zhou, J. Zhang, Z. Zhou, and W. Liu, “Texture Analysis and Volumetry of Hippocampus and Medial Temporal Lobe in Patients with Alzheimer’s Disease,” in *2012 International Conference on Biomedical Engineering and Biotechnology (iCBEB)*, May 2012, pp. 905–908. doi: 10.1109/iCBEB.2012.395.
[134] X. W. Wei Fang Liu, “3D Texture Analysis of Corpus Caliosum Based on MR Images Inpatients with Alzheimer’s Disease and Mild Cognitive Impairment,” *Applied Mechanics and Materials*, vol. 533, pp. 415–420, 2014, doi: 10.4028/www.scientific.net/AMM.533.415.
[135] X. Li, H. Xia, Z. Zhou, and L. Tong, “3D texture analysis of hippocampus based on MR images in patients with alzheimer disease and mild cognitive impairment,” in *2010 3rd International Conference on Biomedical Engineering and Informatics (BMEI)*, Oct. 2010, vol. 1, pp. 1–4. doi: 10.1109/BMEI.2010.5639520.
[136] X. Zhou, Z. Liu, Z. Zhou, and H. Xia, “Study on texture characteristics of hippocampus in MR images of patients with Alzheimer’s Disease,” in *2010 3rd International Conference on Biomedical Engineering and Informatics (BMEI)*, Oct. 2010, vol. 2, pp. 593–596. doi: 10.1109/BMEI.2010.5640016.

[137] C. Salvatore *et al.*, “Magnetic resonance imaging biomarkers for the early diagnosis of Alzheimer’s disease: a machine learning approach,” *Front Neurosci*, vol. 9, p. 307, 2015, doi: 10.3389/fnins.2015.00307.
[138] T.-Y. Kim, J. Son, and K.-G. Kim, “The Recent Progress in Quantitative Medical Image Analysis for Computer Aided Diagnosis Systems,” *Healthc Inform Res*, vol. 17, no. 3, pp. 143–149, Sep. 2011, doi: 10.4258/hir.2011.17.3.143.
[139] M. Blas, S. Turk, and M. Pohar Perme, “Comparison of logistic regression and linear discriminant analysis : a simulation study,” *Metodološki zvezki*, vol. 1, no. 1, pp. 143–161, 2004.
[140] V. N. Vapnik, “An overview of statistical learning theory,” *IEEE Trans Neural Netw*, vol. 10, no. 5, pp. 988–999, 1999, doi: 10.1109/72.788640.
[141] L. Auria and R. A. Moro, “Support Vector Machines (SVM) as a Technique for Solvency Analysis,” DIW Berlin, German Institute for Economic Research, 811, 2008. Accessed: Nov. 10, 2017. [Online]. Available: https://ideas.repec.org/p/diw/diwwpp/dp811.html
[142] A. K. Jain, R. P. W. Duin, and J. Mao, “Statistical pattern recognition: a review,” *IEEE Transactions on Pattern Analysis and Machine Intelligence*, vol. 22, no. 1, pp. 4–37, Jan. 2000, doi: 10.1109/34.824819.
[143] J. V. Tu, “Advantages and disadvantages of using artificial neural networks versus logistic regression for predicting medical outcomes,” *Journal of Clinical Epidemiology*, vol. 49, no. 11, pp. 1225–1231, Nov. 1996, doi: 10.1016/S0895-4356(96)00002-9.
[144] R. A. Fisher, “The Use of Multiple Measurements in Taxonomic Problems.,” 1936, Accessed: Jul. 24, 2016. [Online]. Available: https://digital.library.adelaide.edu.au/dspace/handle/2440/15227
[145] J. P. Lerch *et al.*, “Automated cortical thickness measurements from MRI can accurately separate Alzheimer’s patients from normal elderly controls,” *Neurobiol. Aging*, vol. 29, no. 1, pp. 23–30, Jan. 2008, doi: 10.1016/j.neurobiolaging.2006.09.013.
[146] D. A. Freedman, “Statistical Models,” *Cambridge University Press*, 2009. http://www.goodreads.com/work/best_book/9620152-statistical-models-theory-and-practice (accessed Aug. 23, 2016).
[147] L. deToledo-Morrell *et al.*, “MRI-derived entorhinal volume is a good predictor of conversion from MCI to AD,” *Neurobiol. Aging*, vol. 25, no. 9, pp. 1197–1203, Oct. 2004, doi: 10.1016/j.neurobiolaging.2003.12.007.
[148] C. Cortes and V. Vapnik, “Support-Vector Networks,” *Machine Learning*, vol. 20, no. 3, pp. 273–297, doi: 10.1023/A:1022627411411.
[149] M. C. Evans *et al.*, “Volume changes in Alzheimer’s disease and mild cognitive impairment: cognitive associations,” *Eur Radiol*, vol. 20, no. 3, pp. 674–682, Mar. 2010, doi: 10.1007/s00330-009-1581-5.
[150] G. F. Busatto *et al.*, “A voxel-based morphometry study of temporal lobe gray matter reductions in Alzheimer’s disease,” *Neurobiol. Aging*, vol. 24, no. 2, pp. 221–231, Apr. 2003.
[151] K. Juottonen *et al.*, “Volumes of the entorhinal and perirhinal cortices in Alzheimer’s disease,” *Neurobiol. Aging*, vol. 19, no. 1, pp. 15–22, Feb. 1998.
[152] R. J. Killiany, M. B. Moss, M. S. Albert, T. Sandor, J. Tieman, and F. Jolesz, “Temporal lobe regions on magnetic resonance imaging identify patients with early Alzheimer’s disease,” *Arch. Neurol.*, vol. 50, no. 9, pp. 949–954, Sep. 1993.
[153] E. Braak, K. Griffing, K. Arai, J. Bohl, H. Bratzke, and H. Braak, “Neuropathology of Alzheimer’s disease: what is new since A. Alzheimer?,” *Eur Arch Psychiatry Clin Neurosci*, vol. 249 Suppl 3, pp. 14–22, 1999.

[154] G. B. Karas *et al.*, “Global and local gray matter loss in mild cognitive impairment and Alzheimer’s disease,” *Neuroimage*, vol. 23, no. 2, pp. 708–716, Oct. 2004, doi: 10.1016/j.neuroimage.2004.07.006.
[155] N. Schuff *et al.*, “MRI of hippocampal volume loss in early Alzheimer’s disease in relation to ApoE genotype and biomarkers,” *Brain*, vol. 132, no. Pt 4, pp. 1067–1077, Apr. 2009, doi: 10.1093/brain/awp007.
[156] J. H. Morra *et al.*, “Validation of a fully automated 3D hippocampal segmentation method using subjects with Alzheimer’s disease mild cognitive impairment, and elderly controls,” *NeuroImage*, vol. 43, no. 1, pp. 59–68, Oct. 2008, doi: 10.1016/j.neuroimage.2008.07.003.
[157] C. R. Jack *et al.*, “Medial Temporal Atrophy on MRI in Normal Aging and Very Mild Alzheimer’s Disease,” *Neurology*, vol. 49, no. 3, pp. 786–794, Sep. 1997.
[158] M. Chupin *et al.*, “Anatomically constrained region deformation for the automated segmentation of the hippocampus and the amygdala: Method and validation on controls and patients with Alzheimer’s disease,” *NeuroImage*, vol. 34, no. 3, pp. 996–1019, Feb. 2007, doi: 10.1016/j.neuroimage.2006.10.035.
[159] “ADNI | Alzheimer’s Disease Neuroimaging Initiative.” http://adni.loni.usc.edu/ (accessed Sep. 12, 2015).
[160] C. R. Jack *et al.*, “11C PiB and Structural MRI Provide Complementary Information in Imaging of AD and Amnestic MCI,” *Brain*, vol. 131, no. Pt 3, pp. 665–680, Mar. 2008, doi: 10.1093/brain/awm336.
[161] Y. Li *et al.*, “Regional analysis of FDG and PIB-PET images in normal aging, mild cognitive impairment, and Alzheimer’s disease,” *Eur. J. Nucl. Med. Mol. Imaging*, vol. 35, no. 12, pp. 2169–2181, Dec. 2008, doi: 10.1007/s00259-008-0833-y.
[162] G. W. Small *et al.*, “PET of brain amyloid and tau in mild cognitive impairment,” *N. Engl. J. Med.*, vol. 355, no. 25, pp. 2652–2663, Dec. 2006, doi: 10.1056/NEJMoa054625.
[163] C. Davatzikos, Y. Fan, X. Wu, D. Shen, and S. M. Resnick, “Detection of Prodromal Alzheimer’s Disease via Pattern Classification of MRI,” *Neurobiol Aging*, vol. 29, no. 4, pp. 514–523, Apr. 2008, doi: 10.1016/j.neurobiolaging.2006.11.010.
[164] M. J. West, C. H. Kawas, W. F. Stewart, G. L. Rudow, and J. C. Troncoso, “Hippocampal neurons in pre-clinical Alzheimer’s disease,” *Neurobiol. Aging*, vol. 25, no. 9, pp. 1205–1212, Oct. 2004, doi: 10.1016/j.neurobiolaging.2003.12.005.
[165] G. B. Frisoni, F. Sabattoli, A. D. Lee, R. A. Dutton, A. W. Toga, and P. M. Thompson, “In vivo neuropathology of the hippocampal formation in AD: a radial mapping MR-based study,” *Neuroimage*, vol. 32, no. 1, pp. 104–110, Aug. 2006, doi: 10.1016/j.neuroimage.2006.03.015.
[166] P. M. Szczypiński, M. Strzelecki, A. Materka, and A. Klepaczko, “MaZda--a software package for image texture analysis,” *Comput Methods Programs Biomed*, vol. 94, no. 1, pp. 66–76, Apr. 2009, doi: 10.1016/j.cmpb.2008.08.005.
[167] T. Kaeriyama, N. Kodama, T. Shimada, and I. Fukumoto, “[Application of run length matrix to magnetic resonance imaging diagnosis of Alzheimer-type dementia],” *Nihon Hoshasen Gijutsu Gakkai Zasshi*, vol. 58, no. 11, pp. 1502–1508, Nov. 2002.
[168] N. Kodama, Y. Kawase, and K. Okamoto, “Application of Texture Analysis to Differentiation of Dementia with Lewy Bodies from Alzheimer’s Disease on Magnetic Resonance Images,” in *World Congress on Medical Physics and Biomedical Engineering 2006*, Springer, Berlin, Heidelberg, 2007, pp. 1444–1446. doi: 10.1007/978-3-540-36841-0_354.
[169] B. Reisberg *et al.*, “Stage-specific behavioral, cognitive, and in vivo changes in community residing subjects with age-associated memory impairment and primary

degenerative dementia of the Alzheimer type," *Drug Dev. Res.*, vol. 15, no. 2–3, pp. 101–114, Jan. 1988, doi: 10.1002/ddr.430150203.
[170] S. Duchesne, C. Bocti, K. De Sousa, G. B. Frisoni, H. Chertkow, and D. L. Collins, "Amnestic MCI future clinical status prediction using baseline MRI features," *Neurobiol. Aging*, vol. 31, no. 9, pp. 1606–1617, Sep. 2010, doi: 10.1016/j.neurobiolaging.2008.09.003.
[171] J. Koikkalainen *et al.*, "Multi-template tensor-based morphometry: application to analysis of Alzheimer's disease," *Neuroimage*, vol. 56, no. 3, pp. 1134–1144, Jun. 2011, doi: 10.1016/j.neuroimage.2011.03.029.
[172] S. J. Lupien *et al.*, "Hippocampal volume is as variable in young as in older adults: implications for the notion of hippocampal atrophy in humans," *Neuroimage*, vol. 34, no. 2, pp. 479–485, Jan. 2007, doi: 10.1016/j.neuroimage.2006.09.041.
[173] T. Tapiola *et al.*, "MRI of hippocampus and entorhinal cortex in mild cognitive impairment: a follow-up study," *Neurobiol. Aging*, vol. 29, no. 1, pp. 31–38, Jan. 2008, doi: 10.1016/j.neurobiolaging.2006.09.007.
[174] D. P. Devanand *et al.*, "Hippocampal and entorhinal atrophy in mild cognitive impairment: prediction of Alzheimer disease," *Neurology*, vol. 68, no. 11, pp. 828–836, Mar. 2007, doi: 10.1212/01.wnl.0000256697.20968.d7.
[175] C. R. Jack *et al.*, "Brain atrophy rates predict subsequent clinical conversion in normal elderly and amnestic MCI," *Neurology*, vol. 65, no. 8, pp. 1227–1231, Oct. 2005, doi: 10.1212/01.wnl.0000180958.22678.91.
[176] S. F. Eskildsen, P. Coupé, D. García-Lorenzo, V. Fonov, J. C. Pruessner, and D. L. Collins, "Prediction of Alzheimer's disease in subjects with mild cognitive impairment from the ADNI cohort using patterns of cortical thinning," *NeuroImage*, vol. 65, pp. 511–521, Jan. 2013, doi: 10.1016/j.neuroimage.2012.09.058.
[177] R. S. Desikan *et al.*, "Automated MRI measures predict progression to Alzheimer's disease," *Neurobiol Aging*, vol. 31, no. 8, pp. 1364–1374, Aug. 2010, doi: 10.1016/j.neurobiolaging.2010.04.023.
[178] P. Vemuri *et al.*, "MRI and CSF biomarkers in normal, MCI, and AD subjects," *Neurology*, vol. 73, no. 4, pp. 294–301, Jul. 2009, doi: 10.1212/WNL.0b013e3181af79fb.
[179] J. G. Csernansky *et al.*, "Preclinical detection of Alzheimer's disease: hippocampal shape and volume predict dementia onset in the elderly," *Neuroimage*, vol. 25, no. 3, pp. 783–792, Apr. 2005, doi: 10.1016/j.neuroimage.2004.12.036.
[180] L. G. Apostolova *et al.*, "Conversion of mild cognitive impairment to Alzheimer disease predicted by hippocampal atrophy maps," *Arch. Neurol.*, vol. 63, no. 5, pp. 693–699, May 2006, doi: 10.1001/archneur.63.5.693.
[181] J. H. Morra *et al.*, "Automated mapping of hippocampal atrophy in 1-year repeat MRI data from 490 subjects with Alzheimer's disease, mild cognitive impairment, and elderly controls," *Neuroimage*, vol. 45, no. 1 Suppl, pp. S3-15, Mar. 2009, doi: 10.1016/j.neuroimage.2008.10.043.
[182] T. Gómez-Isla *et al.*, "Neuronal loss correlates with but exceeds neurofibrillary tangles in Alzheimer's disease," *Ann. Neurol.*, vol. 41, no. 1, pp. 17–24, Jan. 1997, doi: 10.1002/ana.410410106.
[183] T. Gómez-Isla, J. L. Price, D. W. McKeel, J. C. Morris, J. H. Growdon, and B. T. Hyman, "Profound loss of layer II entorhinal cortex neurons occurs in very mild Alzheimer's disease," *J. Neurosci.*, vol. 16, no. 14, pp. 4491–4500, Jul. 1996.
[184] C. R. McDonald *et al.*, "Regional rates of neocortical atrophy from normal aging to early Alzheimer disease," *Neurology*, vol. 73, no. 6, pp. 457–465, Aug. 2009, doi: 10.1212/WNL.0b013e3181b16431.

[185] N. C. Fox, R. I. Scahill, W. R. Crum, and M. N. Rossor, “Correlation between rates of brain atrophy and cognitive decline in AD,” *Neurology*, vol. 52, no. 8, pp. 1687–1687, May 1999, doi: 10.1212/WNL.52.8.1687.
[186] C. R. Jack *et al.*, “The Alzheimer’s disease neuroimaging initiative (ADNI): MRI methods,” *J. Magn. Reson. Imaging*, vol. 27, no. 4, pp. 685–691, Apr. 2008, doi: 10.1002/jmri.21049.
[187] P. A. Narayana, W. W. Brey, M. V. Kulkarni, and C. L. Sievenpiper, “Compensation for surface coil sensitivity variation in magnetic resonance imaging,” *Magn Reson Imaging*, vol. 6, no. 3, pp. 271–274, Jun. 1988.
[188] B. Fischl *et al.*, “Whole brain segmentation: automated labeling of neuroanatomical structures in the human brain,” *Neuron*, vol. 33, no. 3, pp. 341–355, Jan. 2002.
[189] D. L. Collins, P. Neelin, T. M. Peters, and A. C. Evans, “Automatic 3D intersubject registration of MR volumetric data in standardized Talairach space,” *J Comput Assist Tomogr*, vol. 18, no. 2, pp. 192–205, Apr. 1994.
[190] B. Fischl and A. M. Dale, “Measuring the thickness of the human cerebral cortex from magnetic resonance images,” *Proc. Natl. Acad. Sci. U.S.A.*, vol. 97, no. 20, pp. 11050–11055, Sep. 2000, doi: 10.1073/pnas.200033797.
[191] B. Fischl *et al.*, “Automatically parcellating the human cerebral cortex,” *Cereb. Cortex*, vol. 14, no. 1, pp. 11–22, Jan. 2004.
[192] C. R. Jack, R. C. Petersen, P. C. O’Brien, and E. G. Tangalos, “MR-based hippocampal volumetry in the diagnosis of Alzheimer’s disease,” *Neurology*, vol. 42, no. 1, pp. 183–183, Jan. 1992, doi: 10.1212/WNL.42.1.183.
[193] T. Du A *et al.*, “Magnetic resonance imaging of the entorhinal cortex and hippocampus in mild cognitive impairment and Alzheimer’s disease,” *J Neurol Neurosurg Psychiatry*, vol. 71, no. 4, pp. 441–447, Oct. 2001, doi: 10.1136/jnnp.71.4.441.
[194] G. M. McKhann *et al.*, “The diagnosis of dementia due to Alzheimer’s disease: Recommendations from the National Institute on Aging-Alzheimer’s Association workgroups on diagnostic guidelines for Alzheimer’s disease,” *Alzheimers Dement*, vol. 7, no. 3, pp. 263–269, May 2011, doi: 10.1016/j.jalz.2011.03.005.
[195] M. W. Weiner *et al.*, “The Alzheimer’s Disease Neuroimaging Initiative: Progress report and future plans,” *Alzheimers Dement*, vol. 6, no. 3, pp. 202–11.e7, May 2010, doi: 10.1016/j.jalz.2010.03.007.
[196] S. F. Eskildsen, P. Coupé, D. García-Lorenzo, V. Fonov, J. C. Pruessner, and D. L. Collins, “Prediction of Alzheimer’s disease in subjects with mild cognitive impairment from the ADNI cohort using patterns of cortical thinning,” *Neuroimage*, vol. 65, pp. 511–521, Jan. 2013, doi: 10.1016/j.neuroimage.2012.09.058.
[197] B. T. Wyman *et al.*, “Standardization of Analysis Sets for Reporting Results from ADNI MRI Data,” *Alzheimers Dement*, vol. 9, no. 3, pp. 332–337, May 2013, doi: 10.1016/j.jalz.2012.06.004.
[198] C. R. Jack *et al.*, “Update on the MRI Core of the Alzheimer’s Disease Neuroimaging Initiative,” *Alzheimers Dement*, vol. 6, no. 3, pp. 212–220, May 2010, doi: 10.1016/j.jalz.2010.03.004.
[199] R. W. Elwood, “The Wechsler Memory Scale—Revised: Psychometric characteristics and clinical application,” *Neuropsychol Rev*, vol. 2, no. 2, pp. 179–201, Jun. 1991, doi: 10.1007/BF01109053.
[200] G. McKhann, D. Drachman, M. Folstein, R. Katzman, D. Price, and E. M. Stadlan, “Clinical diagnosis of Alzheimer’s disease Report of the NINCDS-ADRDA Work Group* under the auspices of Department of Health and Human Services Task Force on Alzheimer’s Disease,” *Neurology*, vol. 34, no. 7, pp. 939–939, Jul. 1984, doi: 10.1212/WNL.34.7.939.

[201] A. Materka, “Texture analysis methodologies for magnetic resonance imaging,” *Dialogues Clin Neurosci*, vol. 6, no. 2, pp. 243–250, Jun. 2004.
[202] A. Materka and M. Strzelecki, “On the importance of MRI nonuniformity correction for texture analysis,” in *2013 Signal Processing: Algorithms, Architectures, Arrangements, and Applications (SPA)*, Sep. 2013, pp. 118–123.
[203] B. Belaroussi, J. Milles, S. Carme, Y. M. Zhu, and H. Benoit-Cattin, “Intensity non-uniformity correction in MRI: existing methods and their validation,” *Med Image Anal*, vol. 10, no. 2, pp. 234–246, Apr. 2006, doi: 10.1016/j.media.2005.09.004.
[204] P. Prasanna, P. Tiwari, and A. Madabhushi, “Co-occurrence of Local Anisotropic Gradient Orientations (CoLlAGe): A new radiomics descriptor,” *Sci Rep*, vol. 6, Nov. 2016, doi: 10.1038/srep37241.
[205] E. Grossner, R. Bernier, E. Brenner, K. Chiou, and F. Hillary, “Prefrontal gray matter volume predicts metacognitive accuracy following traumatic brain injury,” *Neuropsychology*, vol. 32, pp. 484–494, May 2018, doi: 10.1037/neu0000446.
[206] A. M. Dale, B. Fischl, and M. I. Sereno, “Cortical surface-based analysis. I. Segmentation and surface reconstruction,” *Neuroimage*, vol. 9, no. 2, pp. 179–194, Feb. 1999, doi: 10.1006/nimg.1998.0395.
[207] A. M. Dale and M. I. Sereno, “Improved Localizadon of Cortical Activity by Combining EEG and MEG with MRI Cortical Surface Reconstruction: A Linear Approach,” *Journal of Cognitive Neuroscience*, vol. 5, no. 2, pp. 162–176, Apr. 1993, doi: 10.1162/jocn.1993.5.2.162.
[208] B. Fischl, A. Liu, and A. M. Dale, “Automated manifold surgery: constructing geometrically accurate and topologically correct models of the human cerebral cortex,” *IEEE Trans Med Imaging*, vol. 20, no. 1, pp. 70–80, Jan. 2001, doi: 10.1109/42.906426.
[209] B. Fischl, M. I. Sereno, R. B. Tootell, and A. M. Dale, “High-resolution intersubject averaging and a coordinate system for the cortical surface,” *Hum Brain Mapp*, vol. 8, no. 4, pp. 272–284, 1999.
[210] F. Segonne, J. Pacheco, and B. Fischl, “Geometrically Accurate Topology-Correction of Cortical Surfaces Using Nonseparating Loops,” *IEEE Transactions on Medical Imaging*, vol. 26, no. 4, pp. 518–529, Apr. 2007, doi: 10.1109/TMI.2006.887364.
[211] M. Reuter and B. Fischl, “Avoiding asymmetry-induced bias in longitudinal image processing,” *NeuroImage*, vol. 57, no. 1, pp. 19–21, Jul. 2011, doi: 10.1016/j.neuroimage.2011.02.076.
[212] M. Reuter, N. J. Schmansky, H. D. Rosas, and B. Fischl, “Within-subject template estimation for unbiased longitudinal image analysis,” *Neuroimage*, vol. 61, no. 4, pp. 1402–1418, Jul. 2012, doi: 10.1016/j.neuroimage.2012.02.084.
[213] X. Han *et al.*, “Reliability of MRI-derived measurements of human cerebral cortical thickness: the effects of field strength, scanner upgrade and manufacturer,” *Neuroimage*, vol. 32, no. 1, pp. 180–194, Aug. 2006, doi: 10.1016/j.neuroimage.2006.02.051.
[214] J.-H. Cai *et al.*, “Magnetic Resonance Texture Analysis in Alzheimer’s disease,” *Academic Radiology*, Feb. 2020, doi: 10.1016/j.acra.2020.01.006.
[215] M. R. Berthold *et al.*, “KNIME: The Konstanz Information Miner,” in *Data Analysis, Machine Learning and Applications*, 2008, pp. 319–326.
[216] R. M. Haralick, K. Shanmugam, and I. Dinstein, “Textural Features for Image Classification,” *IEEE Transactions on Systems, Man and Cybernetics*, vol. SMC-3, no. 6, pp. 610–621, Nov. 1973, doi: 10.1109/TSMC.1973.4309314.
[217] C. C. Reyes-Aldasoro, “A guide to co-occurrence matrix analysis,” University of Warwick. Department of Computer Science, Report Number 398, Feb. 2004. Accessed: Jan. 31, 2021. [Online]. Available: https://wrap.warwick.ac.uk/61393/

[218] L. Breiman, J. Friedman, C. J. Stone, and R. A. Olshen, *Classification and Regression Trees*. Taylor & Francis, 1984.
[219] A. Sarica, A. Cerasa, and A. Quattrone, "Random Forest Algorithm for the Classification of Neuroimaging Data in Alzheimer's Disease: A Systematic Review," *Front Aging Neurosci*, vol. 9, p. 329, 2017, doi: 10.3389/fnagi.2017.00329.
[220] N. Chow *et al.*, "Comparing 3T and 1.5T MRI for Mapping Hippocampal Atrophy in the Alzheimer's Disease Neuroimaging Initiative," *AJNR Am J Neuroradiol*, vol. 36, no. 4, pp. 653–660, Apr. 2015, doi: 10.3174/ajnr.A4228.
[221] M. A. Bernstein, J. Huston, and H. A. Ward, "Imaging artifacts at 3.0T," *J Magn Reson Imaging*, vol. 24, no. 4, pp. 735–746, Oct. 2006, doi: 10.1002/jmri.20698.
[222] J. F. Schenck, "The role of magnetic susceptibility in magnetic resonance imaging: MRI magnetic compatibility of the first and second kinds," *Med Phys*, vol. 23, no. 6, pp. 815–850, Jun. 1996, doi: 10.1118/1.597854.
[223] C. C. Luk *et al.*, "Alzheimer's disease: 3-Dimensional MRI texture for prediction of conversion from mild cognitive impairment," *Alzheimers Dement (Amst)*, vol. 10, pp. 755–763, Nov. 2018, doi: 10.1016/j.dadm.2018.09.002.
[224] S. G. Costafreda *et al.*, "Automated hippocampal shape analysis predicts the onset of dementia in mild cognitive impairment," *NeuroImage*, vol. 56, no. 1, pp. 212–219, May 2011, doi: 10.1016/j.neuroimage.2011.01.050.
[225] R. S. Briellmann, A. Syngeniotis, and G. D. Jackson, "Comparison of hippocampal volumetry at 1.5 tesla and at 3 tesla," *Epilepsia*, vol. 42, no. 8, pp. 1021–1024, Aug. 2001, doi: 10.1046/j.1528-1157.2001.0420081021.x.
[226] A. J. Ho *et al.*, "Comparing 3 T and 1.5 T MRI for tracking Alzheimer's disease progression with tensor-based morphometry," *Human Brain Mapping*, vol. 31, no. 4, pp. 499–514, 2010, doi: 10.1002/hbm.20882.
[227] K. E. Macdonald *et al.*, "Automated Template-Based Hippocampal Segmentations from MRI: The Effects of 1.5T or 3T Field Strength on Accuracy," *Neuroinform*, vol. 12, no. 3, pp. 405–412, Jul. 2014, doi: 10.1007/s12021-013-9217-y.
[228] E. Busovaca *et al.*, "Is the Alzheimer's disease cortical thickness signature a biological marker for memory?," *Brain Imaging Behav*, vol. 10, no. 2, pp. 517–523, Jun. 2016, doi: 10.1007/s11682-015-9413-5.
[229] B. C. Dickerson *et al.*, "Alzheimer-signature MRI biomarker predicts AD dementia in cognitively normal adults," *Neurology*, vol. 76, no. 16, pp. 1395–1402, Apr. 2011, doi: 10.1212/WNL.0b013e3182166e96.
[230] S. P. Poulin, R. Dautoff, J. C. Morris, L. F. Barrett, and B. C. Dickerson, "Amygdala atrophy is prominent in early Alzheimer's disease and relates to symptom severity," *Psychiatry Res*, vol. 194, no. 1, pp. 7–13, Oct. 2011, doi: 10.1016/j.pscychresns.2011.06.014.
[231] A. J. Ho *et al.*, "Comparing 3 T and 1.5 T MRI for Tracking Alzheimer's Disease Progression with Tensor-Based Morphometry," *Hum Brain Mapp*, vol. 31, no. 4, pp. 499–514, Apr. 2010, doi: 10.1002/hbm.20882.
[232] S. Lee, H. Lee, K. W. Kim, and Alzheimer's Disease Neuroimaging Initiative, "Magnetic resonance imaging texture predicts progression to dementia due to Alzheimer disease earlier than hippocampal volume," *J Psychiatry Neurosci*, vol. 45, no. 1, pp. 7–14, 01 2020, doi: 10.1503/jpn.180171.
[233] D. L. Campbell, H. Kang, and S. Shokouhi, "Application of Haralick texture features in brain [18F]-florbetapir positron emission tomography without reference region normalization," *Clin Interv Aging*, vol. 12, pp. 2077–2086, Dec. 2017, doi: 10.2147/CIA.S143307.

[234] N. Gao *et al.*, “Contourlet-based hippocampal magnetic resonance imaging texture features for multivariant classification and prediction of Alzheimer’s disease,” *Metab Brain Dis*, vol. 33, no. 6, pp. 1899–1909, Dec. 2018, doi: 10.1007/s11011-018-0296-1.
[235] A. J. Ho *et al.*, “Comparing 3 T and 1.5 T MRI for Tracking Alzheimer’s Disease Progression with Tensor-Based Morphometry,” *Hum Brain Mapp*, vol. 31, no. 4, pp. 499–514, Apr. 2010, doi: 10.1002/hbm.20882.
[236] S. Leandrou, S. Petroudi, C. C. Reyes-Aldasoro, P. A. Kyriacou, and C. S. Pattichis, “Quantitative MRI Brain Studies in Mild Cognitive Impairment and Alzheimer #x0027;s disease: A Methodological Review,” *IEEE Reviews in Biomedical Engineering*, vol. PP, no. 99, pp. 1–1, 2018, doi: 10.1109/RBME.2018.2796598.
[237] M. Zhou, F. Zhang, L. Zhao, J. Qian, and C. Dong, “Entorhinal cortex: a good biomarker of mild cognitive impairment and mild Alzheimer’s disease,” *Rev Neurosci*, vol. 27, no. 2, pp. 185–195, Feb. 2016, doi: 10.1515/revneuro-2015-0019.
[238] S. Y. Ryu *et al.*, “Hippocampal and entorhinal structures in subjective memory impairment: a combined MRI volumetric and DTI study,” *Int Psychogeriatr*, vol. 29, no. 5, pp. 785–792, 2017, doi: 10.1017/S1041610216002349.
[239] E. R. DeLong, D. M. DeLong, and D. L. Clarke-Pearson, “Comparing the Areas under Two or More Correlated Receiver Operating Characteristic Curves: A Nonparametric Approach,” *Biometrics*, vol. 44, no. 3, pp. 837–845, 1988, doi: 10.2307/2531595.
[240] S. G. Mueller, N. Schuff, K. Yaffe, C. Madison, B. Miller, and M. W. Weiner, “Hippocampal atrophy patterns in mild cognitive impairment and Alzheimer’s disease,” *Hum Brain Mapp*, vol. 31, no. 9, pp. 1339–1347, Sep. 2010, doi: 10.1002/hbm.20934.
[241] W. Khan *et al.*, “Automated Hippocampal Subfield Measures as Predictors of Conversion from Mild Cognitive Impairment to Alzheimer’s Disease in Two Independent Cohorts,” *Brain Topogr*, vol. 28, no. 5, pp. 746–759, Sep. 2015, doi: 10.1007/s10548-014-0415-1.
[242] E.-J. Hwang *et al.*, “Texture analyses of quantitative susceptibility maps to differentiate Alzheimer’s disease from cognitive normal and mild cognitive impairment,” *Med Phys*, vol. 43, no. 8, p. 4718, Aug. 2016, doi: 10.1118/1.4958959.
[243] A. Chincarini *et al.*, “Local MRI analysis approach in the diagnosis of early and prodromal Alzheimer’s disease,” *Neuroimage*, vol. 58, no. 2, pp. 469–480, Sep. 2011, doi: 10.1016/j.neuroimage.2011.05.083.
[244] S. Leandrou, S. Petroudi, P. A. Kyriacou, C. C. Reyes-Aldasoro, and C. S. Pattichis, “Quantitative MRI Brain Studies in Mild Cognitive Impairment and Alzheimer’s Disease: A Methodological Review,” *IEEE Reviews in Biomedical Engineering*, vol. 11, pp. 97–111, 2018, doi: 10.1109/RBME.2018.2796598.
[245] S. Leandrou, D. Lamnisos, P. A. Kyriacou, S. Constanti, and C. S. Pattichis, “Comparison of 1.5 T and 3 T MRI hippocampus texture features in the assessment of Alzheimer’s disease,” *Biomedical Signal Processing and Control*, vol. 62, p. 102098, Sep. 2020, doi: 10.1016/j.bspc.2020.102098.
[246] S. Leandrou, D. Lamnisos, I. Mamais, P. A. Kyriacou, C. S. Pattichis, and for the A. D. and N. Initiative, “Assessment of Alzheimer’s Disease Based on Texture Analysis of the Entorhinal Cortex,” *Front. Aging Neurosci.*, vol. 12, 2020, doi: 10.3389/fnagi.2020.00176.
[247] M. L. Schroeter, T. Stein, N. Maslowski, and J. Neumann, “Neural correlates of Alzheimer’s disease and mild cognitive impairment: a systematic and quantitative meta-analysis involving 1351 patients,” *Neuroimage*, vol. 47, no. 4, pp. 1196–1206, Oct. 2009, doi: 10.1016/j.neuroimage.2009.05.037.
[248] Y. Yuan, Z.-X. Gu, and W.-S. Wei, “Fluorodeoxyglucose-positron-emission tomography, single-photon emission tomography, and structural MR imaging for

prediction of rapid conversion to Alzheimer disease in patients with mild cognitive impairment: a meta-analysis," *AJNR Am J Neuroradiol*, vol. 30, no. 2, pp. 404–410, Feb. 2009, doi: 10.3174/ajnr.A1357.

[249] C. R. Jack *et al.*, "Serial PIB and MRI in normal, mild cognitive impairment and Alzheimer's disease: implications for sequence of pathological events in Alzheimer's disease," *Brain*, vol. 132, no. 5, pp. 1355–1365, May 2009, doi: 10.1093/brain/awp062.

[250] C. Marcus, E. Mena, and R. M. Subramaniam, "Brain PET in the Diagnosis of Alzheimer's Disease," *Clin Nucl Med*, vol. 39, no. 10, pp. e413–e426, Oct. 2014, doi: 10.1097/RLU.0000000000000547.

[251] Y. LeCun, Y. Bengio, and G. Hinton, "Deep learning," *Nature*, vol. 521, no. 7553, pp. 436–444, May 2015, doi: 10.1038/nature14539.

[252] T. Jo, K. Nho, and A. J. Saykin, "Deep Learning in Alzheimer's Disease: Diagnostic Classification and Prognostic Prediction Using Neuroimaging Data," *Front. Aging Neurosci.*, vol. 11, 2019, doi: 10.3389/fnagi.2019.00220.

[253] K. G. Achilleos, S. Leandrou, N. Prentzas, P. A. Kyriacou, A. C. Kakas, and C. S. Pattichis, "Extracting Explainable Assessments of Alzheimer's disease via Machine Learning on brain MRI imaging data," in *2020 IEEE 20th International Conference on Bioinformatics and Bioengineering (BIBE)*, Oct. 2020, pp. 1036–1041. doi: 10.1109/BIBE50027.2020.00175.

[254] V. Julkunen *et al.*, "Cortical thickness analysis to detect progressive mild cognitive impairment: a reference to Alzheimer's disease," *Dement Geriatr Cogn Disord*, vol. 28, no. 5, pp. 404–412, 2009, doi: 10.1159/000256274.

[255] A. Martínez-Torteya, V. Treviño, and J. G. Tamez-Peña, "Improved Diagnostic Multimodal Biomarkers for Alzheimer's Disease and Mild Cognitive Impairment," *BioMed Research International*, 2015. https://www.hindawi.com/journals/bmri/2015/961314/ (accessed Oct. 30, 2017).

[256] L. Bracoud *et al.*, "DWI and DTI results on normal controls, MCI, and Alzheimer's disease subjects from the rosas study," *Alzheimer's & Dementia: The Journal of the Alzheimer's Association*, vol. 11, no. 7, pp. P801–P802, Jul. 2015, doi: 10.1016/j.jalz.2015.06.1786.

[257] D. Zekry, J.-J. Hauw, and G. Gold, "Mixed dementia: epidemiology, diagnosis, and treatment," *J Am Geriatr Soc*, vol. 50, no. 8, pp. 1431–1438, Aug. 2002, doi: 10.1046/j.1532-5415.2002.50367.x.

[258] C. C. Jaffe, "Imaging and genomics: is there a synergy?," *Radiology*, vol. 264, no. 2, pp. 329–331, Aug. 2012, doi: 10.1148/radiol.12120871.

[259] G. Lee, H. Y. Lee, E. S. Ko, and W. K. Jeong, "Radiomics and imaging genomics in precision medicine," *Precis Future Med*, vol. 1, no. 1, pp. 10–31, Mar. 2017, doi: 10.23838/pfm.2017.00101.

[260] A. M. Rutman and M. D. Kuo, "Radiogenomics: creating a link between molecular diagnostics and diagnostic imaging," *Eur J Radiol*, vol. 70, no. 2, pp. 232–241, May 2009, doi: 10.1016/j.ejrad.2009.01.050.

[261] A. S. Panayides, M. Pattichis, S. Leandrou, C. Pitris, A. Constantinidou, and C. S. Pattichis, "Radiogenomics for Precision Medicine With A Big Data Analytics Perspective," *IEEE J Biomed Health Inform*, Dec. 2018, doi: 10.1109/JBHI.2018.2879381.

[262] E. Prodromou, S. Leandrou, E. Schiza, K. Neocleous, M. Matsangidou, and C. S. Pattichis, "A Multi-User Virtual Reality Application For Visualization And Analysis In Medical Imaging," in *2020 IEEE 20th International Conference on Bioinformatics and Bioengineering (BIBE)*, Oct. 2020, pp. 795–800. doi: 10.1109/BIBE50027.2020.00135.

Appendix A

Table 33 Interpretation of MMSE scores

Score	Dementia stage	Communication skills / Impairement
24-30	Mild Cognitive Impairment	Problems with concentration/ decreased attention span. Starting to have word finding difficulty. No impairments would be recognized in an interview of person Usually are aware of problems and may try to hide or compensate.
20-24	Mild	Diminished visual/spatial abilities Inappropriate social cues (e.g. stand too close to person during conversation). Word finding difficulty Lose train of thought in conversation, Repeats oneself

		Usually aware of problems and may try to hide or compensate.
13-20	Moderate	Difficulty following a conversation. Loss of vocabulary, especially proper nouns. More word finding difficulty Word substitution or making up new words Difficulty following a story or movie. Poor recall Difficulty following directions. Tendency to talk about nothing or ramble.
0-12	Severe	Tendency to ramble or repeat words. Increasing loss of vocabulary Difficult to follow anything but simple conversation/ instructions. Unable to follow a story or movie Major personality/ behavioral changes. Terminal Dementia Inability to speak Difficulty understanding when spoken to Mostly nonverbal communication